SERINE PROTEASE REGULATION OF THE EPITHELIAL SODIUM CHANNEL

by

Adedotun Adebamiro

BA, LaSalle University, 1999

Submitted to the Graduate Faculty of

School of Medicine in partial fulfillment

of the requirements for the degree of

Doctor of Philosophy

University of Pittsburgh

2006

UNIVERSITY OF PITTSBURGH

SCHOOL OF MEDICINE

This dissertation was presented

by

Adedotun Adebamiro

It was defended on

July 13, 2006

and approved by

Daniel C. Devor, Associate Professor, Cell Biology and Physiology

Peter F. Drain, Assistant Professor, Cell Biology and Physiology

John P. Horn, Professor, Neurobiology

Robert J. Bridges, Professor, Cell Biology and Physiology

Thesis Director/Dissertation Advisor: John P. Johnson, Professor, Medicine Renal Electrolyte Division, and Cell Biology and Physiology

SERINE PROTEASE REGULATION OF THE EPITHELIAL SODIUM CHANNEL

Adedotun Adebamiro, PhD

University of Pittsburgh, 2006

Na^+ transport through epithelial cells mediated by the epithelial Na^+ channel (ENaC) is important for maintaining body fluid Na^+ homeostasis, alveolar fluid clearance and normal airway mucocilliary function. A large body of evidence shows significant correlation between serine protease activity, channel fragmentation and transepithelial movement of Na^+. The extracellular protease dependent regulation may play an important role in epithelial cells where the channel activity is intended more for the control of the extracellular environment, such as in airway cells, than in the control of the internal fluid status of the organism. Presented here is evidence supporting the hypothesis that Na^+ channels are inserted into the apical membrane as inactive precursors whereupon they are acted upon by membrane resident serine proteases resulting in active channels. The effects of the serine protease inhibitor, aprotinin, on ENaC single channel properties were studied using transepithelial fluctuation analysis in the A6 amphibian kidney epithelium. Aprotinin causes a potent specific time-dependent inhibition of Na^+ transport. Analysis of blocker induced fluctuations in Na^+ current (I_{Na}) showed linear rate-concentration plots with the same blocker on- and off-rates in control and aprotinin inhibited conditions. Verification of open-block kinetics allowed for the use of a pulse protocol method to study the same cells under different conditions as well as the reversibility of the aprotinin effect on single channel properties. It was shown that protease regulation of I_{Na} is mediated by increasing the number of active channels in the apical membrane. To test the hypothesis that residues on ENaC mediate protease dependent channel activation ENaC was subjected to site-directed mutagenesis and heterologously expressed in Fisher rat thyroid (FRT) model epithelial cells. Activation by exogenous proteases depended on the presence of substrate specific residues in ENaC which dictated the rates of activation and the steady-state current levels.

TABLE OF CONTENTS

LIST OF TABLES

LIST OF FIGURES

PREFACE

It is a great pleasure to have been given the opportunity to study different aspects of Na^+ transport regulation. My interest in Na^+ transport regulation arises from an interesting presentation given by Dr. Pilewski in a journal club for medical scientist training program students describing the effects of Na^+ transport on the pathophysiology of cystic fibrosis. This lead to joining the laboratory of Dr. Bridges where the work described in this thesis was performed. I am immeasurably indebted to Dr. Bridges for his teaching, mentorship, support and accommodation over the last several years. While in his lab, through his relentless attention to detail and willingness to explore, I gained much more than could be reflected by this thesis alone. I expect the lessons learned from him as a scientist, a mentor and a leader will serve me well in future endeavors. I am indebted to my thesis advisor, Dr. Johnson whose support was critical for the completion of my studies. As a mentor and a confidant, I cannot thank him enough. The help of my thesis committee members Dr. Devor, Dr. Drain and Dr. Horn was invaluable in many respects. Their willingness to engage thoroughly in my work, offer criticisms and suggestions and support my endeavor lead to a focused and manageable body of work that is summarized in this dissertation. They are all my mentors.

This work could not have been accomplished without tremendous help from Dr. Cheng, a colleague in Dr. Bridges laboratory. I acknowledge his significant contribution to the generation of reagents and ideas through many lively discussions where honest debate and criticism served to sharpen our thinking and produce exploration of new ideas. The A6 cells were a generous gift from Dr. Van Driessche (KU Leuven, Belgium). The fisher rat thyroid cells were a generous gift from Dr. Snyder (University of Iowa) and the plasmids used in the site-directed mutagenesis studies were gifts from Dr. Rao (Texas Tech) and Dr. Cheng (Rosalind Franklin University). Work with Dr. Mishra on the use of amiloride analogues to generate Na^+ channel noise in Xenopus oocytes and mammalian epithelia, though not presented here, lead to important observations that is a basis for future work in the area. I am indebted to Matt Green for technical help in many areas especially with the Xenopus oocytes. Dr. Bertrand and Dr. Butterworth were wonderful teachers and supportive friends. I cannot be grateful enough for the steadfast support of my family.

1.0 INTRODUCTION

This dissertation addresses a mechanism by which transepithelial Na^+ transport mediated by the epithelial Na^+ channel (ENaC) is activated by proteases in epithelial cells. The transport process considered is the vectorial movement of solutes and water through a monolayer of polarized cells that display targeted distribution of transport proteins. The vectorial movement of Na^+ mediated by ENaC is a passive diffusional process down a Na^+ electrochemical gradient with high capacity and low Na^+ affinity (62, 102) allowing for a large dynamic range in the rates of Na^+ transport. One possible means by which such dynamic range is achieved is the activation of quiescent channels at the apical membrane of epithelial cells by endogenous or exogenous proteases. ENaC is expressed in several tissues where Na^+ absorption is a primary function. The ENaC-mediated Na^+ transport is important in the kidney cortical collecting duct (CCD) for regulated reabsorption of filtered Na^+. The Na^+ reabsorption couples to K^+ secretion to determine plasma levels of Na^+ and K^+. Abnormal up-regulation of Na^+ transport due to gain of function mutations results in Liddles syndrome characterized by hypertension and hypokalemia (170) whereas down regulation results in the syndrome pseudohypoaldosteronism I (PHA-1) characterized by excessive loss of NaCl and hyperkalemia (91). Mice lacking ENaC demonstrate, in addition to PHA-1, neonatal respiratory distress because of the inability to remove fluids from alveoli air spaces (89, 90, 127). Furthermore, increased ENaC activity occurs in cystic fibrosis (22, 23) and is associated with increased absorption of airway surface liquid (124), and decreased mucus clearance (48). ENaC also plays a significant role in salt intake by serving as a hormonally regulated sensor of salt in the dorsal epithelium of the anterior tongue (113) and it functions to modify the secretions of salivary, sweat and pancreatic glands through reabsorption Na^+ along the ducts (5) Regulated ENaC-mediated Na^+ transport is thus implicated in variety of physiological roles critical for life.

1.1 ENAC-MEDIATED SODIUM TRANSPORT

A comprehensive model of epithelial Na^+ transport called the Koefoed Johnsen-Ussing (KU) model emerged from studies in the isolated frog skin (106, 190). The KU model was the culmination of a long series of observations starting with the absorption of Na^+ across frog skin in the absence of a chemical gradient, and the continued absorption against an immense concentration gradient to the dependence of Na^+ transport on energy metabolism (102). According to the KU model, epithelial Na^+ transport is a transcellular process involving two steps. The first is the passive movement of Na^+ from the external environment (lumen) across the apical (luminal) membrane of epithelial cells. The second is the active transport of Na^+ up a chemical gradient from the intracellular compartment across the basolateral (serosal) membrane into the internal (serosa) space mediated by the Na^+/K^+ pump as indicated in Figure 1-1.

The first step in the absorption of Na^+ is the passive diffusion of Na^+ across the apical membrane. This requires an electrochemical gradient for Na^+ and permeability for Na^+. Passive diffusion across the apical membrane was established by the logarithmic dependence of the apical membrane potential difference on luminal Na^+ concentration providing evidence that the apical membrane potential is created in part by the Nernst equilibrium for Na^+ (19, 33). The intracellular Na^+ concentration is low (157, 158), therefore the chemical gradient is oriented inwards. Lindemann and Van Driessche (115) showed that the apical membrane Na^+ permeability was consistent with the presence of discrete channels inhibited by the natriuretic drug amiloride. The apical membrane channels were later studied with patch clamping, which showed that the channels were small conductance, Na^+-selective, non-rectifying channels inhibited by amiloride (140). The channel is a ~ 5 pS conductance channel that gates between a single open state and a single closed state (74, 141).

A

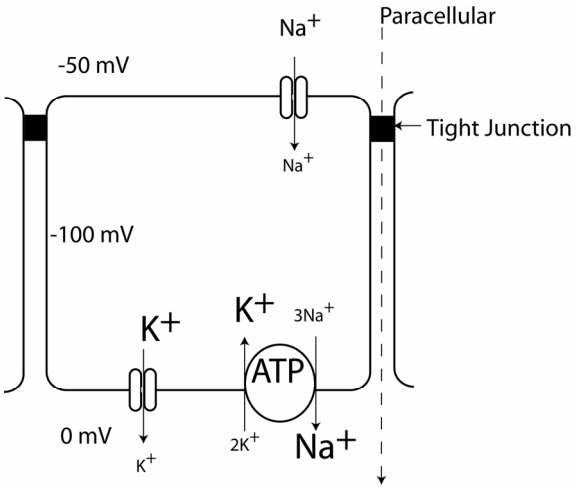

B

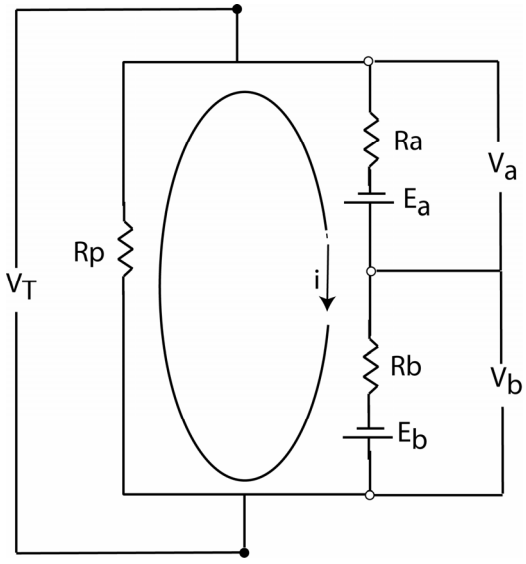

Figure 1-1 A model of Na^+ transport in tight epithelia

A) adapted from Kirschner (102) The apical membrane is permeable to Na^+ through ENaC. The basolateral membrane is permeable to K^+ and has the ubiquitous $3Na^+/2K^+$ pump. When the apical and basolateral sides are bathed in high Na^+, low K^+ solutions, the basolateral membrane resting potential is hyperpolarized and approaches the Nernst equilibrium potential for K^+ (E_K) and the apical resting membrane potential depends on E_{Na}. B, adapted from Schultz (160) At steady state, using the equivalent circuit analysis with the assumption that the apical and basolateral membranes are dominated by the Na^+ and K^+ conductances respectively, the apical membrane potential is $V_a = E_a - iR_a$, the basolateral membrane potential is $V_b = E_b - iR_b$ neglecting the pump. When the paracellular resistance is R_p, then the Na^+ influx current is $(E_a + E_b)/(R_a + R_c + R_p)$. The total electrochemical driving force for Na^+ absorption is therefore $E_{Na} = E_a + E_b$.

The open and closed times are 2 – 5 s. The channel has no known stimuli such as voltage or a ligand that alter the rates of state transitions. In the KU model, Na^+ diffusion across the apical membrane is rate limiting due to a relatively low Na^+ permeability. Biber and Curran (19) showed that the saturable component of Na^+ entry into the cell was in the apical membrane with a K_M similar to that for transepithelial movement. Micro-electrode studies (59, 79) were consistent with Biber and Curran (19) showing that in the frog skin the apical membrane conductance was rate limiting. Consequently, the rate of Na^+ transport is regulated by controlling the permeability of the apical membrane; in other words the functional properties of the Na^+ channels. The second step is extrusion of Na^+ from the cells across the basolateral membrane. Since addition of oubain, a specific inhibitor of the ubiquitous Na^+/K^+ pump, or removal of K^+ from the basolateral bath (thereby inhibiting the pump) inhibits Na^+ transport with resultant increases in intracellular Na^+ and decreases in intracellular K^+ (85, 153), the Na^+/K^+ pump is required at the basolateral membrane. Because decreases in intracellular Na^+ result from inhibition of apical Na^+ entry (153, 158) and application of oubain, an inhibitor of the Na^+/K^+ pump, increases intracellular Na^+ (153), the basolaterally localized Na^+/K^+ pump primarily functions to keep intracellular Na^+ low and K^+ high. The basolateral membrane is 50 – 100 mV hyperpolarized (18, 79, 130) due to a high K^+ permeability (39, 183) and high intracellular K^+ (2, 59, 153). Epithelial cell polarization keeps the K^+ permeability and the Na^+/K^+ pump at the basolateral membrane spatially separated from but electrically coupled to the apical membrane by intercellular tight junctions. When the basolateral membrane is depolarized by increasing basolateral bath K^+, Na^+ transport is decreased because apical membrane depolarization reduces the driving force for Na^+ entry (183). It is clear that the K^+ permeability is important for pump function as well as providing the electrical potential for Na^+ entry at the apical membrane.

1.2 MOLECULAR STRUCTURE AND FUNCTION OF ENaC

The genes encoding ENaC were cloned and, when heterologously expressed in a Xenopus oocyte model system, reconstituted the properties of the apical membrane channels of Na^+ transporting epithelial cells completely (31, 125, 151). The functional channel is made of three homologous

subunits α, β and γ. These subunits are ~ 60-75 kD polypeptides that have two transmembrane spanning domains each (M1 and M2 segments), intracellular amino and carboxyl termini, and the majority of the sequence forms an extracellular domain (30, 173). The topology is conserved for a growing family of cation channels called the DEG(digenetic)/ENaC channels (99). Although each subunit is required, the current experimental results in the literature provide evidence for multiple stoichiometric combinations. Measurement of epitope-labeled subunits suggest that the α subunit was expressed twice as much as the β and γ subunits in the plasma membrane suggesting at least a $\alpha_2\beta_1\gamma_1$ stoichiometry (57). Based on (i) observations that mutational modification of individual subunits is sufficient to impart a functional characteristic such as inhibition by covalent modification of free thiols or changes in zinc and amiloride blockade affinities, and (ii) the expected distribution of channels incorporating the mutant subunit when co-expressed in combination with wild type subunits, it was shown that functional channel stoichiometry was consistent with $\alpha_2\beta_1\gamma_1$ (57, 108). The results contrast with experiments that used similar mutational approaches plus determination of channel complex molecular weights using sucrose gradient sedimentation to postulate a $\alpha_3\beta_3\gamma_3$ stoichiometry (174). Recent results from Förster resonance energy transfer (FRET) of subunits labeled with green and yellow fluorescent protein FRET pairs suggest that there are equal numbers of α, β and γ subunit per channel (177). Although solving the stoichiometry controversy awaits higher resolution techniques, the current literature is unequivocal that the functional channel contains all three subunits.

A representation of the membrane topology of the α ENaC subunit is shown in Figure 1-2. At least part of the ion permeation pathway is formed from all three subunits with a conserved pre-M2 sequence implicated. Mutations within this sequence results in altered ion selectivity of the channels as well as changes in channel gating (96-98, 152, 172). Because of the voltage sensitivity of amiloride block (61, 162), and competitive interactions with Na^+ (112), amiloride may block at the pore entry site. Consistent with this, mutations in the pre-M2 segment also reduced amiloride block affinity (159). These results suggest that the pore of the channel comprises residues in the pre-M2 domain. Amiloride block affinity is however not determined solely by the pre-M2 segment since an α subunit region closer to the M1 segment also determine the affinity (92). Similarly, channel gating is modulated by mutations in the

cytoplasmic amino terminal "HG" motif (72, 73). Thus, while the pore region is highly important for channel gating, parts of the channel far removed from the pore also affect gating.

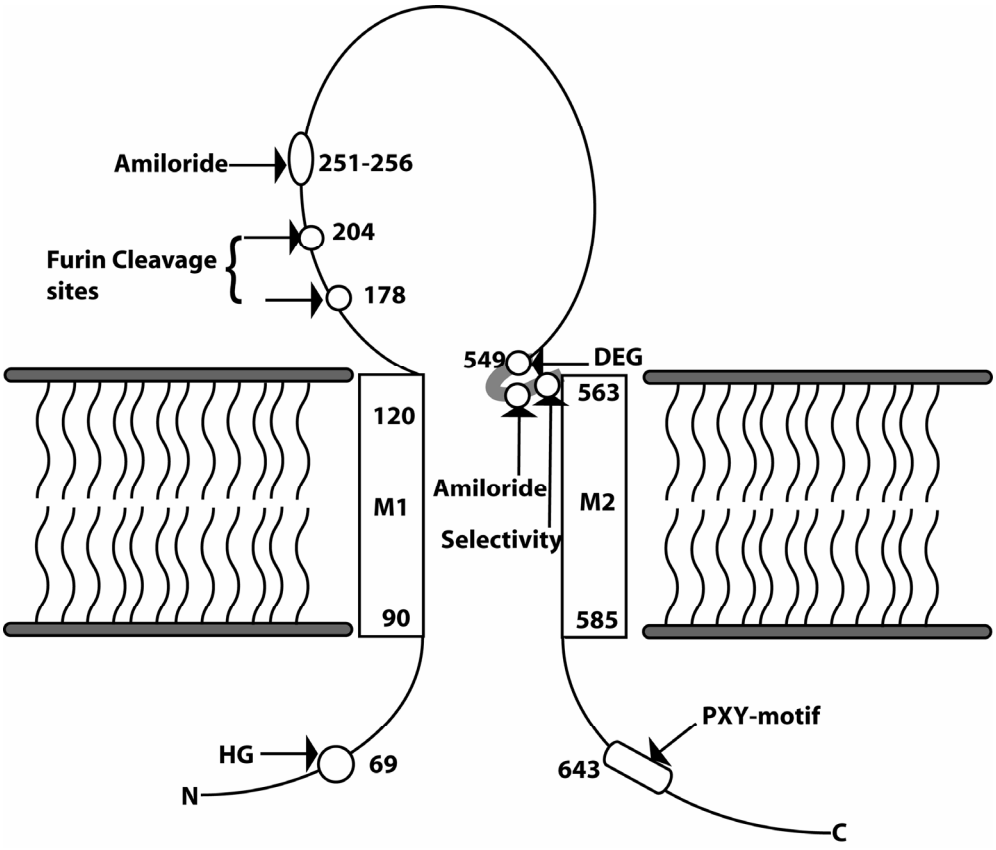

Figure 1-2 Disposition of the α subunit of ENaC in the membrane

The Disposition of the α subunit of ENaC in the membrane is based on sequence information and selective proteolysis. The N-termini cytoplasmic sequence has the residues HG that results in reduced channel P_O when mutated. The sequence after the first transmembrane domain has two cleavage sites that are furin consensus sequences. The potency of amiloride inhibition of the channel is determined in part by a sequence WRYFHY at residues 251-256. The shaded portion before M2 is known as the pre-M2 region and is thought to form part of the channel pore. This region contains the DEG site at position 549. Mutation of this residue leads to altered gating properties in ENaC and degenerin family ion channels. The pre-M2 region also has residues that determine the potency of amiloride blockade and the selectivity properties of the channel. The C-terminal cytoplasmic domain has consensus phosphorylation sites for protein kinase C, protein kinase A, and extracellular regulated kinase 1 / 2. In addition, the C-terminal region contains a PXY motif, that allows for regulation of ENaC by the ubiquitin ligase Nedd4-2. Mutation of the PXY motif results in increased surface expression.

1.3 REGULATION OF SODIUM REABSORBTION

The driving force for tissues to reabsorb Na^+ is high over vast differences in luminal Na^+ concentration, and the absorption rate is determined by the apical membrane Na^+ permeability under the influence of various hormones. Consequently, many of the dynamic regulatory processes involved in epithelial Na^+ transport center on controlling apical Na^+ channel activity through three identifiable means: i) regulation of channel synthesis, ii) endocytic-exocytic processes where membrane vesicle associated channels are trafficked between apical membrane and intracellular pools and iii) regulation of the functional properties of channels already in the apical membrane.

Control of subunit synthesis is accomplished by aldosterone through mineralocorticoid receptor but only partly mediated by transcriptional up-regulation of the subunits (63). In different tissues aldosterone selectively increased mRNA transcripts of the subunits, for instance increasing β and γ but not α subunit mRNA in the rat colon (11). In general, the increases in mRNA and the time courses were not commensurate with increases in the Na^+ current suggesting that the transcriptional regulation of subunits is not the primary response to aldosterone but may result from chronic aldosterone stimulation (9, 10, 66, 139). Similarly the rate of increase Na^+ current was faster than the rate of increase of subunit protein so that the increase in current cannot be attributed to synthesis (6). Although it's effect on subunit synthesis does not explain the Na^+ current increase completely, aldosterone induces transcription of several other proteins that potentially may modulate the trafficking and function of the channel (196).

The trafficking of channels between intracellular pools and the apical membrane is the second possibility for the regulation of Na^+ transport. The average number of channels at the apical membrane results from the balance between channel insertion into the membrane and retrieval from the membrane. Regulation of trafficking may result from an effect on insertion, retrieval or both. There is currently significant evidence to support the notion that retrieval of ENaC from the apical membrane is a regulatory step. Truncation of the carboxyl termini of all three subunits result in extended apical membrane residence time of the channel and increased Na^+ currents (69, 166). The carboxyl termini have sequences recognized by the clathrin

dependent endocytosis as well as by the ubiquitin ligase Nedd4-2 (179, 203). Clearly, Nedd4-2 dependent retrieval of ENaC from the membrane occurs and down regulates Na^+ current. Phosphorylation of Nedd4-2 interferes with its ability to cause down regulation of Na^+ transport (45, 176). Regulatory pathways that result in phosphorylation of Nedd4-2, such as increased synthesis (by aldosterone mediated transcription) and phosphorylation (insulin receptor activation of phosphoinositol dependent kinase) of SGK mediate channel expression at the surface (145). The phosphorylation activity of SGK has been shown to increase subunit expression at the surface as well as membrane surface area as measured by membrane capacitance (7). Phosphorylation at conserved sites in the C-termini prevents the Nedd4-2 dependent down regulation as well as prevents endocytic retrieval by other mechanisms (178, 205). There is also evidence that insertion can be regulated. The action of cAMP on Na^+ transport is mediated in part by the trafficking of channels from an intracellular recycling pool to the apical membrane (27).

The third level of regulation is modification of channel function. Modification of channel function may occur through changing the channel open probability or through recruitment from a quiescent channel population at the apical membrane. This is accomplished primarily through covalent modifications and non covalent interactions. The C-termini of ENaC subunits is known to be phosphorylated in response to stimulation by aldosterone and insulin; and blockade of the phosphorylation prevents increases in Na^+ currents (165, 207). Similarly, a response to aldosterone stimulation is the methylation of the C-terminus of the β subunit in renal epithelial cells (155). Methylation was recently shown to stimulate Na^+ currents in epithelial cells (50). Non-covalent interactions also appear to modify channel function. Unlike many channels that open in response to known ligands, a ligand for ENaC has not been identified. However, recent studies show that phosphatidylinositol 4,5 bisphosphate and phosphatidylinositol 3,4,5-triphosphate whose concentrations change in response to hormonal stimulation of renal epithelial cells directly interact with the amino and carboxyl termini of the β and γ subunits respectively and increase the open probability of ENaC (55, 121, 149, 186, 187). This interaction is probably mediated by binding to positively charged amino acids in a track of the γ subunit intracellular carboxyl terminal domain (148). A growing body of evidence suggests that endogenous and exogenous proteases act to increase ENaC-mediated Na^+ transport in part by recruitment of

inactive channels (29). The evidence for protease dependent regulation is reviewed in the next section and the elucidation of a mechanism is the subject of the rest of the dissertation.

1.4 PROTEASE ACTIVITY AND SODIUM TRANSPORT

A strong correlation exists between extracellular luminal protease activity and epithelial Na^+ transport. Studies looking at alterations in hormonal levels and salt dietary intake found that conditions which facilitate Na^+ reabsorption resulted in increased urinary kallikrien activity (67, 119, 120). Kallikriens are serine proteases known to have kininoginase activity that hydrolyzes the inactive peptide precursor (kininogen) to an active peptide agonist (kinin) (118). To stimulate Na^+ reabsorption in the kidney, animals were maintained on reduced salt intake. Reduced salt intake is a strong activator of the mineralocorticoid aldosterone, a steroid hormone that stimulates Na^+ transport in renal cortical collecting duct (CCD) cells. These animals had higher levels of urinary kallikrien activity (67). Animals injected with aldosterone but without the restricted salt intake also had higher urinary kallikrien activity (67, 119, 197). Increased urinary kallikrien activity was also detected in animals on increased K^+ intake, which is an aldosterone inducing stimulus (84). Consequently increased plasma aldosterone was strongly associated with increased urinary kallikrien. The presence of hormonally up-regulated urinary kallikrien activity raised questions about its origin, the molecular identity of the kallikrien activity, whether or not the protease activity was directly involved in regulating Na^+ transport and how the regulation is accomplished.

The protease activity found in the urine originates from renal CCD epithelial cells (35). The kallikrien-like protease and its kininogenase activity was also found in amphibian epithelial cells of the toad bladder and skin (118), and amphibian renal CCD derived A6 epithelial cells. These epithelial cells all share the property of amiloride-sensitive electrogenic Na^+ transport mediated by ENaC. Several experiments using biochemical, histochemical and physiological approaches localized the protease activity to the apical membrane, facing the luminal environment (169). Secretion of the kallikrien enzyme activity into the luminal environment follows the development of a functional transport monolayer by the A6 cells (95). The cellular

distribution and sub-cellular localization of the protease activity places it in close proximity with the apical membrane ENaC and is consistent with its accumulation in the urine.

Several experiments attempted to distinguish whether involvement of protease activity in Na^+ transport regulation was direct or indirect. While the up-regulation of urine kallikrien activity may cause up-regulation of Na^+ transport, it may also result from feedback mechanisms modulating the level of hormone mediated up-regulation (for instance to protect against excessive increases in intracellular Na^+) or from completely unrelated processes. Initial suggestions that kallikrien-like protease activity regulates Na^+ transport came from studies of amiloride inhibition of the urinary kallikrien protease activity and protease activities derived from frog skin extracts and renal CCD cell suspensions (118). Amiloride is a K^+-sparing diuretic known to potently inhibit Na^+ transport in epithelial cells. Since amiloride inhibits Na^+ transport and inhibits the extracellular protease activity from Na^+ transporting epithelial cells, it was suggested that amiloride inhibition of the extracellular protease activity explains its inhibition of Na^+ transport. While amiloride does inhibit the isolated kallikrien-like proteases, the inhibition was two orders of magnitude less potent than amiloride inhibition of Na^+ transport (118). The preponderance of evidence from noise analysis and single channel measurements is consistent with the hypothesis that amiloride inhibition of Na^+ transport is via a direct blocking mechanism of ENaC. The macromolecular protease inhibitor, aprotinin that inhibits the urinary kallikrien protease activity with high potency also inhibits transepithelial Na^+ transport, a key observation for the present work. In particular, the addition of aprotinin to toad bladder epithelium inhibited Na^+ transport (137). Furthermore, several epithelial cells respond to apical protease inhibitors with reduced Na^+ transport (49, 116, 132, 191). However, it remains a possibility, like the case with amiloride, that the macromolecular protease inhibitor directly interacts with and blocks the channels.

In isolated epithelial up-regulation of the kallikrien activity alone is not sufficient for aldosterone mediated increases in Na^+ transport. In contrast to an activating role of the extracellular proteases, in many cases, an inhibitory effect of exogenously added extracellular proteases was observed. The addition of exogenous kallikrien to the apical surface of mammalian urinary bladder caused irreversible inhibition of Na^+ transport interpreted as progressive hydrolysis of the Na^+ channel (110). However, the epithelium gained an amiloride insensitive conductance with near equal Na^+ and K^+ permeability that was interpreted as non-

selective degraded channels. In the toad bladder epithelium, addition of trypsin to the apical surface also inhibited Na^+ transport (64). In both cases, apical amiloride prevented protease mediated inhibition. Because amiloride does not inhibit trypsin nor inhibit kallikrien at the concentrations used, but interacts with and blocks the channel, the protective amiloride effect was consistent with the protease recognizing specific site/s on the channel that could be masked by amiloride binding or an amiloride induced conformational change in the channel.

Vallet et al. identified a serine protease, channel activating protease 1 (xCAP1), that increased ENaC-mediated Na^+ transport when co-expressed with ENaC in Xenopus oocytes (191). The increase in Na^+ current mediated by xCAP1 was inhibited by the serine protease inhibitor aprotinin. Consequently xCAP1 and its homologues may be the aprotinin sensitive proteases mediating Na^+ transport in many epithelial cells. A related human membrane associated protease, prostasin, increased Na^+ transport when co-expressed with ENaC in Xenopus oocytes (3, 49). Other membrane associated proteases CAP2 and CAP3 have been identified that also increased Na^+ transport when co-expressed with ENaC in Xenopus oocytes (200). The proteases found to up-regulate ENaC-mediated Na^+ transport in oocytes have in common an extracellular serine protease domain and either a transmembrane segment (CAP2 and CAP3) or a glycophosphatydil inositol (GPI)-anchor (CAP1) (200). Prostasin and CAP3 are known to be membrane associated; with active extracellular serine protease domains (182, 206). Although not exclusive to Na^+ transporting epithelia, prostasin and similar channel activating proteases can be found in many epithelia with aprotinin sensitive Na^+ transport. Interestingly, prostasin was upregulated by aldosterone in rat CCDs. Tong et al used the small interfering RNA (siRNA) technique to reduce the expression of prostasin in a model Na^+ transporting airway epithelial cell. The airway cells with reduced prostasin expression had diminished Na^+ transport. In contrast to exogenously added trypsin and kallikrien, the observations suggest that an endogenous protease can activate Na^+ transport. These results also suggest that the endogenous protease activity is fully capable of maintaining the steady-state Na^+ transport in native Na^+ transporting epithelia such that inhibition of the protease reduces the steady-state transport but addition of exogenous protease to uninhibited cells does not increase the transport. Furthermore, in heterologous expression studies such as Xenopus oocytes injected with ENaC cRNAs, and fibroblasts transfected with ENaC, the proteases trypsin, chymotrypsin, neutrophil elastase and cathepsin G increased Na^+ transport (28). The overall picture suggests that

proteases may play both an activating role and perhaps an inhibitory role in the regulation of Na^+ transport. The channel may sojourn in a protease dependent manner through "inactive quiescent", "activated" and "inactivated periods" in its lifetime at the apical membrane. The "inactive quiescent" state occurs prior to an essentially irreversible proteolytic activation, the active state represents channels with finite open probability whose activity can be regulated by covalent and non-covalent interactions and perhaps and the possible "inactivated period" may represent channels that have been irreversibly inactivated prior to retrieval from the apical membrane. Measurements of the apical membrane channel density by amiloride binding and immunodetection gave results two orders of magnitude or higher than can be accounted for by active channels (7, 40). The population of quiescent and inactivated channels may explain the discrepancy.

1.5 SODIUM CHANNEL CLEAVAGE AND ACTIVITY

The notion that protease activation of Na^+ transport results from cleavage of ENaC arises from the correlation between the appearance of cleaved forms of the α and γ subunit and the measured ENaC activity (54). First, salt restriction or aldosterone infusion (stimuli for increasing Na^+ reabsorption in the kidney) were associated with the appearance of a lower molecular weight γ subunit in the rat cortical collecting duct while control rats had only the heavier γ subunit (123). Two molecular weight species of the α and γ subunit were found in whole rat kidneys where up regulation of Na^+ transport in collecting duct cells correlated with increase of the lower molecular γ subunit and decrease of the higher molecular weight species suggesting a conversion (54). Aldosterone up-regulation of prostasin in the cortical collecting duct cells (133) may generate the γ subunit cleavage. Further, preventing internalization of ENaC in epithelial cells heterologously expressing ENaC increased the Na^+ current, increased the lower molecular weight isoforms of the α and γ subunits at the apical membrane and decreased sensitivity to exogenous trypsin activation (105). Finally, mutation of the furin cleavage consensus sequences found in the extracellular domains of the α and γ subunits prevented endogenous cleavage of these subunits and reduced Na^+ transport rates (86).

1.6 HYPOTHESIS AND SPECIFIC AIMS

1.6.1 Hypothesis

ENaC arrives at the apical membrane as an inactive precursor whereupon activation by membrane associated extracellular proteases occurs to regulate the extent of apical membrane ENaC activity.

1.6.2 Specific Aim 1:

From the basic mechanism of Na^+ transport in epithelial cells, there are only three primary possibilities that can lead to an increase in Na^+ entry; a change in the driving force for Na^+ entry across the apical membrane, a change in the Na^+ permeability of the apical membrane or a combination of the two. There is no *a priori* expectation that the driving force is being directly regulated by extracellular proteases to increase Na^+ since oocyte expression system experiments demonstrate a protease dependent change in Na^+ transport despite holding the driving force constant by clamping the membrane potential and fixing the Na^+ gradient. The experiments under fixed driving forces neither rule out a protease effect on driving forces nor indicate the significance of changes in the driving force in native epithelia. In other words, the experiments suggest the second possibility but do not exclude the third. The experiments in the first part of the dissertation were carried out in a well characterized native Na^+ transporting epithelial cell line to understand how epithelial cells regulate Na^+ transport via the extracellular protease dependent mechanism. In intact epithelial cells, perturbation in the number of active channels, the single channel open probability and single channel currents were measured as Na^+ transport responds to changes in extracellular protease activity. In conjunction with immunochemical detection of membrane ENaC density, a protease dependent change in the number of active channels can be determined from the electrophysiological measurements. The results directly implicate the protease mechanism to Na^+ channel regulation, provide evidence for the presence of quiescent channels and unmask possible further heterogeneity of the active channels.

1.6.3 Specific Aim 2:

Many proteolytic regulatory mechanisms use the hydrolysis of a peptide agonist precursor to generate a signaling molecule that interacts with specific membrane receptors. A well known example is the rennin-angiotensin system. Another mechanism involves activation of protease activated receptors (PARs). The known PARs are G protein coupled receptors with intramolecular tethered peptide ligands that are exposed by proteolysis. The peptide ligands for the PARs are sufficient for receptor activation (138) but they were unable to up-regulate Na^+ transport in epithelia cells (41). A possibility for ENaC is the activation by hydrolysis of its extracellular domains. There is currently correlative evidence for this possibility based on many recent studies showing an association between ENaC fragments at the apical membrane and channel activity (54, 86, 105)

The second part of the dissertation focuses on the question of ENaC as the target of proteolytic activation. Divided into two sections, the first section considers the possibility that ENaC is the direct target of proteases that activate Na^+ transport and that hydrolysis is a requirement for transport activation. The first section shows the development of a suitable expression system for studying protease regulation followed by the use of site-directed mutagenesis to probe ENaC for protease responsive residues. It was shown that there are residues on ENaC that are required for the current-activating responses to specific proteases activation and these residues correspond to the protease cleavage sites. The second section utilizes the expression system to study the sequences on ENaC that are utilized by the endogenous channel activating proteases to mediate Na^+ transport. These experiments demonstrate the utility of a heterologous expression system to study ENaC-mediated Na^+ transport by providing evidence that the transformation of quiescent channels into electrically active channels can be mediated by proteolytic cleavage of channels already at the apical membrane.

2.0 PROTEASE INHIBITION AND SINGLE CHANNEL PROPERTIES

Absorption of fluids and electrolytes is a function of many epithelia characterized often characterized by electrogenic Na^+ transport where the rate limiting step is apical membrane entry mediated by the epithelial Na^+ channel ENaC (65). In addition to well known endocrine regulation of ENaC through intracellular steroid receptors (63) and 2nd messengers such as cAMP (16) and Ca^{2+} (109), an alternate means of regulation, by extracellular proteases, was described (191) and referred to as channel activating protease (CAP) regulation of ENaC. CAP regulation of ENaC may play a role in a variety of physiological functions from blood pressure regulation (170), to mucocilliary clearance in the airways (21) and hearing (156). Three putative CAPs, CAP1 (prostasin), CAP2 (TMPRSS4) and CAP3 (matriptase) that stimulate ENaC-mediated amiloride-sensitive Na^+ transport (I_{Na}) in *Xenopus* oocytes have been cloned (200). These CAPs were predicted to be membrane anchored proteins with extracellular serine protease domains. The importance of serine protease activity in ENaC regulation has been demonstrated in renal epithelial cell-lines (132, 191, 201) and primary airway cells (25, 49) by serine protease inhibition.

Vallet et al. (192) reported that both membrane anchoring and proteolytic activity were required for CAP1 activation of ENaC. However, the exogenous addition of chymotrypsin and trypsin have also been shown to stimulate I_{Na} in *Xenopus* oocytes (37) and trypsin stimulates I_{Na} in fibroblasts expressing ENaC (29). Recently, it was shown that the appearance of apparently smaller molecular weight forms of ENaC from MDCK cells heterologously expressing ENaC could be blocked by mutations that remove putative cleavage sites in ENaC α and γ subunits for the protein convertase furin (86). These mutations were associated with a significant decrease of I_{Na} in *Xenopus* oocytes expressing ENaC. Although exogenous proteases have no effect on the spontaneous I_{Na} in several native Na^+ transporting epithelia, trypsin enhanced recovery of I_{Na} following inhibition by the serine protease inhibitors aprotinin and bikunin (25, 49, 191).

Therefore, inhibition of the CAP pathway by specific protease inhibitors is sufficient to inhibit Na^+ transport in numerous epithelia.

ENaC regulation by the CAP pathway could be mediated by changes in the single channel current (i_{Na}), the open probability (P_o), or the number of active channels (N_T) which are related to the transepithelial Na^+ current (I_{Na}) according to equation 2-1.

$$I_{Na} = N_T \cdot P_o \cdot i_{Na} \qquad \textbf{2-1}$$

Studies using ENaC heterologously expressed in oocytes (3, 37) and fibroblasts (29) have yielded contradictory results in regards to how extracellular proteases regulate ENaC. In an effort to further clarify how ENaC is regulated by the CAP pathway, transepithelial current fluctuation analysis was carried out in the amphibian renal epithelial cell line A6. The results demonstrate that the protease inhibitor aprotinin reversibly inhibits I_{Na}. The decrease in I_{Na} was accompanied by a decrease in the number of open channels (N_o), an increase in i_{Na} and a paradoxical increase in P_o. Because only the decrease in N_o can explain the decrease in I_{Na} it can be concluded that the CAP pathway regulates sodium transport by modulating the number of active ENaCs in the apical membrane.

2.1 MATERIALS AND METHODS

2.1.1 Cell culture

A6 cells were maintained in amphibian medium (Biowhitaker) and 10 % fetal bovine serum (Gibco) in an incubator with humidified air and 4 % CO_2 at 28°C as previously described (154). The cells were expanded on plastic tissue culture dishes and then seeded on Costar Transwell permeable supports (polycarbonate membrane of 0.4 μm pore size and 1cm^2 area). Experiments were performed 14 to 21 days after seeding on the permeable supports and 24 to 48 hours after media replacement.

2.1.2 Short-circuit current (I_{SC}) measurement

Costar Transwell cell culture inserts were mounted in Costar Ussing chambers with identical bath solutions in the apical and basolateral chambers containing (in mM) 100 NaCl, 2.4 $KHCO_3$, 1 $CaCl_2$, 5 glucose. The pH of the solution was 8.0 when gassed with ambient air. All experiments were carried out at room temperature. Gassing and continuous voltage-clamping to 0 mV was achieved with a four electrode automatic voltage clamp (Department of Bioengineering, University of Iowa) as shown in Figure 2-1. The open circuit voltages for the monolayers ranged from 40 mV to 80 mV. Four millivolt bipolar pulses were applied every min. generating current deflections used to calculate the transepithelial resistance (R_T) with Ohms law. I_{sc} traces were digitized at 10Hz and recorded using a DASA 6600 acquisition board and Acquire 6600 recording software (Gould Instrument System). The small molecule amiloride potently and specifically inhibit ENaC so that the difference in I_{SC} after addition of amiloride (10 μM) is equal to I_{ENaC}. In A6 cells, the primary transepithelial Na^+ pathway is through ENaC; therefore I_{ENaC} is practically equivalent to I_{Na}. Consequently the I_{SC} inhibited by 10 μM amiloride is taking as the measure of I_{Na}. Furthermore, under the experimental conditions the amiloride insensitive current was very small such that I_{Na} was 95 to 100 % of the I_{SC}. The current after addition of amiloride was extrapolated throughout the short-circuiting period as a constant; therefore, the I_{Na} reported at any point before addition of amiloride may only deviate from the actual amiloride-sensitive I_{SC} by 0 – 5 %.

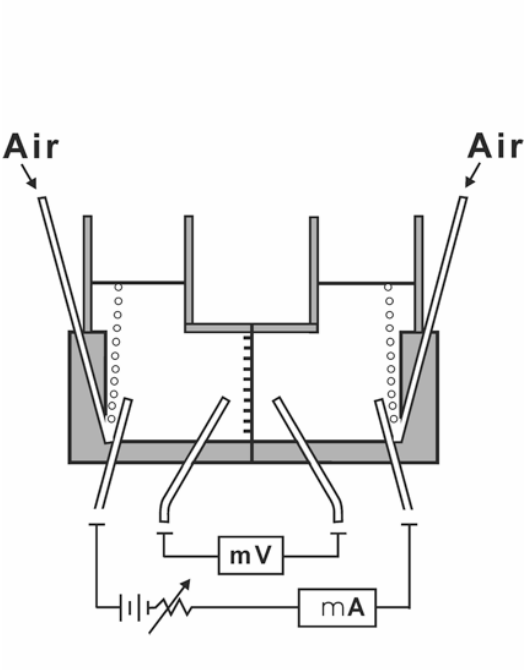

Figure 2-1 Ussing chamber apparatus

The Ussing chamber setup shows the two voltage sensing electrodes and the two current passing electrodes and the air input shafts. The half-chambers are separated such that electrical continuity is achieved solely through the mounted epithelial monolayer. In practice, the voltage sensing electrodes are connected to an amplifier that drives the current output to fix the transepithelial potential (for short-circuiting, 0 mV). The airshafts provide a gas-lift circulation that minimizes the unstirred layer across of the monolayer.

2.1.3 Blocker induced fluctuation analysis

2.1.3.1 Theory

From single channel studies, the apical Na^+ channels in A6 cells (74, 122), mammalian cortical collecting tubules (141, 142), and ENaC heterologously expressed in Xenopus oocytes (151) undergo spontaneous gating between an open (conducting) and a closed (non-conducting) state with no demonstrable subconductance states. The gating can therefore be described by equation 2-2.

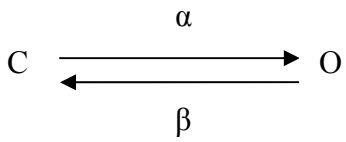

2-2

where C is closed state, O is an open state and α and β represent the rate constants for the transitions. The spontaneous open probability P_o is given by equation 2-3

$$P_O = \frac{N_O}{N_O + N_C} = \frac{N_O}{N_T} = \frac{\alpha}{\alpha + \beta}$$

2-3

where N_T is the total number of active channels or the number of open channels (N_O) plus closed channels (N_C). In the apical membrane, the N_T channels, assumed to be independent, have single channel currents i_{Na} under short-circuit conditions. The spontaneous transitions between closed and open states would therefore result in a variance (σ_I^2) of the mean macroscopic Na^+ current (I_{Na}) given by equation 2-4 (83).

$$\sigma_I^{\,2} = N_T \cdot i_{Na}^{\,2} \cdot P_O \cdot (1 - P_O)$$

2-4

When at least one of the single channel parameters is known from an independent experiment, equations 2-1 and 2-4 can produce the other two. Aside from the requirement for *a priori* determination of one of the parameters, a second limitation from equation 2-4 is that the variance of short-circuit currents can also arise from several sources besides the spontaneous fluctuations of Na^+ channels and these must be separated from the channel noise. The measurement of the spectral density or power density spectra (PDS) of current noise can allow for separating the noise of the channel openings and closings from other noise sources. Noise arising from exponential relaxation processes such as channel opening and closing will yield Lorentzian PDS which are of the form (80):

$$S(f) = \frac{S(0)}{1 + \left(\frac{f}{f_c}\right)^2}$$

2-5

where f is the frequency, S(0) and f_c are the low frequency plateau and corner frequency of the Lorentzian. The corner frequency is given by

$$2 \cdot \pi \cdot f_c = \alpha + \beta$$

2-6

and S(0) is given by

$$S(0) = \frac{4 \cdot \sigma_I^{\,2}}{\alpha + \beta}$$

2-7

From the Lorentzian spectral density the variance of spontaneous transitions arising from the exponential relaxation process can be separated from other noise sources and the upper limit on α and β can be estimated but α and β cannot be individually determined.

Although Lorentzian spectral density was expected for the apical Na^+ channels, it has remained impossible to observe in short-circuited epithelia for $0.1 < f < 1000$ Hz. Since the mean open and closed states life times for single ENaC channels in polarized A6 cells are 2 s or more (140), the upper limit for Lorentzians arising from the spontaneous gating of the channel (i.e. in the absence of blocking molecules) is 0.16 Hz necessitating measurements down to 0.01 Hz for any hope of observing spontaneous Lorentzians. Because I_{Na} was not perfectly stationary, and excess noise with 1/f spectral density arises at low frequencies, it was impractical to measure spontaneous low frequency Lorentzians that would characterize the channel transitions observed in cell-attached mode patch-clamping of Na^+ channels in the apical membrane of A6 cells. High frequency spontaneous fluctuations were never observed. An alternative approach is the measurement of Lorentzians induced by the application of compounds that block the Na^+ channel (103, 111, 112).

Blocker induced noise is based on a simple three state scheme that accounts for the blocker concentration dependent changes in spectral density and macroscopic currents where the blocker interacts solely with, and blocks the open state of the Na^+ channel with rate coefficients k_{on} and k_{off} (equation 2-8). This scheme gives rise to a relaxation process that is a sum of two exponentials which produces a sum of two Lorentzian components in the PDS (195).

$$C \underset{\beta}{\overset{\alpha}{\rightleftharpoons}} O \underset{k_{off}}{\overset{k_{on}[B]}{\rightleftharpoons}} \text{Blocked} \qquad \textbf{2-8}$$

The corner frequencies, in radians, are the two characteristic eigenvalues of the solution to the linear differential equations describing the scheme which are both functions of all four rate coefficients. Separately, the spontaneous (r^S) and blocker induced (r^B) transition processes have relaxation rates

$$r^S = \alpha + \beta \qquad \textbf{2-9}$$

$$r^B = k_{off} + k_{on} \cdot B \qquad \textbf{2-10}$$

The differential equations for the three state model in matrix notation is

$$\frac{d}{dt}\begin{pmatrix} N_C \\ N_O \\ N_B \end{pmatrix} = \begin{pmatrix} -\alpha & \beta & 0 \\ \alpha & -(\beta + k_{on} \cdot B) & k_{off} \\ 0 & k_{on} \cdot B & -k_{off} \end{pmatrix} \cdot \begin{pmatrix} N_C \\ N_O \\ N_B \end{pmatrix} \qquad \textbf{2-11}$$

where the variables N_C, N_O and N_B represent the number of closed, open and blocked channels respectively. Since N_T is the sum of closed, open and blocked channels and is a constant, one of the variables is not independent. If N_C is chosen as the dependent variable, the transition matrix reduces to a 2×2 matrix

$$\begin{pmatrix} -(r^S + k_{on} \cdot B) & k_{off} - \alpha \\ k_{on} \cdot B & k_{off} \end{pmatrix}$$

with eigenvalues

$$\lambda = \frac{1}{2}\left[(r^S + r^B) \pm \sqrt{(r^S + r^B)^2 - 4 \cdot (r^S \cdot k_{off} + \alpha \cdot k_{on} \cdot B)} \right] \qquad \textbf{2-12}$$

The determination of the λs at different blocker concentrations can be used to calculate the matrix parameters k_{on}, k_{off}, α and β. From α and β, equations 2-3 2-4 and 2-7 can be used to

calculate N_T, i_{Na} and P_o explicitly. However the low frequency corner, as previously indicated, is impractical to resolve under short-circuit conditions. Thus the PDS reveals one blocker dependent Lorentzian. The effect of the slow spontaneous gating on the corner frequency of this Lorentzian is very small. Equation 2-11 reveals this phenomenon when rearranged to

$$\lambda = \frac{1}{2}\left[\left(r^S + r^B\right) \pm r^B \cdot Q\ \right]$$

where

$$Q = \sqrt{\left(1 + \frac{r^S}{r^B}\right)^2 - 4 \cdot \left(\frac{\alpha \cdot k_{off}}{r^{B^2}} + \frac{\beta}{r^B}\right)}$$

From inspection Q ranges between $1\text{-}r^s/k_{off}$ and 1. Therefore at any blocker concentration the high frequency $\lambda \leq r^B + 0.5\ r^S$. For $r^S < 0.62\ s^{-1}$ the shift of the high corner frequency λ will be less than $0.62\ s^{-1}$ or 0.1 Hz. For typical high rate blockers with corner frequencies resolved at greater than 1 Hz, the effect of the spontaneous transitions is quite small. In the case of the compound used in the following experiments, corner frequencies were greater than 40 Hz making the effect of the spontaneous transitions negligible. The parameter i_{Na} at a given blocker concentration is calculated directly from the blocker induced Lorentzian. P_o is calculated from equilibrium considerations as described in the Section 2.1.3.2 from which N_T was subsequently obtained.

2.1.3.2 Implementation of Fluctuation Analysis

A6 cells on Costar Transwell inserts were placed in Costar Ussing chambers and continuously short-circuited with a low noise voltage clamp previously described (194). The I_{sc} was high-pass filtered (cut off 0.25 Hz) to remove the DC component then subjected to anti-aliasing filtering and amplification. The resulting signal was digitized and Fourier transformed to generate power density spectra (PDS) normalized to the tissue surface area (193). PDS were collected at 0.5 Hz fundamental frequency as averages of 30 sweeps over a frequency range of 0.5 to 350 Hz. The data was then fitted to equation 2-5 plus a low frequency component defined as $S1/f^{\alpha}$ (144). "One over f" noise, also called flicker noise, is the excess noise that results from fluctuations in conductance of porous membranes held away from electrical equilibrium that

decreases as 1/f (46). S1 is the low frequency power of the "one over f noise" with its decay characterized by α ranging from .5 to 1.5. We determined the plateau power (S_o) and corner frequency (f_c) from fits of 44 data points in the 0.5 to 200 Hz range. Blocker dependent parameters were determined as previously described (51, 78, 82). We determined aprotinin dependent changes in single channel parameters using two approaches: a cumulative 6-chloro-3,5-diaminopyrazine carboxamide (CDPC) concentration step and a pulse protocol (82). CDPC was chosen because its low affinity and high off-rate (see below) permit measurements of Lorentzians at relatively uninhibited states and affords a number of experimental advantages. These advantages were well described by Helman and Baxendale (78). Firstly, low affinity CDPC blockade minimizes the poorly understood "autoregulatory" responses to significant current inhibition that occurs with higher affinity blockers. Secondly, CDPC permits simultaneous measurement of changes in steady-state current and blocker kinetics from spectral analysis necessary for the determination of the open probability from the three-state model. Thirdly, a low affinity blocker by virtue of a high off-rate reduces the relative error in the estimation of the off-rate from the linear regression of the corner-frequency versus blocker concentration.

The cumulative concentration step approach was carried out by mounting A6 cells in a fixed bath volume (5 ml). Either 4 μM of the serine protease inhibitor aprotinin or an equivalent volume of the vehicle phosphate buffered saline (PBS) was added to the apical side. Apical and basolateral solutions were continuously mixed and oxygenated by a gas lift using air. After incubating in 4 μM aprotinin or PBS for 30 min., increasing doses of CDPC (in DMSO) were added to the apical bath to yield a cumulative increase in CDPC concentration. The concentrations used were 10, 20, 30, 40, and 50 μM CDPC. PDS were obtained 2 min. after addition of each dose of CDPC and following establishment of a new steady-state I_{sc}. The ENaC-mediated Na^+ current (I_{Na}) was taken as the I_{sc} before minus the I_{sc} remaining after addition of 10 μM amiloride and usually accounted for greater than 90% of the I_{SC}. Blocker rate coefficients where calculated from the linear regression of $2\pi f_c$ vs. blocker concentration using a pseudo-first order kinetic description where $2\pi f_c = k_{off} + k_{on} \cdot [B]$ (k_{on} and k_{off} are the apparent

on- and off- coefficients of the blocker (B) interacting with the open channel) and the dissociation constant was calculated as $K_d = \frac{k_{off}}{k_{on}}$.

For the pulse protocol, the Ussing chamber was modified to reduce the apical volume to 1.5 ml. The cells were continuously perfused at 5 ml/min with Ringer solution containing 10 μM CDPC. At indicated time points PDS were obtained, the solution was switched to one with 30 μM CDPC, PDS were again obtained and then the solution was switched back to one with 10 μM CDPC. Three experimental periods were evaluated; i) control, thirty min. of perfusion without aprotinin, ii) aprotinin, 45 min. of perfusion with a solution containing 10 μM aprotinin and iii) washout, thirty min. of perfusion without aprotinin. PDS were obtained at 10 and 30 μM CDPC at 10, 20 and 30 min. of the control and washout periods and at 25, 35 and 45 min. of the aprotinin period. The blocker rate coefficients were calculated from the two blocker concentrations and corner frequencies as

$$k_{on} = \frac{2\pi(f_c(30) - f_c(10))}{30\mu M - 10\mu M}$$

2-13

where $f_c(10)$ and $f_c(30)$ are the corner frequencies at 10 and 30 μM CDPC and

$$k_{off} = 2\pi f_c(10) - k_{on} \cdot 10\mu M$$

2-14

The single channel current amplitude (i_{Na}) was calculated as

$$i_{Na} = \frac{S_0 \cdot (2\pi f_c(10))^2}{4 \cdot I_{Na}(10) \cdot k_{on} \cdot 10\mu M}$$

2-15

where I_{Na} is the amiloride-sensitive current thus allowing determination the number of open channels at 10 μM CPDC as

$$N_o = \frac{I_{Na}(10)}{i_{Na}}$$

2-16

It has been repeatedly verified that CDPC and its analogs interact with ENaC-mediated amiloride-sensitive Na^+ transport in a manner described satisfactorily by a three state model (1, 14, 15, 51-53, 78, 82, 112, 114). The use of a closed-open blocked three-state model instead of a two-state or more complicated four-state models is not the focus of this work and arguments for the use of a three-state model of CDPC blockade of I_{Na} in A6 cells can be found in (78, 82). Therefore, the open probability (P_o) was calculated assuming a three state model where the blocker interacts predominantly with the open state using

$$P_o = \frac{\left(1 - \frac{I_{Na}(30)}{I_{Na}(10)}\right) \cdot K_d}{30 \cdot \mu M \cdot \frac{I_{Na}(30)}{I_{Na}(10)} - 10 \cdot \mu M} \qquad \textbf{2-17}$$

where $I_{Na}(10)$ and $I_{Na}(30)$ are the amiloride-sensitive current at 10 and 30 μM CDPC (82). The number of active channels (N_T) was calculated from

$$N_T = N_o \cdot \left(\frac{1}{P_o} + \frac{10}{K_d}\right) \qquad \textbf{2-18}$$

2.1.4 Cell surface biotinylation and western blotting of ENaC

Confluent A6 cell monolayers grown on permeable filters (Costar; 75 mm diameter) were treated with PBS, 10 μM aprotinin for 1 hour or 100 nM aldosterone for 6 hours and then kept on ice. Cell surface biotinylation and Western blot analysis of ENaC subunits were performed according to the modified method as described by Gottardi et al. (68, 75). Briefly, cells were washed three times in ice-cold PBS-CM (PBS with 1 mM $MgCl_2$ and 0.1 mM $CaCl_2$) and incubated with 1.5 mg/ml EZ-link™ Sulfo-NHS-S-S-biotin (Pierce) in cold biotinylation buffer (10 mM triethanolamine, 2 mM $CaCl_2$, 150 mM NaCl, pH 9.0) with gentle agitation. Cells were washed once with quenching buffer (192 mM glycine, 25 mM Tris in PBS-CM) and incubated for 20

min with quenching buffer. Cells were then rinsed twice with PBS-CM, scraped in cold PBS and pelleted at 2,000 rpm at 4 ^{0}C. The cells were lysed in lysis buffer (1.0% Triton X-100, 150 mM NaCl, 5 mM EDTA, 50 mM Tris) and incubated on ice for 60 min before centrifugation (10 min at 14,000 × g, 4 ^{0}C). Supernatants were transferred to new tubes and protein concentration was determined with Commassie® plus protein assay kit (Pierce). 750 µg of supernatant from each sample were incubated with 100 µl of 50 % slurry of streptavidin-agarose beads for 2 hours at 4 ^{0}C. Beads were pelleted by brief centrifugation and then were washed three times with HNTG (20 mM HEPES, pH 7.5, 150 mM NaCl, 0.1 % Triton X-100, 10 % glycerol). Biotinylated proteins were eluted by boiling in sample buffer supplemented with 5 % β-mercaptoethanol. Proteins were separated on 4-20 % SDS-PAGE and were transferred to Immobilon-P membranes (Millipore). Proteins were detected by Western blot with polyclonal antibodies against α, β and γ ENaC subunits. ENaC antibodies were generously provided by Dr. Cecilia Canessa. The signal was developed with Supersignal® west femto maximum sensitivity substrate (Pierce) and detected with X-Omat Blue XB-1 imaging film (Kodak). Signal intensities were quantified with scanning densitometry (Bio-Rad Lab).

2.1.5 Statistical Analysis

Data points represent the mean of n individual experiments +/- SEM. Statistical comparisons were performed with either unpaired t-Tests when comparing across experiments or paired t-Tests when comparing across conditions in the same cells. The $p < 0.05$ was considered significant. The p values are reported relative to 0.01 and 0.05 in the text and figure legends. Linear regressions were performed with Origin (Microcal). Non-linear curve fitting were performed with Matlab (Mathworks).

2.2 RESULTS

2.2.1 Effect of aprotinin on I_{Na}

Administration of 10 μM aprotinin to the apical side of the Ussing chamber resulted in a decrease of I_{sc}. Short circuit current traces of the effects of PBS and aprotinin on A6 cell sodium transport are shown in Figure 2-2. After a 25 to 30-min. equilibration period following initiation of transepithelial voltage-clamping, PBS or aprotinin was added to the apical side for 50 min. followed by 10 μM amiloride to obtain a measure of net electrogenic sodium transport mediated by the amiloride-sensitive sodium channel ENaC (I_{Na}). Application of amiloride inhibited 90% of the I_{SC} under these experimental conditions which is typical for A6 epithelial cells (81). Thus any change in the I_{SC} can be attributed to a change in I_{Na}. The I_{sc} taken after the equilibration period is referred to as the control I_{sc}. As can be seen, aprotinin caused a time-dependent decrease in the I_{SC} that was not observed in the PBS (vehicle control) treated cells. The decrease in I_{sc} caused by aprotinin was apparent following a variable short lag phase of ~ 30 s. In this subset of experiments, the PBS treated monolayers had a control I_{sc} of 8.4 +/- 1.36 μA/cm^2 (n = 12) that was not significantly changed (8.9 +/- 1.08 μA/cm^2, $p > 0.05$) 50 min. after addition of PBS but was reduced to 0.8 +/- 0.13 μA/cm^2 upon addition of 10 μM amiloride. In monolayers where 10 μM aprotinin was added to the apical side had control I_{sc} of 7.5 +/- 1.25 μA/cm^2 (n = 12) that was reduced to 2.2 +/- 0.55 μA/cm^2 ($p < 0.01$) 50 min. after addition of aprotinin and further reduced to 0.5 +/- 0.12 μA/cm^2 with the addition of 10 μM amiloride. Thus I_{Na} was reduced from 8.1 +/- 1.1 μA/cm^2 in the PBS treated cells to 1.7 +/- 0.53 μA/cm^2 in the aprotinin treated cells. These results are summarized in Figure 2-2 C.

The inhibition of I_{Na} by aprotinin was time-dependent. The decrease in I_{Na} as a percentage of control I_{Na} following addition of 10 μM aprotinin was fitted to an exponential decay

$$I_{Na}(t) = A \cdot \exp(-t/\tau) + B,$$

where A is the aprotinin sensitive current and B the aprotinin insensitive current; as illustrated in Figure 2-3 A. Using the period starting 5 min. and ending 45 min. after addition of aprotinin, τ was 18 +/- 1.2 min. Aprotinin (10 μM) inhibited 84 +/- 10.5% of the control I_{Na} in this subset of filters. The effect of aprotinin on I_{Na} was also concentration dependent (Figure 2-3 B). The half

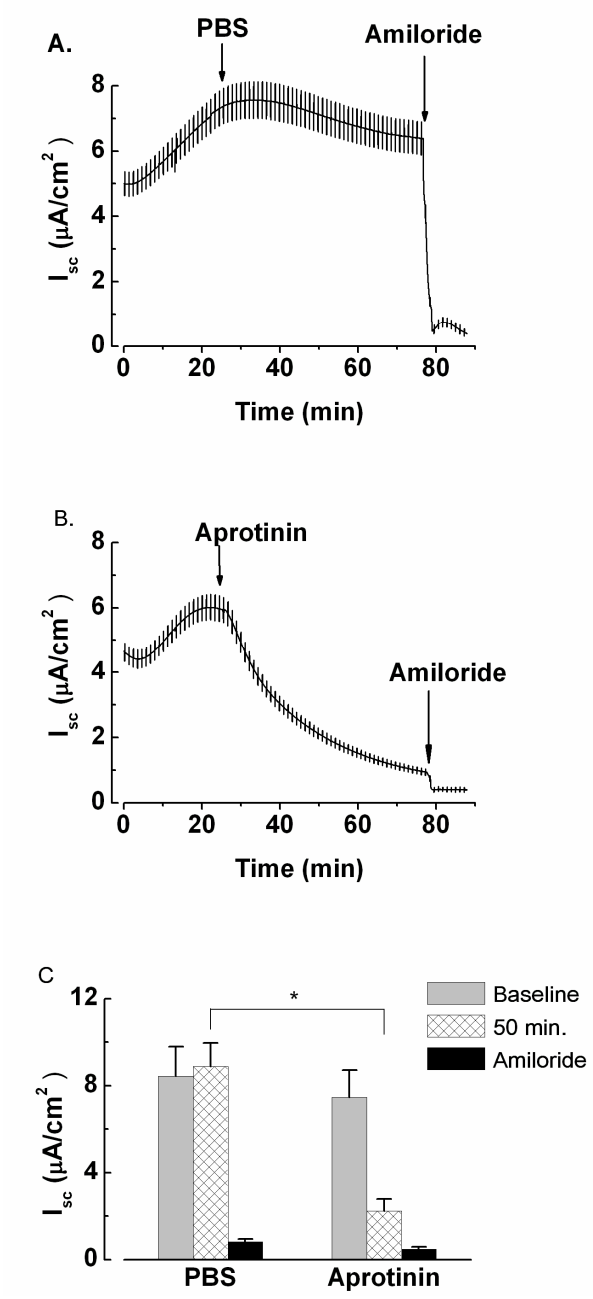

Figure 2-2 Aprotinin inhibition of I_{Na} in A6 cells

Effect of apically administered aprotinin on amiloride-sensitive I_{SC} in A6 cell monolayers. A6 cells in Ussing chambers with symmetrical bath solutions continuously gassed with air were voltage-clamped at 0 mV and I_{SC} monitored. After a 25-30 min. equilibration period (A) PBS or (B) aprotinin 10 μM was added to the apical bath. I_{SC} was monitored for 50 min. then 10 μM amiloride was added to the apical bath to determine I_{Na}. The current deflections are responses to 4 mV bipolar pulses used to measure transepithelial resistance (R_T). (C) The mean values of I_{SC} before (*shaded bar*), 50 min. after addition of PBS/aprotinin (*hatched bars*) and following addition of amiloride (*filled bars*) indicate substantial decrease of I_{SC} by aprotinin. The error bars are +/- SEM. Significant decrease was found in comparing I_{SC} values before and 50 min. following addition of aprotinin but not PBS with n = 12 and 14 filters for PBS and aprotinin experiments respectively (* $p < 0.01$).

maximal inhibition constant ($K_{1/2}$), determined by fitting the I_{Na} as a percentage of control I_{Na} versus aprotinin (Apr) concentration to a simple inhibition curve,

$$I_{Na}([Apr]) = \frac{A \cdot K_{1/2}}{K_{1/2} + [Apr]} + B,$$

was 1.0 +/- 0.13 μM with a maximal inhibition of 80 +/- 12 %. The concentration dependence suggests a high affinity inhibition of the majority of the I_{Na} by aprotinin. The transepithelial resistance (R_T) was maintained after addition of 10 μM aprotinin. The decrease in I_{Na} caused by aprotinin was accompanied by a tendency towards increasing R_T particularly in filters that had relatively high control I_{Na}. The R_T before addition of PBS and aprotinin was 5.15 +/- 0.46 and 4.90 +/- 0.57 kΩcm^2 respectively. Following the addition of PBS and aprotinin for 50 min. the R_T was 4.6 +/- 0.46 and 6.1 +/- 0.53 kΩcm^2 respectively, thus the integrity of the epithelial monolayer was not compromised by aprotinin incubation.

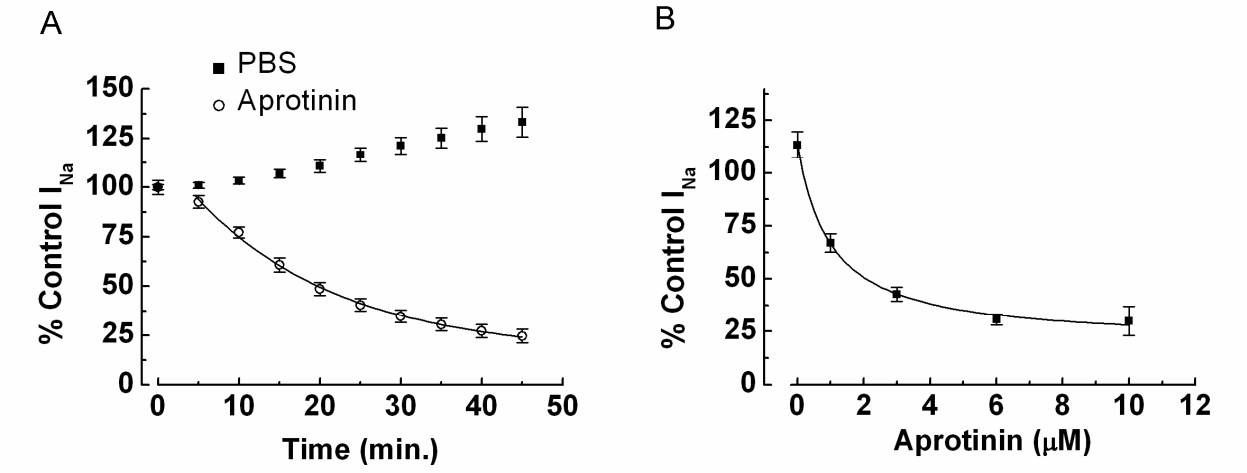

Figure 2-3 Time and concentration dependence of the aprotinin effect

(A) I_{Na} after apical administration of PBS (*filled squares*) or 10 μM aprotinin (*open circles*) was plotted as a percentage of I_{Na} before administration (control) using data recorded at 5 min. intervals. The data points plotted represent the mean values of 12 filters each for PBS and aprotinin addition with error bars corresponding to +/- SEM. A small time-dependent increase in I_{Na} could be seen with PBS addition but was not consistently observed in all the filters measured. The solid line through the aprotinin data points represents a fit to an exponential decay. The mean control I_{Na} for the set of 24 filters used in this experiment was 8.2 +/- 0.36 μA/cm^2. (B) The %control I_{Na} was measured at 50 min. after adding the indicated concentration 0, 1, 3, 6, 10 μM of aprotinin (*filled squares*) and demonstrated a concentration dependence to the aprotinin inhibition of I_{Na}. The solid line represents a fit to the inhibition curve. The mean control I_{Na} for the set of 25 filters used in this experiment was 4.1 +/- 0.30 μA/cm^2. Error bars are +/- SEM.

2.2.2 Effect of aprotinin on CDPC block of ENaC

The blockade of I_{Na} by CDPC for PBS and aprotinin treated A6 was first measured by a cumulative concentration response determination using a step protocol. PBS or 4 μM aprotinin was introduced to the apical side of the A6 filters for 30 min. before commencing the CDPC concentration step protocol, which was carried out over 30 min. The concentration of 4 μM aprotinin was used because this concentration was capable of significantly inhibiting I_{Na} but sufficient current remains at the higher CDPC blocker concentrations to ensure adequate measurement of the Lorentzian component in the PDS. As shown in Figure 2-4 A, PBS treated cells had significantly higher I_{Na} (6.1 +/- 0.40 $\mu A/cm^2$) compared to aprotinin treated cells (2.8 +/- 0.59 $\mu A/cm^2$, $p < 0.01$) at 0 μM CDPC and also at all other concentrations studied (10, 20, 30, 40 and 50 μM). CDPC caused a concentration dependent decrease in I_{Na} in both PBS and aprotinin treated A6 cells thus the sensitivity to blockade of I_{Na} by CDPC was maintained in the presence of aprotinin. The PDS in both PBS and aprotinin treated A6 had Lorentzian components that varied with CDPC concentration (Figure 2-4 A and B). As expected from a smaller I_{Na}, the Lorentzian S_o values were also significantly decreased in aprotinin treated cells ($p < 0.01$) at the blocker concentrations studied. The S_o values remained biphasic with respect to blocker concentration in both the PBS and aprotinin studies. The data was fitted to the equation describing the S_o of a two-state kinetic scheme and a biphasic curve was obtained. The S_o maxima were at 18.7 +/- 0.28 μM and 15.5 +/- 0.71 μM CDPC for PBS and aprotinin treated A6 respectively (Figure 2-4 B).

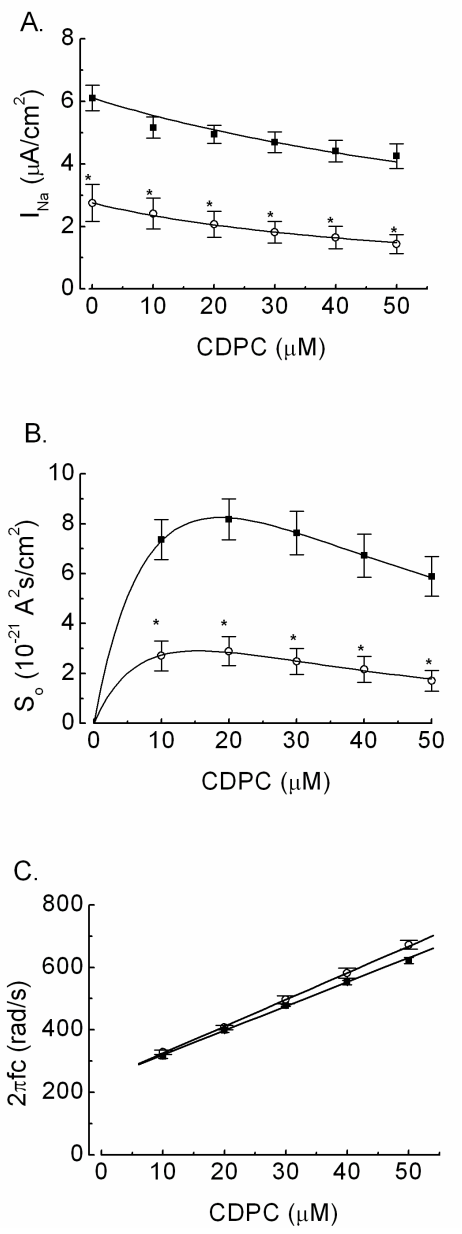

Figure 2-4 Aprotinin effect on blocker parameters

A6 cells in Ussing chambers were continuously voltage clamped at 0 mV and the I_{SC} monitored on a strip chart for 30 min. following addition of PBS (*filled squares*) or aprotinin 4 μM; (*open circles*). Cumulative step increases in the concentration of CDPC in the apical bath were carried out, the I_{SC} and power density spectra were obtained at each blocker concentration 10,20,30,40 and 50 μM. The values are given as the mean (n = 8 for PBS and n = 6 for aprotinin treated A6 filters) +/- SEM. (A) The I_{Na} following 30 min. of PBS addition was significantly higher than I_{Na} following aprotinin addition (*$p < 0.01$). In both conditions CDPC decreased the I_{Na} and the decrease could be explained by simple Michaelis-Menten inhibition kinetics (*solid lines*). (B) The S_o at increasing concentration of CDPC was biphasic and was fitted to a two-state channel blocking model (*solid lines*) in both cases. The difference in magnitude of S_o between PBS and aprotinin treated A6 cells was significant (*$p < 0.01$). (C) $2\pi f_c$ plots with linear regressions (*solid lines*) from which k_{on} and k_{off} were calculated were virtually identical for PBS and aprotinin treated cells.

The S_o values are the first indication that the blocker-ENaC interaction is not significantly affected by aprotinin[1]. The second indication came from measurement of the $2\pi f_c$ values at the CDPC concentrations used. For both PBS and aprotinin treated A6 cells, the $2\pi f_c$ increased linearly with respect to blocker concentration. A linear regression of the data demonstrated that the apparent rate coefficients were not different (Figure 2-4 C). The k_{off} and k_{on} were 242 +/- 5.40 s^{-1} and 7.8 +/- 0.19 $\mu M^{-1}s^{-1}$ for PBS experiments (n = 8). These constants were not significantly different in aprotinin experiments (n = 6) at 240 +/- 3.78 s^{-1} and 8.6 +/- 0.15 $\mu M^{-1}s^{-1}$ respectively ($p > 0.05$). The blocker dissociation constant K_d was 31.2 and 28.1 μM CDPC for PBS and aprotinin treated A6 cells respectively. The biphasic dependence of S_o on blocker concentration and the linear dependence of $2\pi f_c$ on blocker concentration, in PBS and aprotinin treated A6, is expected from a pseudo-first order blocker-ENaC reaction. Consequently, only two concentration points were required to determine the blocking kinetics as well as the single channel parameters as previously described (82). To avoid autoregulatory responses of I_{Na} to prolonged blocker-induced decreases in I_{Na} caused by cumulative increases in blocker concentration (1, 53, 183), a pulse-protocol approach was employed to measure the single channel properties.

---

[1] The S_0 values for the open to block transition can be expressed by rearranging equation (1) as $S_0 = \frac{4 \cdot I \cdot i \cdot k_{on} \cdot B}{(2\pi f_c)^2}$. Using $I = N \cdot i \cdot \frac{k_{off}}{k_{off} + k_{on} \cdot B}$ and $2\pi f_c = k_{off} + k_{on} \cdot B$, we obtained $S_0 = 4 \cdot N \cdot i^2 \cdot \frac{k_{off} \cdot k_{on} \cdot B}{(k_{off} + k_{on} \cdot B)^3}$. The S_0 values clearly depend on the blocker rate coefficients k_{on} and k_{off}. In addition, provided that i and N were constants with respect to B, the maximum value of S_0 occurs at the blocker concentration, $B_{Max} = 1/2 \cdot (koff / kon)$. The lack of a change in B_{Max} in the absence or presence of aprotinin argues that the ratio k_{off}/k_{on} and hence the dissociation constant of the blocker was unaltered.

2.2.3 Single Channel Properties: Pulse Protocol

To avoid blocker induced autoregulation of ENaC and to study the single channel properties of the same cells in control and aprotinin treated periods as well as measure reversibility of the aprotinin effect a pulse protocol approach was employed pulsing between 10 and 30 μM CDPC (82). Typical PDS in control and aprotinin treated periods at 10 and 30 μM CDPC are shown in Figure 2-5. The two CDPC concentrations were chosen because they were close to the S_o maxima as shown in the step protocol experiments (Figure 2-4), thus providing the highest signal for the Lorentzian component in the PDS while producing measurable changes in I_{Na} and significant changes in $2\pi f_c$. Secondarily, 10 and 30 μM CDPC could be used in both the control and aprotinin periods because the blocker kinetics were identical in the absence and presence of aprotinin. The I_{Na}, i_{Na}, P_o and N_o were measured before (control), while perfusing with aprotinin (aprotinin) and following removal of aprotinin from the apical side (washout) in 8 filters as illustrated in Figure 2-6. The I_{Na} was 3.4 +/- 0.17 μA/cm^2 under control conditions and was reduced to 1.4 +/- 0.17 μA/cm^2 35 min. after addition of 10 μM aprotinin ($p < 0.01$).

Following washout of aprotinin, I_{Na} recovered to control levels (3.2 +/- 0.11 μA/cm^2). The recovery appears to be complete by 10 min. after washout as subsequent time points did not show further increases in I_{Na}. The i_{Na} was 0.46 +/- 0.037 pA in the control period, increased to 0.70 +/- 0.069 pA ($p < 0.05$) 35 min. after addition of aprotinin and returned to 0.45 +/- 0.018 pA following removal of aprotinin. The P_o was 0.23 +/- 0.031 before aprotinin addition, approached a maximum of 0.41 +/- 0.075 ($p < 0.05$) 15 min. after aprotinin addition then returned to 0.23 +/- 0.019 after removal of aprotinin. The changes in N_o paralleled changes in I_{Na} with N_o of 8.03 +/- 0.812 before, 2.26 +/- 0.523 ($p < 0.01$) after aprotinin addition and 7.21 +/- 0.445 million channels /cm^2 following washout of aprotinin. Since changes in I_{Na} cannot be explained by changes in i_{Na} or P_o, these changes must result from changes in N_T as shown in Figure 2-7. N_T was 42 +/- 8.24 million channels /cm^2 before aprotinin addition. N_T was reduced to 8.93 +/- 3.35 million channels /cm^2 after addition of aprotinin and returned to 34.4 +/- 5.42 million channels /cm^2 following aprotinin washout.

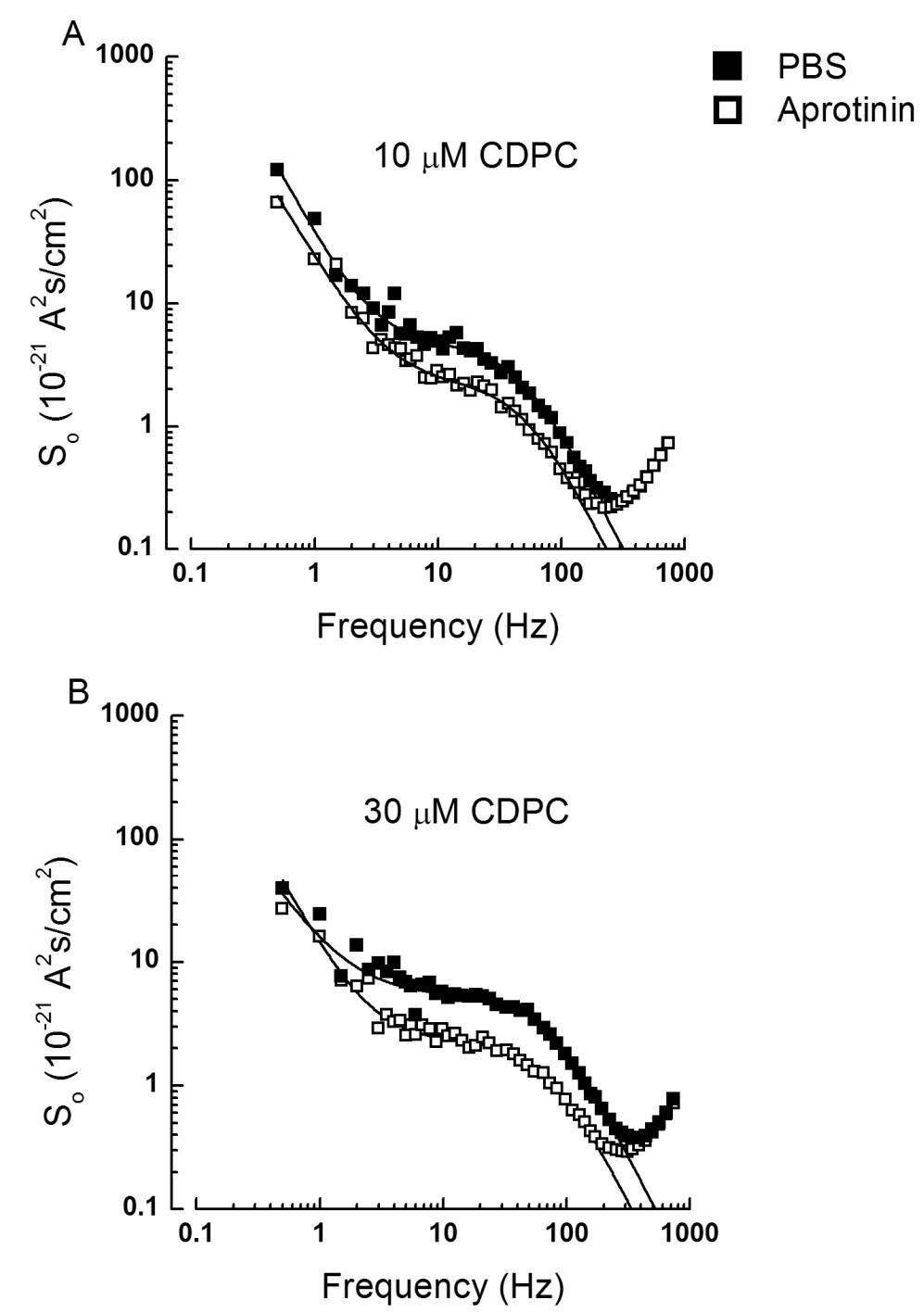

Figure 2-5 Representative current spectral densities

Typical current noise power spectral density in the absence (*solid squares*; 3.87 μA/cm^2 I_{Na}) and presence (*open squares*; 1.67 μA/cm^2 I_{Na}) of aprotinin are shown at 10 μM CDPC (A) and 30 μM CDPC (B). Corner frequencies were 47.6 and 50.2 Hz (A); and 72.4 and 72.7 Hz (B) in the absence and presence of aprotinin respectively. The solid lines represents the fit of the data to the sum of Lorentzian plus low frequency "1/f" noise.

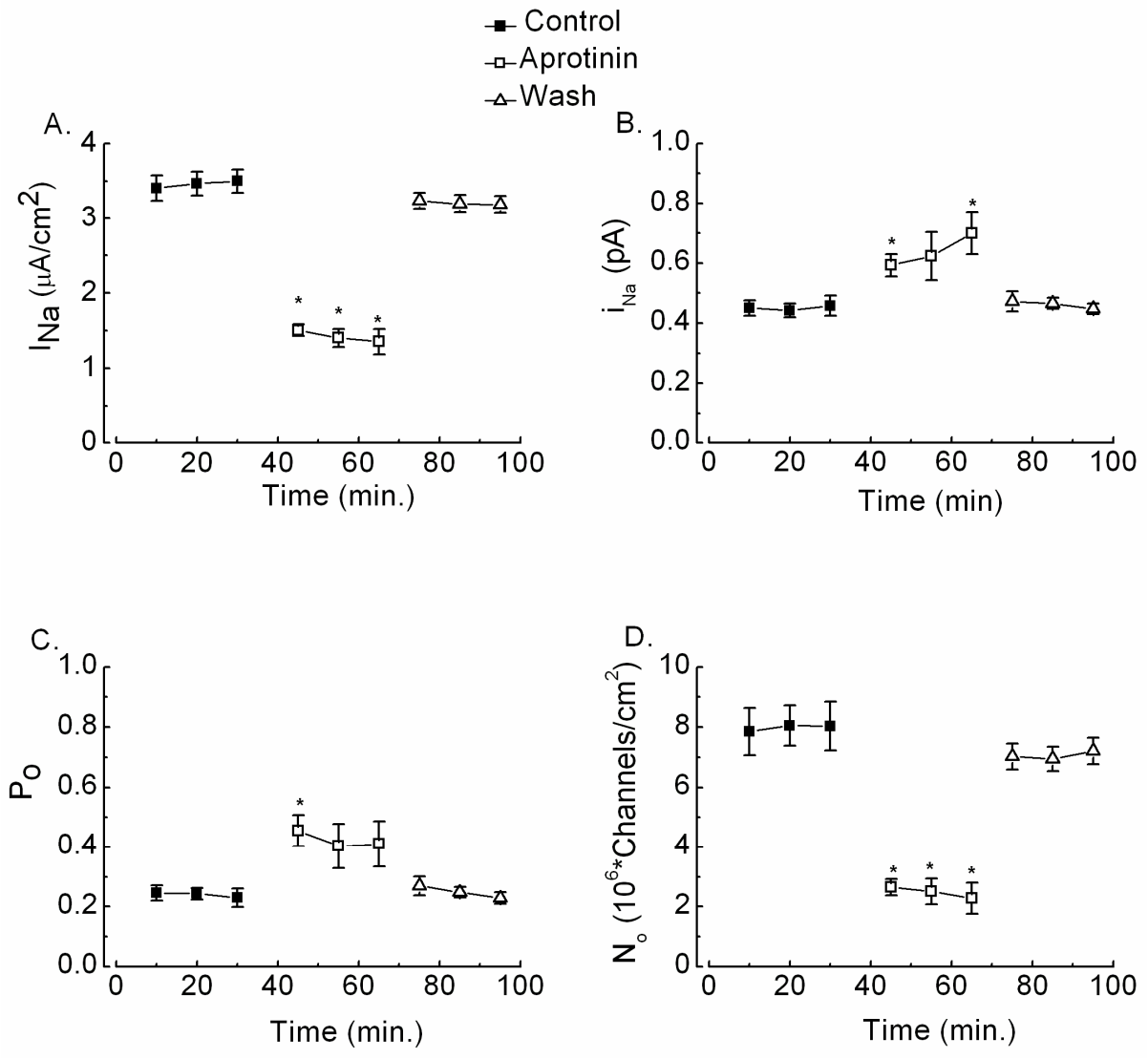

Figure 2-6 Changes in single channel parameters with aprotinin addition

(A) Summary of reduction in I_{Na} by aprotinin in the pulse protocol experiments. I_{Na} of cells continuously perfused with a ringer solution containing 10 μM CDPC was measured at 10 min. intervals prior to addition of aprotinin (*filled squares*), then the cells were perfused with 10 μM aprotinin and I_{Na} measured at the indicated times (*open squares*) after which aprotinin was washed out (*open triangles*). At 10 min. intervals, the CDPC concentration was pulsed to 30 μM and returned to 10 μM for analysis of blocker-induced fluctuations. (B) Summary of changes in i_{Na} following perfusion of aprotinin and washout. The increase in i_{Na} caused by aprotinin was significant (*$p < 0.01$) and reversible. (C) Summary of changes in P_o. The increase in P_o were significant (*$p < 0.01$) at 15 min. after perfusing with aprotinin and returned to the pre-aprotinin control values following washout of aprotinin. (D) Summary of changes in N_o following aprotinin perfusion showed a significant decrease in No (* $p < 0.01$) that was completely reversed upon removal of aprotinin. Values are reported as mean +/- SEM for n = 8.

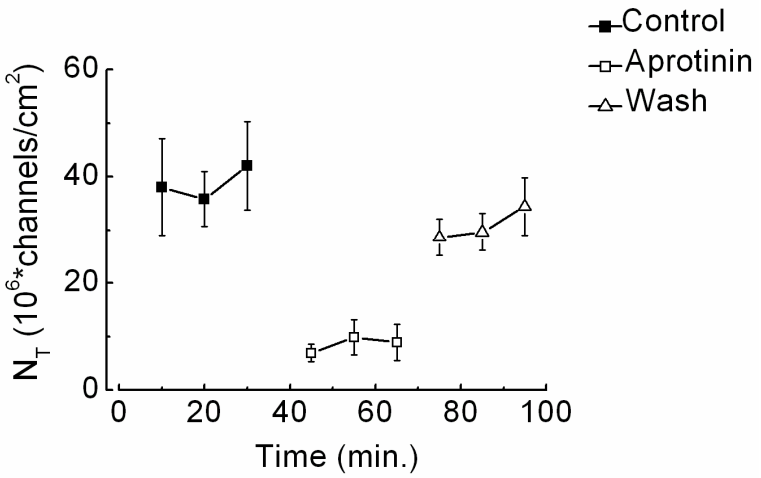

Figure 2-7 N_T calculated from P_o N_o and K_d

N_T calculated from the P_o and K_d decreased by ~ 80% following 35 min. of inhibition by aprotinin (*open squares*) compared to control conditions (*solid squares*). Inhibition of N_T was reversed following washout of aprotinin (*open triangles*) and returned to control values within 30 min. of washout.

2.2.4 Relationship between single channel properties and I_{Na}

To examine how the single channel properties change with I_{Na} we quantified their relationship to I_{Na} by linear regression analysis (Figure 2-8) using the experimental data set shown in Figure 2-6. Because of the apparent differences in the relationship of the single channel properties to I_{Na} in the control, aprotinin and washout conditions we determined the regressions using data points in each condition. The linear parameters are summarized in Table 2-1. The values of i_{Na} versus I_{Na} in the control and aprotinin treated conditions are plotted in Figure 2-8. Over the range of control I_{Na} (2.78 – 4.17 μA/cm^2) i_{Na} decreased with increases of I_{Na} (r = - 0.62). The i_{Na} also decreased with increases of I_{Na} (r = - 0.80) over the aprotinin I_{Na} range (0.87 – 2.08 μA/cm^2). However, the slope was ~ 3 fold steeper and the intercept ~ 50 % higher during the aprotinin treatment period compared to the control period. No correlation was observed between i_{Na} and I_{Na} during the wash condition (r = 0.02). Plotted also are the P_o values versus I_{Na} in the control and aprotinin treated conditions (Figure 2-8 B). The P_o also decreased

with increases of I_{Na} (r = - 0.46) in the control condition as well as in the presence of aprotinin (r = - 0.75). In the presence of aprotinin the slope was ~ 4 fold steeper and the intercept increased by ~ 100 %. No correlation was observed between P_o and I_{Na} in the wash condition (r = - 0.17). We also plotted the N_o versus I_{Na} in the control and aprotinin treated conditions (Figure 2-8 C). We found that N_o increased with increases of I_{Na} in the control condition (r = 0.86). This positive correlation remained in the aprotinin (r = 0.92) and wash conditions (r = 0.61) so that transport is determined primarily by changes of N_o in each condition studied.

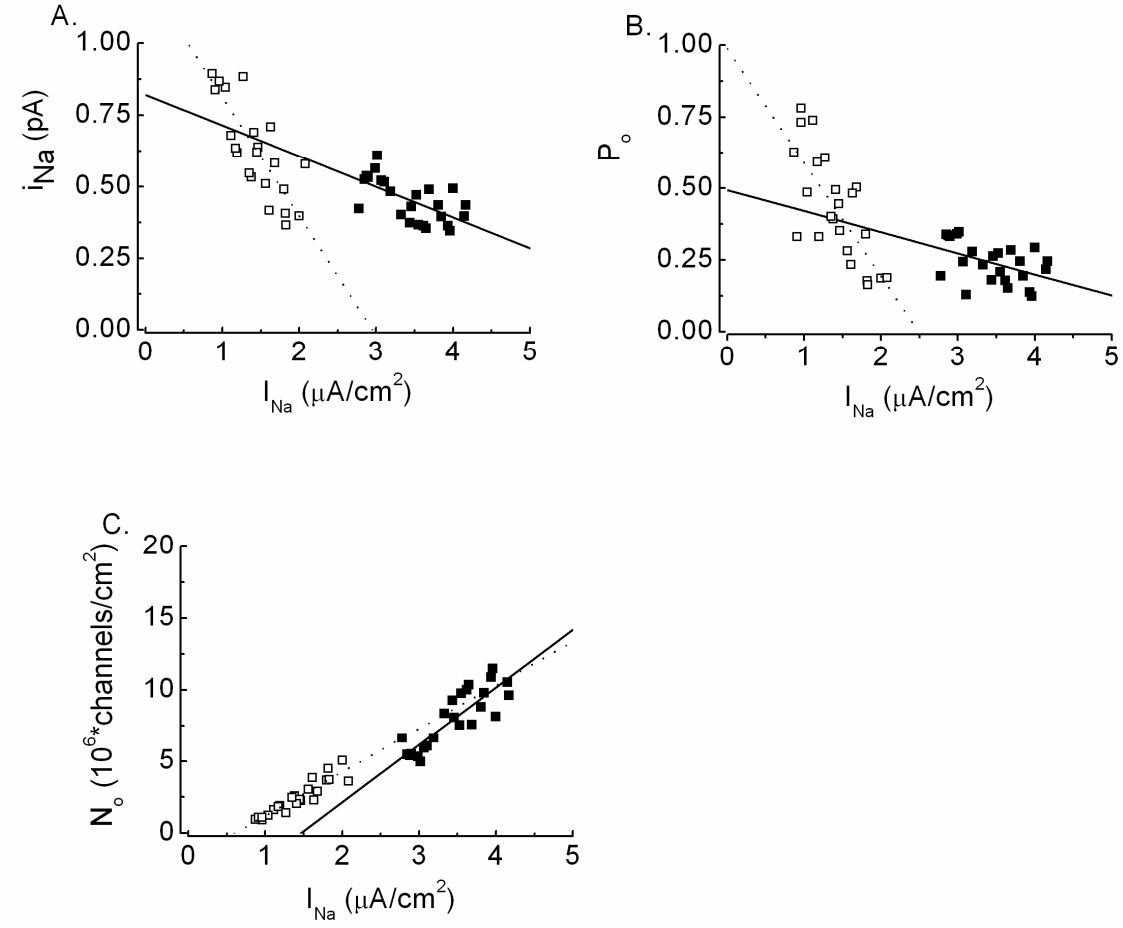

Figure 2-8 Relationship of Single Channel Parameters to I_{Na}

Individual values of (A) i_{Na}, (B) P_o and (C) N_o under control conditions (*filled squares*) and during aprotinin treatment (*open squares*) plotted against I_{Na}. The data points from the wash conditions have been omitted for clarity. The lines are linear regressions to the control period data (*solid line*) and aprotinin period data (*dotted line*). The regressions for all three periods are summarized in Table 2-1.

Table 2-1 Dependence of the Single Channel Properties on the ENaC-mediated Na+ current

"Intercept" and "Slope" are the linear parameters of the regression with regression coefficient r. Brackets indicate the lower and upper bounds of the 95 % confidence interval of the estimated linear parameters. The regressions are statistically significant ($p < 0.025$) except where stated otherwise. [a] $p > 0.05$

	r	Intercept	Slope
		i_{Na}	
		pA	pA/(μA/cm^2)
Control	-0.62	0.82 [0.61, 1.03]	- 0.11 [- 0.17, - 0.05]
Aprotinin	-0.80	1.23 [1.03, 1.43]	- 0.42 [-0.55, -0.28]
Wash	0.02[a]	0.45 [0.14, 0.75]	0.00 [-0.09, 0.10]
		P_o	
			(μA/cm^2)$^{-1}$
Control	-0.46	0.49 [0.27, 0.71]	- 0.07 [- 0.14, - 0.01]
Aprotinin	-0.75	0.99 [0.76, 1.22]	-0.40 [-0.55, -0.24]
Wash	-0.17[a]	0.35 [0.07, 0.66]	-0.04 [- 0.13, 0.06]
		N_o	
		10^6 Channels/cm^2	10^6 Channels/μA
Control	0.86	- 5.86 [- 9.56, - 2.17]	4.01 [2.95, 5.07]
Aprotinin	0.92	-1.84 [- 2.66, -1.03]	3.04 [2.49, 3.60]
Wash	0.61	-0.24 [-4.43, 3.96]	2.28 [0.973, 3.58]

2.2.5 Single channel conductance (γ_{Na}), basolateral resistance (R_b) and membrane Hyperpolarization

First, it is assumed that under a specific condition, such as in the control period, γ_{Na}, R_b and the transcellular Na^+ electromotive force, E_{Na}, are constants. E_{Na} measured in A6 cells in the same Ringer solution as used in the present studies averages 120 mV (81). Second, it is assumed that under a given condition, the sample to sample variation in I_{Na} results from variation in apical membrane expression and activity of ENaC. This assumption is based on the fact that I_{Na} strongly correlates with the apical conductance in examples of identically maintained A6 cells but no correlation was seen with the basolateral conductance (70). Third, the apical membrane conductance is predominantly mediated by ENaC (81). Under short-circuit conditions, the equivalent circuit (Figure 1-1 B) gives

$$I_{Na} = \frac{E_{Na}}{R_a + R_b}$$

R_a can be expressed in terms of I_{Na} as

$$R_a = \frac{E_a}{I_{Na}} - R_b$$

At the apical membrane

$$V_a - E_a = I_{Na} R_a$$

Since

$$i_{Na} = \gamma_{Na} \cdot (V_a - E_a),$$

$$i_{Na} = \gamma_{Na} E_{Na} - \gamma_{Na} R_b I_{Na} \qquad \textbf{2-19}$$

Therefore, for constant γ_{Na}, E_{Na} and R_b, i_{Na} decreases linearly with I_{Na}; with intercept $\gamma_{Na}E_{Na}$ and slope $\gamma_{Na}R_b$. The regression of i_{Na} versus I_{Na} (Figure 2-8, Table 2-1) can thus be used to estimate γ_{Na} and R_b. These values are 6.8 pS and 16 kΩcm^2. R_a, calculated as $1/(\gamma_{Na} \bullet N_o)$, is 19kΩ giving an $R_{cell} = R_a + R_b$ of 35 kΩ. The values of R_{cell} and R_b are close to previously reported values (81, 144). Assuming constant γ_{Na}, the R_a increased under aprotinin treated conditions to 74 kΩcm^2 with a parallel increase in R_b to 60 kΩcm^2. Based on the standard error on the slope and intercept and the error on the estimates of E_{Na} (144) a change of >20% in R_b is considered significant. This gives an average fractional apical resistance, fR_a, of ~ 0.55 in both

control and aprotinin treated tissues. Assuming E_a is constant, the apical membrane is hyperpolarized by $\Delta i_{Na}/\gamma_{Na}$ = 30 mV. Under short-circuit conditions $V_a = -V_b$, therefore the basolateral membrane is also hyperpolarized by 30 mV. This coupling of the apical membrane conductance to the basolateral membrane has been previously reported (42, 43, 144) and suggest that in some Na^+ transporting cells therefore, apical membrane Na^+ permeability changes alone may be inadequate to explain the Na^+ transport rate changes.

2.2.6 Cell surface expression of ENaC

The above results indicate aprotinin decreases the number of active channels in the apical membrane. To determine if this effect is also reflected in changes in ENaC apical membrane protein levels we performed cell surface protein biotinylation studies. We biotinylated apical membrane proteins of A6 cells grown on permeable supports (75mm diameter). Biotinylated proteins were recovered with streptavidin-agarose beads and we determined subunit density by Western blotting using specific antibodies to each of the ENaC subunits α, β, γ as described by Alvarez de la Rosa et al., (2002 and 2004), Gottardi et al., (1995), and Hanwell et al., (2002). Western blots were examined from A6 cells treated with PBS or 10 μM aprotinin for 1 hour, or cells treated with 100nM aldosterone for 6 hours. There were two immunoreactive bands for the α subunit at 85 and 65 Kd, two for the β subunit at 115 and 100 Kd while one predominant band at 90 Kd was observed for the γ subunit. As shown in Figure 2-9, quantification of the relative changes in apical membrane subunits indicated that aldosterone increased subunit density 2-4 fold as previously reported by Alvarez de la Rosa et al., (2002). In contrast aprotinin had no detectable effect on the cell surface density of any of the three ENaC subunits. The results summarized in Fig. 2-9 represent 3 independent experiments. Alvarez de la Rosa et al. (6) reported aldosterone increased cell surface expression of ENaC subunits proportional to an observed increase in I_{SC}. These results confirm that it is possible by biochemical methods to detect changes in N_T and thereby I_{Na} when A6 cells are stimulated with aldosterone. In contrast the large decreases in N_T in the presence of aprotinin did not correlate with a biochemically detectable decrease in cell surface subunit density.

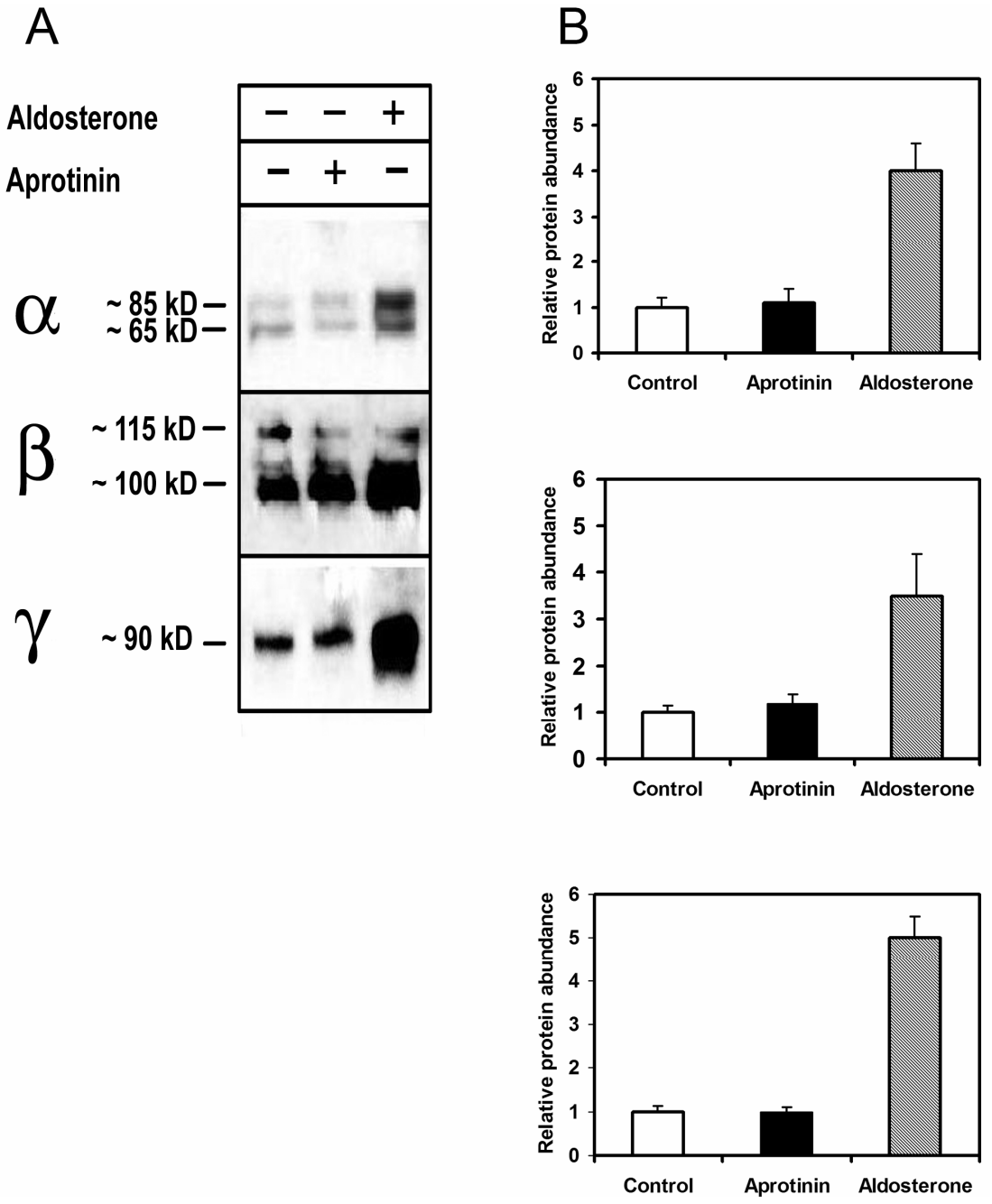

Figure 2-9 Cell surface abundance of ENaC subunits

The effect of aprotinin and aldosterone on the relative abundance of ENaC subunits in the apical membrane of A6 cells. A) A6 cells grown on permeable supports were treated either with PBS or 10 μM aprotinin for 1 hour or 100 nM aldosterone for 6 hours. Apical proteins were biotinylated and recovered with streptavidin-agarose beads. The recovered proteins were analyzed with antibodies against α, β and γ Xenopus ENaC subunits. Representative Western blots are shown with the arrows indicating the migration of molecular mass standards. B) Mean of relative changes in apical membrane abundance measured by scanning densitometry and normalized to the control density. The bars represent three independent experiments with error bars corresponding to ± SEM.

2.3 DISCUSSION

Aprotinin is a 6.5 kD protein that is a potent and reversible Kunitz type inhibitor of several serine proteases including trypsin, plasmin and kallikreins (198). The inhibition of Na^+ transport by apical administration of aprotinin has been reported in toad urinary bladder (137), the A6 cell line (191), the mouse cortical collecting duct cell mpkCCD14 cell line (116), human bronchial epithelial cells (25, 49) and rat and mouse lung alveolar epithelial cells (147). In all cases aprotinin inhibition of I_{Na} was much slower than the effect caused by the ENaC blocker amiloride. Inhibition of I_{Na} by aprotinin was evident within 10 min. of addition and approached a non-zero nadir with time. The inhibition was characterized by a time constant of ~18 min. The plateau level of inhibition was concentration dependent with high affinity and a maximum inhibition of 70 to 80%. The micromolar affinity reported here is consistent with measurements carried out on the urinary toad bladder (Orce et al., 1980). The concentration dependence and time course suggests aprotinin inhibits a specific protease dependent pathway that regulates a large fraction of the epithelial Na^+ transport. The identity of this regulatory protease(s) is a matter of some conjecture.

Kallikrein-like protease activity has been identified at the apical surface and in the apical medium of A6 cells forming a tight monolayer as well as from toad urinary bladder (95). The kallikrein-like protease activity was inhibited by aprotinin at a concentration that inhibited Na+ transport in A6 cells and toad bladder (118). Further, exogenous addition of trypsin and chymotrypsin have been shown to activate I_{Na} in epithelia pretreated with protease inhibitors and activate Na^+ mediated currents in *Xenopus* oocytes expressing ENaC (25, 49, 116, 191). Vallet et al., (1997), using expression cloning methods, identified a channel activating protease (CAP) from A6 cells that increased ENaC-mediated I_{Na} in *Xenopus* oocytes. The mammalian homologue of xCAP1 is prostasin/hCAP1 and coexpression of prostasin with ENaC also increases Na^+ mediated currents (3, 201). Similar to the secretion of kallikrein-like proteases by amphibian renal cells, prostasin has been found to be secreted in an aldosterone regulated manner in rat urine (133). Bikunin, a Kunitz type serine protease inhibitor with two Kunitz domains, has a submicromolar potency for inhibiting Na^+ transport in human bronchial epithelia

(25) and this correlates with the nanomolar inhibition constant reported for aprotinin inhibition of prostasin enzymatic activity (167). These findings support the idea that prostasin and CAP1 are endogenous proteases that can regulate epithelial Na^+ transport. Consistent with this view is that RNA silencing of CAP1 was sufficient to inhibit I_{Na} in the CF15 airway epithelial cell line to the extent observed with aprotinin on A6 and HBE cells (188). Expression cloning has identified two other such CAPs in mammalian renal cells that are capable of stimulating current in *Xenopus* oocytes co-expressing ENaC in an aprotinin sensitive manner (200). Another possible protease that may regulate Na^+ transport is the ubiquitous convertase furin, which modulated ENaC-mediated currents in the Chinese hamster ovary expression system (86). However furin is not inhibited by aprotinin; consequently, the aprotinin inhibition of I_{Na} cannot be attributed to a furin pathway of channel activation in A6 cells and human bronchial epithelia. The relative importance of the individual proteases and the mechanism of their action in regulating Na^+ transport are yet to be determined. The studies reported here were designed to investigate the mechanism of action of aprotinin inhibition of epithelial Na^+ transport and thereby how aprotinin sensitive proteases regulate Na^+ transport.

2.3.1 Single channel properties

Using noise analysis we studied the apical Na^+ channels in the presence and absence of aprotinin and found that the decrease in I_{Na} caused by aprotinin can be explained by a decrease in the number of open channels (N_o) and these effects of aprotinin were fully reversible upon aprotinin wash out. In contrast, aprotinin caused both i_{Na} and P_o to increase and thus these changes cannot account for the decrease in I_{Na}. The i_{Na} averaged 0.45 pA under control conditions in the present study, which is similar to previously reported values in short-circuited A6 cells by noise analysis (7, 82). Given the i_{Na} of 0.45 pA under control conditions and a single channel conductance of 4-6 pS for the highly selective Na^+ channel in A6 cells (140, 151), a driving force of ~ 90 mV can be estimated for apical Na^+ entry. A 90 mV effective electromotive force for Na^+ movement across the apical membrane has been reported in A6 cell monolayers with resistances and I_{Na} in the range that we have measured (70). The average i_{Na} presented here is therefore consistent with the characteristic driving forces across the apical membrane of A6 cell monolayers and the conductance of sodium channels. Application of aprotinin to the apical bath caused a significant

increase in i_{Na}. Therefore, the inhibition of I_{Na} by aprotinin cannot be explained by changes in i_{Na}. By definition, $N_o = N_T * P_o$ where N_T is the number of electrically detectable or active channels gating between the open and closed states. A decrease in N_o may arise from a decrease in N_T or a decrease in P_o of the active channels. The P_o of active channels at the apical membrane was measured and in the control condition averaged 0.2. This value of P_o is well within the range that has been measured by noise analysis and patch clamping for ENaC (80). With application of aprotinin the P_o doubled. The increase in P_o would be expected to increase N_o; however, aprotinin causes a reduction in N_o. Therefore, aprotinin inhibition of I_{Na} is explained by a decrease in N_T (Figure 2-7). The timing of the reciprocal changes in i_{Na} and P_o were not explicitly measured but it can be inferred that the time course for the changes in i_{Na} and P_o are similar to the time course for aprotinin inhibition of I_{Na}. If the effects on P_o, i_{Na} or both occurred rapidly, a substantial initial rise, with a theoretical maximum of three-times the I_{Na}, would have been observed in the I_{SC} traces. Aprotinin caused P_o to increase two-fold and i_{Na} to increase from 0.45 pA to 0.69 pA. Because $I_{Na} = i \bullet P_o \bullet N_T$, I_{Na} should have increased three fold if N_T remained constant in the presence of aprotinin. An increase in the I_{SC} was never observed with the addition of aprotinin. Alternatively, if the effects on P_o and i_{Na} occurred later than the effect on inhibiting I_{Na}, then the I_{SC} would pass through a nadir before rising back to the final plateau value, and this was also not observed. Such biphasic effects resulting from rapid changes in P_o and slower effects on N_o have been reported for inhibition of I_{Na} by inhibitors of phosphatidylinositol 3-kinase (144) but were absent in the present studies. We are led to surmise that changes in i_{Na}, P_o and N_o occur concurrently with changes in I_{Na}.

To further elucidate the relationship between I_{Na} and the single channel properties we examined the individual data points from our pulse-protocol experiments. Considering the control conditions, we found a weak negative correlation between i_{Na} and I_{Na}. A negative correlation is expected because increased Na^+ transport rates depolarize the cells reducing the electromotive force across the Na^+ channels (20, 71). The strength of the correlation is expected to be weak because the driving force across the apical membrane is variable due in part to a high variation in the basolateral resistance from one monolayer to another (70). Following apical administration of aprotinin, the negative correlation between i_{Na} and I_{Na} became stronger. Such a correlation cannot explain the decrease in I_{Na}. It however suggests that the effect on i_{Na} is not simply due to the presence of aprotinin but follows the amount of inhibition of I_{Na} caused by the

presence of aprotinin. It was found that a negative correlation occurs between the ratio $I_{Na}^{control}/I_{Na}^{aprotinin}$ and $i_{Na}^{control}/i_{Na}^{aprotinin}$ (data not shown) thereby confirming that inhibition of I_{Na} by aprotinin produces the steep inverse relationship seen in the presence of aprotinin. In a similar manner, the P_o from cells under control conditions showed significant variation but a weak negative correlation was evident. This increasing P_o with decreasing I_{Na} may be related to a previously reported hyperpolarization induced increase in ENaC P_o (141, 142). As observed in the case of i_{Na}, with aprotinin treatment the negative correlation between P_o and I_{Na} was intensified supporting the notion that the P_o changes accompanies the decreasing I_{Na} and is not simply due to the presence of aprotinin. For N_o, we found a strong positive correlation with I_{Na} both in the control condition and the in the presence of aprotinin. Since the apical conductance has been shown to be strongly positively correlated with I_{Na} in A6 cells (70, 81) and the apical conductance is in large part given by the product of N_o and the single channel conductance, it is expected that under control conditions N_o would have a positive correlation with I_{Na}. This correlation persists following treatment with aprotinin. The decrease in I_{Na} following aprotinin treatment is only explained by a decrease in N_o that results from a decrease in N_T.

2.3.2 Mechanism of Apical-Basolateral Cross-talk

It was shown that as the apical membrane conductance is decreased by aprotinin, there is also a decrease in the basolateral membrane conductance. The data were consistent with previous results showing that increasing the apical resistance also increased the basolateral resistance. Although an effect of aprotinin on the basolateral resistance cannot be completely ruled out, many observations suggest a cross talk exists at least in the apical to basal direction. First, amiloride dependent increase in the apical resistance results in simultaneous increases in the basolateral resistance from microelectrode studies of the toad bladder (42, 134). In both cases, there was remarkably constant fR_a despite significant inhibition of the apical membrane. The increase in basolateral resistance can be explained to a large degree by inhibited K^+ conductance of the basolateral membrane following amiloride inhibition of the apical membrane (43). Although the aprotinin results are consistent with the previous reports there is a significant difference between the time scales (tens of minutes versus seconds) of the aprotinin experiments

(this dissertation) and the amiloride experiments (42) so that different mechanisms may be in effect.

Assuming similar mechanisms are in effect, what connects the apical membrane to the basolateral membrane? There may be a direct electrical coupling if the basolateral membrane conductance is voltage sensitive. There is an implicit voltage dependence if the basolateral membrane K^+ conductance follows Goldman-Hodgkin-Katz (GHK). However the voltage dependence due to GHK cannot explain 3 fold increases in R_b. A voltage dependence of basolateral membrane K^+ channel kinetics cannot be ruled out to explain the cross talk. On the other hand changes in intracellular ions may be responsible for the cross talk. It is known that the basolateral membrane of A6 cells have Na/Ca exhange that has a role in intracellular Ca^{2+} homeostasis (26). Further, the intracellular Ca^{2+} concentration is raised/lowered by increasing/decreasing apical Na^+ presumably mediated by changes in intracellular Na^+ (24). Intracellular Ca^{2+} increases can stimulate basolateral K^+ channels (34, 41, 47, 135). An hypothesis that explains the coupling is that changes in intracellular Na^+ caused by inhibiting ENaC may result in decreased intracellular Na^+, increased Ca^{2+} efflux at the basolateral membrane mediated by the Na/Ca exchanger and decreased basolateral Ca^{2+} resulting in inhibition of basolateral K^+ channels. Other possibilities involve sensitivity of both the apical Na^+ conductance and the basolateral K^+ conductance to changes in intracellular pH (77). Also, sensitivity of basolateral potassium channels to intracellular Na^+ has been observed in the thick-ascending limb of the renal nephron (143) so that Na^+ influx could directly regulate basolateral K^+ conductance.

2.3.3 Mechanism of aprotinin inhibition of N_T

Out of several possible explanations for the decrease in N_T, caused by aprotinin an intriguing explanation is that at the apical membrane there is a turnover of active channels into inactive channels in the presence of aprotinin. The inactive channels can be considered to be “capped” while the active channels are “uncapped”. Because multiple proteases have been shown to increase ENaC activity in a variety of systems in a manner dependent on their proteolytic activity, it is possible that ENaC is the substrate for proteolytic uncapping. Alternatively, ENaC uncapping may occur through proteolysis of a closely associated ENaC regulatory protein,

proteolytic generation of a stimulatory ligand, protein-protein interactions of ENaC extracellular domain and the protease or through generation of intracellular 2nd messengers. Activation of the trypsin receptor, *protease activated receptor* 2 (PAR2) does not stimulate ENaC (41) and ENaC activation is independent of PAR2 (37). Furthermore, ENaC activation by serine proteases is independent of G protein coupled receptors in oocytes (37) and fibroblasts (29), yet to date all known PARs are G-protein coupled receptors. There is no finding to support an intracellular 2nd messenger requirement for the protease mediated uncapping of ENaC. Protein-protein interactions in the extracytoplasmic domain between the protease dipeptidyl aminopeptidase-like protein, DPPX, and neuronal A-Type K^+ channels has been implicated in the redistribution of the neuronal channels from the ER to the plasma membrane as well as in the regulation of channel gating (129). The function of DPPX is not associated with proteolytic activity; however it remains to be determined that the protease-like domain is required for DPPX channel regulating activity. It is difficult to imagine that apically administered aprotinin is rapidly trafficked to the ER were it disrupts a possible DPPX-like interaction of ENaC with a serine protease or that once disrupted reconstitution and trafficking occur on the time scale observed with exogenous protease re-activation of aprotinin inhibited I_{Na} in epithelia cells. Trafficking from a compartment closer to the apical membrane or direct activation by the protein-protein interaction may cause the uncapping event. If aprotinin inhibits a protease dependent trafficking of ENaC to the apical membrane from intracellular pools, then the physical channel density is expected to decrease. The quantitation of apical membrane ENaC subunits by cell surface biotinylation however shows that the steady-state density of α, β and γ subunits were unchanged in the presence of aprotinin. Thus it appears unlikely that aprotinin mediates ENaC trafficking to alter steady-state sodium current in A6 cells. Recent investigations suggest that the biochemically detected apical membrane protein subunit density may be 1-2 orders of magnitude greater than electrically detectable channels (7). Although the aldosterone mediated changes in subunit density and I_{SC} were both observed a similar correlation could not be observed for the aprotinin mediated changes in I_{Na}. These results may mean aprotinin does not alter cell surface expression of ENaC subunit or that any changes are beyond the resolution of present biochemical methods. The high level of subunit protein at the apical surface would also impair the detection of proteolytically cleaved ENaC subunits.

There is however some evidence to support the idea that uncapping may occur through proteolysis of ENaC. A low apparent molecular weight form of the γ subunit immunoreactive band on Western blots was induced by aldosterone (123). The new size was consistent with excision of an amino terminal region immediately after the first transmembrane domain. Aldosterone up-regulation of CAP1 (133) and subsequent ENaC cleavage may explain the observations by Masilamani et al. (123). Molecular weight reductions attributable to proteolytic cleavages in α and γ subunits in MDCK cells expressing ENaC was recently reported and found critical for channel activity (86, 88). In A6 cells, a fast and slow migrating α ENaC immunoreactive band has been reported with the fast form seen primarily at the apical membrane (6). However, this fast migrating band form appears to result from the formation of stable disulfide bonds following maturation. Although extensive processing of ENaC resulting in the change of the apparent molecular weight of its subunits have been observed, the data remains inconclusive as to whether ENaC is proteolytically cleaved in A6 cells and whether the cleavage results in the phenomenon we term uncapping. Independent of the mechanism, protease mediated uncapping was apparently irreversible in oocyte studies suggesting that channels cannot be recapped (37).

A simple hypothesis that explains aprotinin inhibition of I_{Na} is that endocytosis of uncapped channels (i.e., active channels) is responsible for the loss of current in the presence of aprotinin as aprotinin prevents the uncapping of capped channels (i.e., inactive channels) newly inserted into the apical membrane. The half-life (11-17 min) measured for the α, β and γ ENaC subunits in the A6 apical membrane (6) is in good agreement with the time constant (18 min) for the decay in I_{Na} following administration of aprotinin. Taking changes in I_{Na} as a measure of the changes in $N_{T,}$ the decrease is consistent with the retrieval of active channels from the apical membrane. This implies that aprotinin prevents a constitutive replacement of active channels while retrieval of already activated channels continues leading to an apparent turnover of uncapped channels into capped channels. If this notion is correct aprotinin should not cause a change in cell surface protein subunit density, an expectation consistent with the biotinylation studies shown in Figure 2-9. However, much higher half-life values have been reported for ENaC subunits (>24 Hrs for α and γ, 6 Hrs for β) in the apical membrane of A6 cells (104, 204). The discrepancies in the measurements of ENaC subunit half-lifes at the apical membrane are yet to be resolved. Since subunit half-life measurements do not necessarily correlate with the actual

half-life of an active channel, we emphasize that the remarkable agreement of the estimate of the time constant for the inhibition of I_{Na} by aprotinin with the biochemical half-life observed by Alvarez de la Rosa et al., 2002 provides a working hypothesis whereby we can test the requirement of trafficking in the regulation of ENaC by endogenous proteases.

A protease mediated uncapping that increases the N_T is at odds with recent findings that trypsin stimulates increases in "NP_o" which is equivalent to N_o (29). However, the increase in NP_o was only demonstrated for channels with very low NP_o resulting in 10 – 100 fold increases of NP_o. Inhibition by aprotinin did not reveal the presence of these 100 fold lower P_o "near-silent" channels. If these very low P_o channels were present in the absence or in the presence of aprotinin they probably contribute a very small fraction to the total I_{Na}. If the near silent channels are present, they do not explain the aprotinin insensitive current and would not be detected in the presence of high P_o channels remaining in the membrane. From the perspective of transepithelial blocker-induced fluctuation analysis, the "near-silent channels if present are virtually inactive. Consequently, the reduction of N_T measured here is not inconsistent with a turnover of channels with high P_o to near-silent channels in the presence of aprotinin. However, our results suggest that the higher P_o channels observed in the presence of aprotinin results either from functional heterogeneity of the Na^+ channels in the apical membrane or from compensatory increases in the P_o of active channels remaining in the membrane.

2.3.4 Effect of channel heterogeneity on measured P_o and N_T

If it is presumed that aprotinin's effect is mediated by CAP1 and that CAP1 may be mimicked by exogenous trypsin, the effect on N_T measured here is at odds with reported instances of CAP1 and trypsin increasing the P_o of ENaC (29, 191). In one instance, the P_o was calculated by estimating the number of open channels via dividing the whole cell current by the single channel current and then dividing this estimate by the estimated number of channels obtained from subunit labeling. This approach invariably gives in absolute terms very low P_o values of 0.004 to 0.014 (58). CAP activation of current would imply that the P_o increases, at the most, to just 0.04 to 0.14 (200). Measurements of ENaC P_o by single channel analysis with and without CAP activation averaged 0.4 despite three-fold increases in I_{Na} (3). In the second instance, single channel measurements show that trypsin increased the P_o from very low values of 0.02 to ~ 0.6

(29). A possible explanation for the discrepancies is that CAP1/trypsin activates low P_o channels but has no effect on high P_o channels. This will result in measurement of changes in N_T if a population of high P_o channels persists after conversion of some channels to the low P_o form when aprotinin is present.

In the experiments we have assumed a homogenous channel population with identical P_o. Next we consider the effects on the calculated P_o and N_T from noise analysis if the channels form a heterogeneous population. For simplicity, it is assumed that channels can be found at either a fixed high P_o ($P_o^H = 0.5$) or a variable P_o (P_o^V). The fraction of channels with P_o^V is F. The blocker dependence of I_{Na} is then given by:

$$I_{Na}(B) = i_{Na} \cdot N_T \cdot K_d \cdot \left(\frac{(1-F)}{\frac{K_d}{P_0^H} + B} + \frac{F}{\frac{K_d}{P_0^V} + B} \right)$$

2-20

where B is the blocker concentration and K_d the dissociation constant from the $2\pi f_c$ versus concentration plot. The values of I_{Na} from equation 2-20 are determined for a range of F and P_o^V and at the blocker (CDPC) concentrations (10 and 30 μM). Using these values, we plot the P_o calculated from equation 2-17 and N_T (normalized) from equation 2-18 for some values of P_o^V and F (Figure 2-10).

To illustrate the effect of channel heterogeneity on the open probability derived from noise analysis we consider examples, from the literature, of patch clamp analysis of ENaC showing measurements of high P_o channels and low P_o channels but no intermediate P_o channels were observed. The first example comes from measurement of the effect of aldosterone on the single channel properties of ENaC in A6 epithelial cells. Here withdrawal of aldosterone resulted in a time-dependent decrease in I_{Na}; however, the measured P_o did not decrease gradually but rather abruptly and did not track exactly with t decrease in I_{Na}. A decrease in P_o (from 0.3 to 0.04) was not observed until I_{Na} was reduced by 70% (100). Afterwards, no further decreases in P_o were measured despite continued decreases in I_{Na}. From these results it is possible that the change in P_o resulted not from gradual changes affecting all the channels simultaneously but instead from inter-conversion between high P_o and low P_o channels. The values $P_o^H = 0.3$ and $P_o^V = 0.04$ were chosen to determine the effect on measured P_o as F increases as shown in (Figure 2-10 A). It is observed that measured P_o was a maximum (0.3) for

F = 0 and a minium (0.04) for F = 1. Between these extremes, only small decreases in measured P_o can be observed until a large fraction of channels have been converted. For instance, only a 13% decrease in P_o is measured for a 50% conversion and a 50% decrease in P_o requires a 85% conversion of high P_o to low P_o channels. This possibility may also partly explain apparent differences observed between single channel and noise analysis measurements of the effect of aldosterone on P_o and N_T in A6 cells. Single channel studies indicate that aldosterone dramatically increases the P_o (100) in A6 cells whereas noise analysis indicates in increase in N_T (82).

The second example is from protease treatment of membrane patches form fibroblasts expressing ENaC. The protease treatment led to an increase in single channel P_o from 0.02 to 0.57 (29). Yet, protease treatment did not yield such vast increases in whole cell I_{Na} suggesting that a fraction of channel had the low P_o which could be increased by trypsin whereas others had relatively high P_o (Dr. Caldwell, Seminar 2005). Using a $P_o^H = 0.5$ and $P_o^v = 0.02$, a plot of measured P_o versus F (Figure 2-10) shows an even greater tendency of the measured P_o to remain unchanged despite significant increases in F. For example, a 50% decrease in P_o is measured only when F is greater than 95%. For such a case, noise analysis primarily attributes the changes in I_{Na} to changes in N_T. This possibility may partly explain apparent differences observed between single channel and noise analysis measurements of the effect of aldosterone and aprotinin on P_o and N_T in A6 cells. Single channel studies had previously indicated that aldosterone dramatically increases the P_o in A6 cells (100) whereas noise analysis previously indicated an increase in N_T (82).

Next we examine the effect of changing P_o^V on the measured P_o when F is held constant. As shown in Figure 2-10 B, if F is 0.9, then as P_o^V decreases, the measured P_o also decreases until a minima is reached at $P_o^V = 0.1$. Then further decreases in P_o^V results in increasing the measured P_o towards 0.5. This implies that there is a range of P_o^V for which noise analysis can measure decreases in P_o. For instance decrease of measured P_o to 0.25 implies a decrease of P_o^V to 0.2. For this range only small changes in N_T are measured (1 to 0.9). However, for further decreases in P_o^V, measured P_o is expected to increase and significant decreases in N_T can be observed. For example, when P_o^V drops to 0.02, the measured P_o is 0.33 and N_T drops to 0.25. In other words, if the conversion of a large fraction of channels occurs from P_o of 0.5 to 0.2 a decrease in measured P_o is expected from noise analysis; however, if the decrease is to a much

smaller value (e.g 0.02) a change in N_T is to be expected. A plot of the effect of changing both P_o^V and F on measured P_o and N_T is shown respectively in Figure 2-10A and B. It shows that when F is 1 the measured P_o changes linearly with P_o^V and the measured N_T is constant. As F gets smaller, P_o varies in a biphasic manner with P_o^V starting with an initial decrease (from P_o^V = 0), a minimum and an increase. N_T is no longer perfectly constant but rolls off to value of 1 – F as P_o^V gets smaller. It can be observed that if aprotinin addition caused a shift in the open probability of 90 % of the channels (F = 0.9) from a starting value 0.5 with the rest of the channels having $P_o^H = 0.5$, a decrease in P_o will be calculated if the drop is not too extreme. For extreme decreases, or for changes in a smaller fraction of channels (F = 0.5) minimal shifts in calculated P_o will occur. However, a change in the P_o^V of a small fraction of channels will only cause a significant effect on current if that change is extreme.

From the preceeding discussion our results are not consistent with a uniform decrease in P_o of all the channels. Our results are also not consistent with an intermediate decrease of the P_o of a significant fraction of the channels (which will result in measured decrease of the P_o). But our results are consistent with a partitioning of a fraction of channels from high P_o to very low P_o; or with a decrease in N_T, which is essentially partitioning of a fraction of the channels from high P_o to a P_o of zero. In either the case of protease regulation or aldosterone regulation, some functional heterogeneity is suggested by the different measurements obtained from noise analysis and single channel patches.

The difference in the current measured at the two blocker concentrations is critical for noise analysis. This difference becomes very small proportionally to the zero blocker current as P_o decreases. A P_o of 0.02 will result in a 1% difference in measured current between 10 and 30 μM CDPC. As moment to moment variation of 1% is evident in the short-circuit current records, such a small difference is not useful for calculating the P_o. Measuring such low P_o will require the use of an extended blocker concentration difference that still permits accurate determination of the Lorentzian in the power density spectra. Blockers may have to be optimized specifically for this purpose.

In conclusion, our data suggests that there is an aprotinin sensitive protease in the apical membrane that serves to uncap newly inserted inactive ENaC channels. It remains of interest to show whether the size of the uncapped (active) channel pool is regulated by direct proteolytic activation of apical membrane channels or via the proteolysis of co-protein(s) that in turn regulate channel activity. The possible involvement of intermediate second messengers in the protease-mediated regulation of ENaC channels will also require further investigation.

A

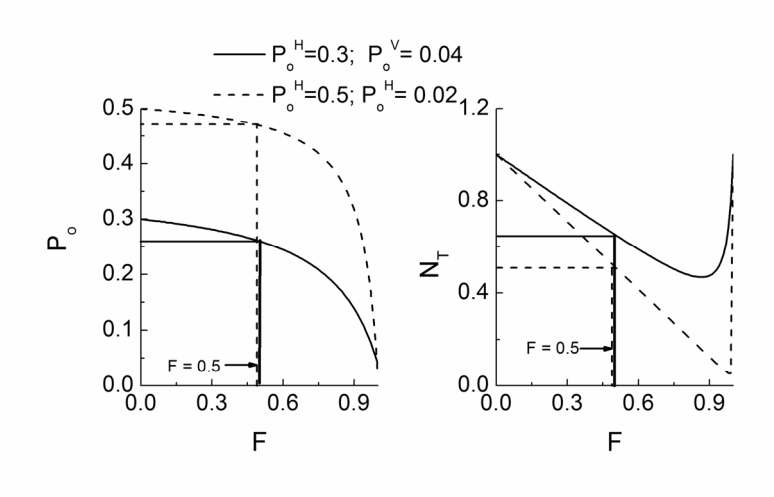

B

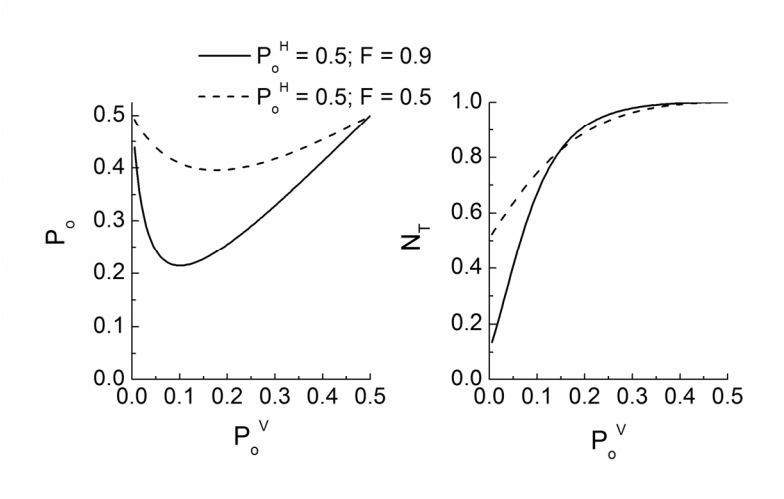

Figure 2-10 Effect of channel P_o heterogeneity on measured parameters

A) Plot of the expected P_o (left) and N_T (right) from noise analysis giving the heterogeneity described by F, the fraction of channels having variable P_o (P_o^V) with respect to the channels having fixed high P_o^H. These are plotted for P_o^H = 0.3 and P_o^V = 0.04 from Kemendy et al (1992) as well as for a second set of values from Caldwell et al. (2004) where P_o^H = 0.5 and P_o^V = 0.02. The drop in calculated P_o from noise analysis is not linear and is delayed until a large fraction of channels have converted and the delay increases with smaller values of the P_o^V. During this delay, N_T measurement shows significant decreases (see section 2.3.4 for details). B) A plot of calculated P_o (left) and N_T (right) from noise analysis versus P_o^V based on P_o^H = 0.5 and F = 0.5 and 0.9. As P_o^V decreases, decreases in the calculated P_o are observed whose extent depends on F until a nadir whereupon calculated P_o increases towards P_o^H. Thus for decreases in P_o^V to values less than 0.1 for present example the calculated P_o remains unchanged or increases dependending on the starting point. Whereas small decreases in P_o^v will not appear as significant changes in N_T, decreasing P_o^V to very small values will result in large decreases in the calculated N_T. The plots in A and B, correspond to families of curves that gives a surface plot for measured P_o and N_T versus P_o^V and F.

3.0 PROTEASE ACTIVATION VIA THEGAMMA-SUBUNIT

The regulated transepithelial transport of Na^+, critical for maintaining body fluid homeostasis in terrestrial organisms, is attributable to the expression of the heteromeric epithelial Na^+ channel (ENaC) (65). ENaC consists of α, β and γ subunits (31, 126). It was previously observed that exogenous aprotinin, a serine protease inhibitor, inhibited Na^+ transport in cortical collecting duct cells from the kidney (118, 132, 137, 191, 200) and human bronchial epithelial cells from the lung (25). Epithelial derived serine proteases such as the channel activating proteases (CAPs) and prostasin activated ENaC-mediated Na^+ transport when co-expressed in Xenopus oocytes (49, 191, 200). The ability of some of these proteases, CAP1 (whose human homologue is prostasin), to increase Na^+ transport in the co-expression studies was inhibited by aprotinin. In addition to the CAPs, which represent endogenous proteases, ENaC-mediated Na^+ transport can also be activated by exogenous trypsin, chymotrypsin and neutrophil elastase and cathepsin G (28, 37).

The notion that protease activation of Na^+ transport results from cleavage of ENaC arises from the correlation between the appearance of cleaved forms of the α and γ subunit and the measured ENaC activity. First, salt restriction or aldosterone infusion (stimuli for increasing Na^+ reabsorption in the kidney) were associated with the appearance of a lower molecular weight γ subunit in the rat cortical collecting duct while control rats had only the heavier γ subunit (123). Two molecular weight species of the α and γ subunit were found in whole rat kidneys where up-regulation of Na^+ transport in collecting duct cells correlated with preferential increase of the lower molecular γ subunit and decrease of the higher molecular weight species (54) suggesting a conversion. Aldosterone up-regulation of prostasin in the cortical collecting duct cells (133) may generate the γ subunit cleavage. Further, preventing internalization of ENaC in epithelial cells heterologously expressing ENaC increased the lower molecular weight isoforms of the α and γ subunits at the apical membrane which correlated with decreased sensitivity to exogenous trypsin

activation (105). Second, mutation of the furin cleavage consensus sequences found in the α and γ subunits prevented endogenous cleavage of these subunits and reduced Na^+ transport rates (86).

The single channel studies by Caldwell et al. provided evidence that exogenously added serine proteases could activate the channel by direct proteolysis (28, 29). These results suggest that proteases can directly bind to the channel and induce activation by cleavage. Based on the observation that trypsin and human neutrophil elastase could maximally activate silent channels, we tested the hypothesis that proteases directly interact with ENaC causing activation of Na^+ transport in a model epithelial cell by site-directed mutagenesis and analysis of the kinetics of current activation. Using related proteases neutrophil elastase and porcine pancreatic elastases as well as thrombin we show that specific protease interactions with ENaC must occur in a segment of the γ subunit.

3.1 MATERIALS METHODS

3.1.1 Construction of human α, β, γ ENaC tricistronic expression vector and site-directed mutagenesis.

The hENaC plasmid was obtained from Dr. Cheng (Rosalind Franklin University). Briefly, the human α, β, and γ ENaC subunit cDNAs were isolated from human lung epithelial cells. All three cDNA sequences were identical to the sequence reported by McDonald et al., 1994 and 1995 (accession numbers L29007, L36592 and L36593). The α cDNA was subcloned into pECFPN1 and a stop codon introduced at the 3' end of the α subunit to prevent the expression of the CFP. The β and γ subunits were subcloned into the pEGFPN1 vector (Clontech, CA) to obtain pEGFPN1/β and pEGFPN1/γ. Appropriate start and stop codons were inserted to allow for the expression of the β and γ subunits without the C-terminal expression of EGFP. The DNA fragments from pEGFPN1/β and pEGFP/γ vectors comprising the CMV promoters and the subunit cDNA without the GFP sequences were isolated and then subcloned into pECFPN1/α to generate a 13.4 kb tricistronic hENaC vector shown in

Figure 3-1. The important features of this ENaC tricistronic vector are that all three ENaC subunits are arranged in tandem and expression of each subunit is under an independent CMV promoter allowing for the separate expression of each subunit without the expression of ECFP or EGFP.

Site-directed mutagenesis was performed using Quick Change II XL (Stratagene) for single amino acid substitutions. Briefly, 28-33 bp long oligonucleotides containing the substituted nucleotide bases for changing the amino acids were synthesized as forward and reverse primers overlapping the base to be mutated. PCR using the hENaC template is carried out with the primers and the subsequent reaction digested by Dpn I to remove methylated template DNA. Top10® competent *E. coli* are transformed and plated. Usually, plasmid DNA is obtained from several colonies and checked by digestion with Xho I (New England Biolabs). DNA properly digested into three fragments by Xho I is sent for sequencing. Overlap PCR was performed using Phusion™ high-fidelity DNA polymerase (Finnzymes) to introduce a human thrombin cleavage site (LVPRG) by multiple contiguous substitutions in the $\gamma_{186\text{-}190}$ sequence of hENaC. Overlapping fragments were synthesized by PCR with forward and reverse primers 5'-**CTCGTGCCAAGAGGC**TCAAATGTCATGCACATCGAGTCC-3' and 5'-GCTCCTCAGCAGAATAGCTCATGTTGATTTTCTTCTCC-3'. A second set of forward and reverse primers, 5'-CTGCAGGCCACCAACATCTTTGCACAGGTGCCACAGC-3' and 5'-GCCTCTTGGCACGAGCAACATCTTTGCACAGGTGCCACAGC -3', containing Sbf I and BbvC I restriction sites were used in a second round of PCR to yield the blunt end product that was subcloned into the pCR® 4Blunt-TOPO® vector (Invitrogen), digested with Sbf I/BbvC I and ligated to the appropriate Sbf I/BbvC I digest fragment of hENaC. The sequences of all mutations were verified by DNA sequencing.

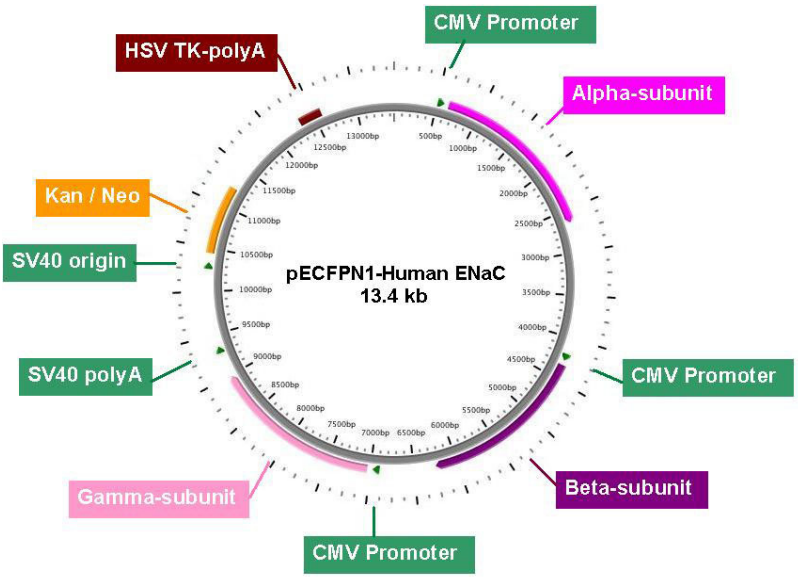

Figure 3-1 Tricistronic ENaC Vector

3.1.2 Cell culture and transfection

Fisher rat thyroid (FRT) cells were grown in sodium bicarbonate buffered Hams's F-12 media (Sigma, St Louis MO) modified with 10% FCS (Hyclone), 100 U/ml penicillin and 100 U/ml streptomycin at 37^0 C and 5 % CO_2 as previously described (164). The cells were expanded in plastic tissue culture flasks. Confluent monolayers were stably transfected with hENaC or mutant plasmids using Lipofectamine 2000 (Invitrogen, Carlsbad CA) and Opti-MEM media (GIBCO BRL Baltimore, MD) as described by the manufacturer's instructions and selected with G418 (500 µg/ml; GIBCO). The selected cells were fed with media containing 50 µM amiloride. FRT cells were seeded onto permeable tissue culture inserts (Transwell Clear, 0.4 µM pore size, 6 mm diameter, Corning) and fed three times a week with or without supplementation with dexamethasone (30 nM) or aldosterone (30 nM). The cells matured for at least 10 days and amiloride was removed from the feeding media two feeding cycles before short-circuit current measurements.

3.1.3 Short circuit current (I_{SC}) measurements

Current measurements were carried out 10 to 14 days after seeding. The epithelial cell monolayers were studied by placing the Transwell tissue culture inserts into Costar Ussing chambers with apical and basolateral bathing solution containing (in mM) 120 NaCl, 25 $NaHCO_3$, 3.3 KH_2PO_4, 0.8 K_2HPO_4, 1.2 $MgCl_2$, 1.2 $CaCl_2$ and 10 glucose as previously described (25). The apical and basolateral solutions were continuously circulated with a gas lift. The pH of the solution was 7.4 at 37^o C when gassed with a mixture of 95 % O_2: 5 % CO_2. The monolayers were continuously short-circuited with a voltage clamp (Department of Bioengineering, University of Iowa, Iowa City, IA) and transepithelial resistance was monitored by periodically applying a 4 mV bipolar pulse and calculating resistance from the current change. The amiloride-sensitive I_{SC} (I_{Na}) obtained from the difference in current with and without amiloride (50 μM) in the apical bath, was taken as a measure of ENaC-mediated electrogenic Na^+ transport. The amiloride insensitive current was minimal (< 5% of the baseline I_{SC}). The proteases trypsin (Sigma), human neutrophil elastase (NE; EPC, Owensville, MO), porcine pancreatic elastase (PE; EPC) and human alpha thrombin (TH; Sigma) were added to the apical bath and mixed by rapid pipetting with a transfer pipette.

To observe significant and reproducible protease activation it was necessary to pre-treat the cells with the serine protease inhibitor aprotinin. Many epithelial cells appear to have constitutive activation of Na^+ transport which can be inhibited by aprotinin in a time-dependent manner and the transport rate rapidly reverts to control levels upon addition of exogenous trypsin (25, 191). The slow time dependence of inhibition and rapid reversal by aprotinin suggests that in the presence of aprotinin active channels are continually retrieved or degraded whereas newly inserted channels were not activated. This pool of newly inserted channels can then be activated by exogenous proteases. The time course of aprotinin inhibition of current in mammalian airway cells has a half-life of ~ 45 min (4, 25). To ensure maximal inhibition for all constructs examined in experiments involving pre- protease inhibition, the protease inhibitor, aprotinin (10 μM; Sigma) or a vehicle control (PBS) was added to the apical surface of the monolayers overnight as previously reported (191) in the modified Ham's F-12 media and remained in the apical bath solution during I_{SC} measurements The proteases, the protease inhibitor aprotinin, and amiloride had no effect on I_{SC} in untransfected FRT cells.

3.1.4 Data Evaluation and Analysis

The effects of the proteases were assessed in two ways. First, steady-state I_{Na} was assessed before protease addition (baseline I_{Na}), then after the I_{Na} reached a steady-state 20-30 min. after addition of NE, PE or TH (I_{PR}). Trypsin was then added in excess over the aprotinin concentration to obtain I_{Tryp}. To compare the effects of NE, PE and TH to that of the maximum effect of trypsin we used the ratio I_{PR}/I_{Tryp} and the normalized value $\Delta I_{PR}{}^{Norm}$ where $\Delta I_{PR}{}^{Norm} = (I_{PR} - \text{baseline } I_{Na})/(I_{Tryp} - \text{baseline } I_{Na})$. Second, following addition of NE, PE or TH the time course of the $\Delta I_{PR}{}^{Norm}$ in each experiment was analyzed according to two reactions. The first reaction is shown in equation 3-1 below.

$$C + E \leftarrow \frac{k_{on}}{k_{off}} \rightarrow A$$

3-1

The quantity C is the inactive channel at the membrane, E is the added enzyme concentration and A is the channel activated by proteases. The rate coefficients k_{on} and k_{off} have their usual meanings. The differential equation from equation 3-1 is:

$$\frac{d}{dt}(A) = k_{on} E \cdot C_0 - (k_{off} + k_{on} E) A$$

3-2

Under the assumption that the enzyme concentration is constant due to being in excess and no autolysis the differential equation is solved to yield exponential functions in time that can be fitted to the whole time course of current activation (Appendix). The time courses for individual experiments were fitted using Matlab (The Mathworks, Natick MA) to equation 3-3.

$$\Delta I_{PR}{}^{Norm}(t) = \Delta I_{PR}{}^{Norm}(\infty)\left(1 - e^{-t/\tau}\right)$$

3-3

A linear term was added to equation 3-3 to account for long time decreasing trend in the current records. The reciprocal of the time constant τ was taken as a measure of the apparent relaxation rate constant k_{obs}. It is shown in the Appendix that the k_{obs} is given by

$$k_{obs} = k_{off} + k_{on}E$$

3-4

The second reaction is of the form shown in equation 3-5.

$$C + E \leftarrow \frac{k_{on}}{k_{off}} \rightarrow CE \xrightarrow{k_{cat}} A$$

3-5

The differential equations from equation 3-5 are

$$\frac{d}{dt}(CE) = k_{on}E \cdot C_0 - (k_{cat} + k_{off} + k_{on}E) \cdot CE - k_{on}E \cdot A$$

3-6

$$\frac{d}{dt}(A) = k_{cat} \cdot CE$$

3-7

The k_{off} and k_{on} have their usual meanings and k_{cat} is simply used to express a rate limiting enzyme concentration independent step. It is shown in the appendix that the time course of activation can be approximated also by equation 3-3 but here the k_{obs} is given by equation 3-8:

$$k_{obs} = \frac{k_{cat}E}{K_M + E}$$

3-8

where,

$$K_M = \frac{k_{off} + k_{cat}}{k_{on}}$$

Linear and non-linear regression analysis of the k_{obs} versus enzyme concentration was carried out in OriginPro (OriginLab, Northampton MA).

3.1.5 Matrix-assisted Laser Desorption Ionization-Time of Flight Analysis (MALDI-TOF)

The sites of cleavage by NE and PE were searched by MALDI-TOF mass spectrometry on a 23-mer peptide designated peptide T^{176}-S^{198} (Ac-TGRKRKVGGSIHKASNVMHIES-NH_2) and corresponding to the amino acid sequence T176 to S198 of the γ subunit of ENaC. Enzymatic

digestions were performed at 37°C with NE and PE at final enzyme concentration of 200 nM and peptide T^{176}-S^{198} at 200 μM in 200 mM Tris acetate, pH 7.4. Following the incubation period, 20 μl of the reaction was quenched by lowering the pH to 3 with addition of 20 μl of 0.5 % trifluoroacetic acid (TFA). The reaction without and with the enzymes were submitted to MALDI-TOF measurements. A ZipTip C_{18} solid-phase extraction sorbant (Millipore, Bedford MA) was washed with 10 μl of acetonitrile/water (1:1, v/v) and then equilibrated with aqueous 0.1% TFA. Peptide samples acidified with 5% aqueous TFA to enhance peptide retention on the stationary phase of the C_{18} sorbant were loaded onto the tip and eluted with 0.1% TFA in acetonitrile/water (1:1, v/v). The matrix solution was prepared by dissolving 10 mg of cyano-4-hydroxycinnamic acid in 1 ml of acetonitrile/water (1:1, v/v) containing 0.1% TFA. 0.5 μl of the matrix solution was mixed with 0.5 μl of peptide solution. About 0.5 μl of the mixture was deposited onto the MALDI stage and air-dried. Positive ion MALDI-TOF Mass spectra were acquired on an Applied Biosystems (Foster City, CA) Voyager DE-Star mass spectrometer operated in reflector mode. Following time-delayed extraction, the ions were accelerated to 20 kV for TOF analysis. A total of 100 laser shots were acquired and signal averaged per spectrum.

3.1.6 Statistics

Effects of the proteases on steady-state I_{Na} within a given construct were determined using unpaired double sided t tests of (1) I_{Na} at baseline versus I_{PR} or I_{Tryp} and (2) I_{PR} versus I_{Tryp}. Comparison of the ratioΔI_{PR}^{Norm} and τ across multiple mutants were carried out with one way ANOVA followed by individual comparisons versus wild type ENaC using the Bonferroni corrected t- test. in Origin . $P < 0.05$ was considered significant.

3.2 RESULTS

3.2.1 Expression of ENaC-mediated Na^+ transport in FRT cells and regulation by corticosteroids and protease

FRT epithelial cells stably transfected with the α, β and γ human ENaC subunits in a single tricistronic vector (hENaC) had an I_{SC} that was blocked by addition of amiloride (50 μM) to the apical side (Figure 3-2 A and B). The magnitude of the amiloride-sensitive I_{SC} (I_{Na}) averaged 3.4 ± 0.12 μA/cm^2 (*n* = 11) and is similar to what has been typically observed by transiently transfecting FRT cells simultaneously with the three ENaC subunits in separate plasmids (171). Untransfected cells had no I_{Na}. The transepithelial epithelial resistance (R_T) averaged 1.2 ± 0.13 kΩ•cm^2. Feeding the cells in media supplemented with either aldosterone (30 nM) or dexamethasone (30 nM) for 72 hrs or more before short-circuiting significantly increased I_{Na} with no increase in the amiloride insensitive $I_{SC.}$. Aldosterone induced a 1.5-fold (n = 7) increase in I_{Na} while dexamethasone induced an 8-fold (n = 11) increase in I_{Na} (Figure 3-2 B). The half maximal inhibitory concentration (K_i) for amiloride was 570 ± 86 nM with a maximal inhibition of 96 ± 1.2%. Transepithelial resistances were 0.9 ± 0.13 and 1.1 ± 0.08 kΩ•cm^2 in aldosterone and dexamethasone treatments respectively after the addition of amiloride. To determine whether proteases regulate Na^+ transport in FRT cells stably expressing hENaC, the effect of exogenously added trypsin and protease inhibitor were examined. The cells were first pre-incubated either with the protease inhibitor aprotinin (10 μM) or a vehicle control (PBS) on the apical side for 16 to 24 hrs. The cells that were pre-incubated with aprotinin had decreased I_{Na} compared to cells pre-incubated with PBS. During short-circuiting addition of trypsin (15 μM) to the apical bath, in a 5 μM excess over the aprotinin concentration, caused no statistically significant increase in the I_{Na} of PBS pre-incubated cells (3.9 ± 0.87 to 4.5 ± 1.03 μA/cm^2; n = 11) but significantly increased I_{Na} in aprotinin pretreated cells. The baseline I_{Na} in the aprotinin pretreated cells was 3.1 ± 0.68 and the maximal I_{Na} after addition of trypsin (I_{Tryp}) was 5.9 ± 0.68 μA/cm^2 (n = 12). No differences were found in the plateau current observed between PBS and aprotinin treated cells following addition of trypsin. Thus, in the presence of aprotinin trypsin addition causes an increase in current whereas in the absence of aprotinin trypsin addition does not result in a significant increase in current. Consequently, aprotinin unmasks a portion of I_{Na}

that can be regulated by extracellular protease activity similar to the previously reported effects of aprotinin and trypsin. The absolute values of the aprotinin and trypsin effects on I_{Na} were greatly enhanced in dexamethasone treated cells but displayed the same qualitative pattern (Figure 3-3, A and B). As already noted dexamethasone treatment greatly increased the I_{Na}. Trypsin did not significantly increase I_{Na} in PBS pretreated dexamethasone stimulated cells where I_{Na} was 37.1 ± 1.66 μA/cm^2 before trypsin and 39.6 ± 1.96 μA/cm^2. Pretreatment with aprotinin caused a 50% decrease in the baseline I_{Na} to 21.3 ± 0.8 μA/cm^2 and in these aprotinin inhibited cells trypsin doubled the I_{Na} to 40.8 ± 2.09 μA/cm^2 (Figure 3-3 A and B). Because the dexamethasone stimulated hENaC expressing FRT cells gave a more robust and reproducible I_{Na} and the protease regulatory pattern persists in dexamethasone treated cells, dexamethasone treated cells were used in the remainder of the study.

3.2.2 Sub-micromolar neutrophil and porcine elastase activate ENaC in FRT cells

It was previously shown that, like trypsin, human neutrophil elastase (NE) can activate ENaC-mediated Na^+ current (28). We examined the effect of NE and porcine pancreatic elastase (PE), a similar elastase (13, 189), on the I_{SC} in FRT cells expressing ENaC. Elastase is not inhibited by aprotinin (13, 136) therefore an excess over the aprotinin concentration was not required to stimulate I_{Na}. Addition of NE (300 nM) or porcine elastase (300 nM) to the apical side of FRT cells expressing ENaC had no effect on cells pretreated with PBS (Figure 3-4). Similar to the effects of trypsin NE and PE increased the I_{SC} in cells that were pre-treated with 10 μM aprotinin (Figure 3-4). The rise in the I_{SC} following elastase addition occurred over a 5 min period and increased to a plateau value equal to the baseline I_{SC} of uninhibited cells that were pre-incubated with PBS. Addition of trypsin subsequent to NE or PE did not further increase the I_{SC} in either PBS treated or aprotinin treated cells. Thus, trypsin, NE or PE were sufficient to increase I_{SC} in aprotinin inhibited cells back to the values observed in control PBS treated cells. Trypsin did not significantly increase the I_{Na} after NE or PE stimulation of aprotinin inhibited cells, consequently the maximal protease stimulation was not additive.

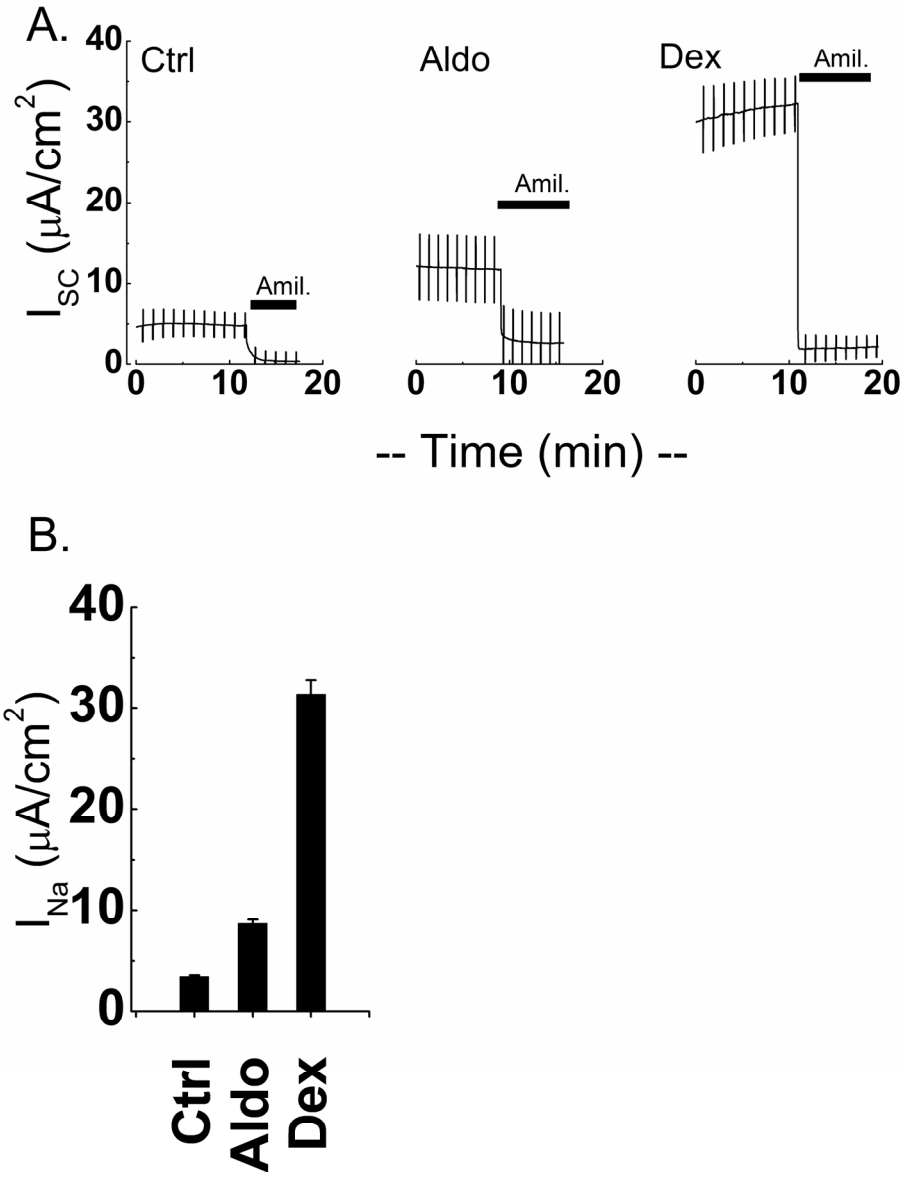

Figure 3-2 Expression of ENaC and corticosteroid stimulation of Na^+ transport in FRT cells

FRT cells stably transfected with the tricistronic vector containing the α, β and γ human ENaC subunits were short-circuited in Ussing chambers with symmetrical NaCl, $NaHCO_3$ buffered ringers. (A) Representative current traces of unstimulated (Ctrl), aldosterone (30 nM) and dexamethasone (30 nM) stimulated cells. The vertical deflections are current responses to 4 mV bipolar pulses for monitoring transepithelial resistance. Amiloride (50 μM), was added to the apical side for the indicated period (*bars*) to determine I_{Na}, the amiloride-sensitive component of the I_{SC}. (B) Summary of the amiloride-sensitive I_{Na} (mean ± SEM; N = 7 - 11).

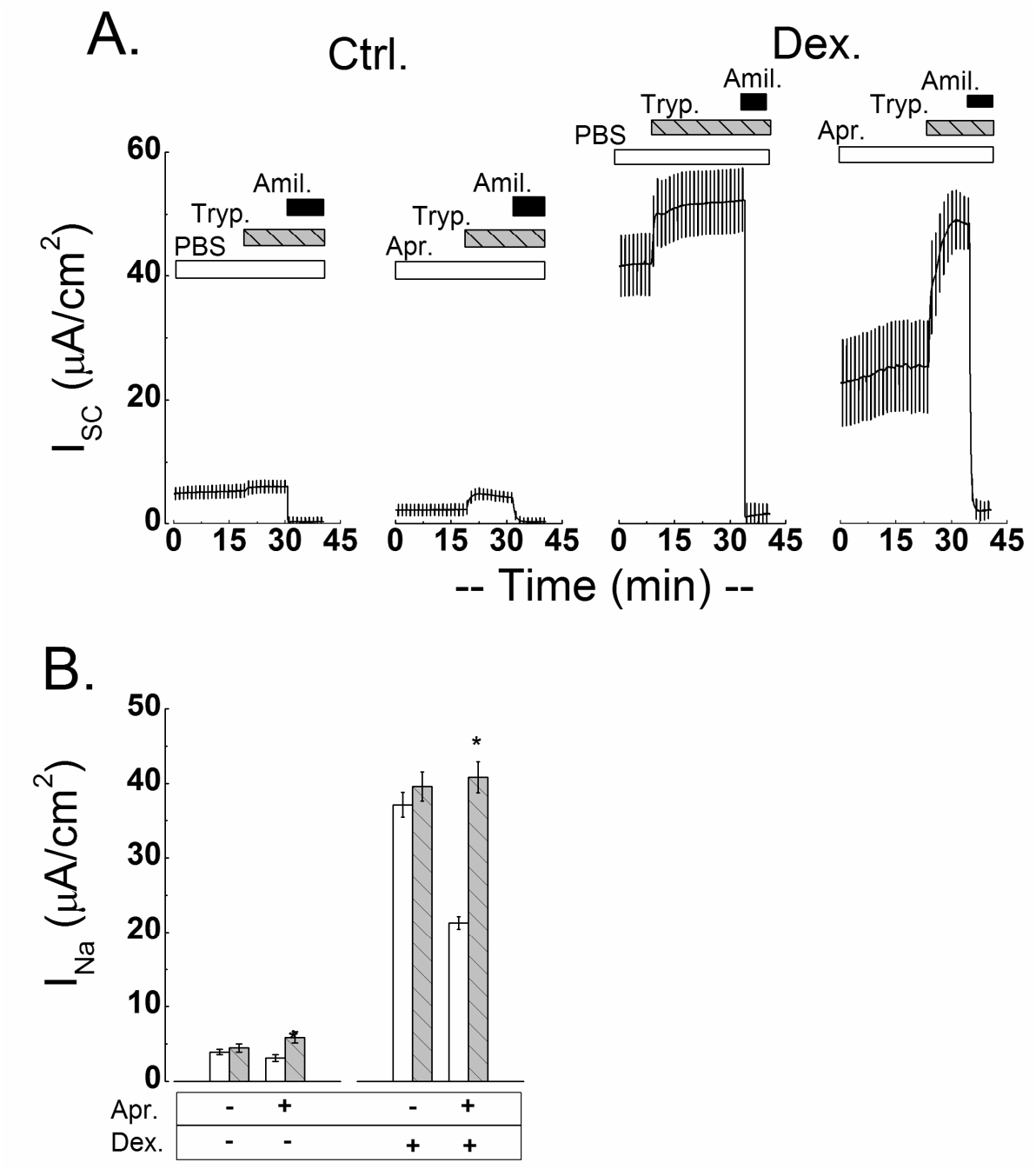

Figure 3-3 Na^+ transport regulation by aprotinin and trypsin in FRT cells

(A) Representative I_{SC} traces in FRT cells expressing ENaC, pre-incubated with and kept in vehicle (PBS) control or aprotinin (APR; 10 μM) during short-circuiting as indicated by the bars. Also shown are traces from cells pre-stimulated with dexamethasone (30 nM). Trypsin (15 μM) and amiloride (50 μM) were added to the apical side as indicated (*horizontal bars*). (B) I_{Na} (mean ± SEM, N = 11 - 17) before (*open bars*) and after (*solid bars*) addition of trypsin in PBS pre-incubated cells and aprotinin pre-incubated cells without or with dexamethasone stimulation as indicated. *P < 0.05 by Student's t test comparison of I_{Na} at baseline and after addition of trypsin (I_{Tryp}).

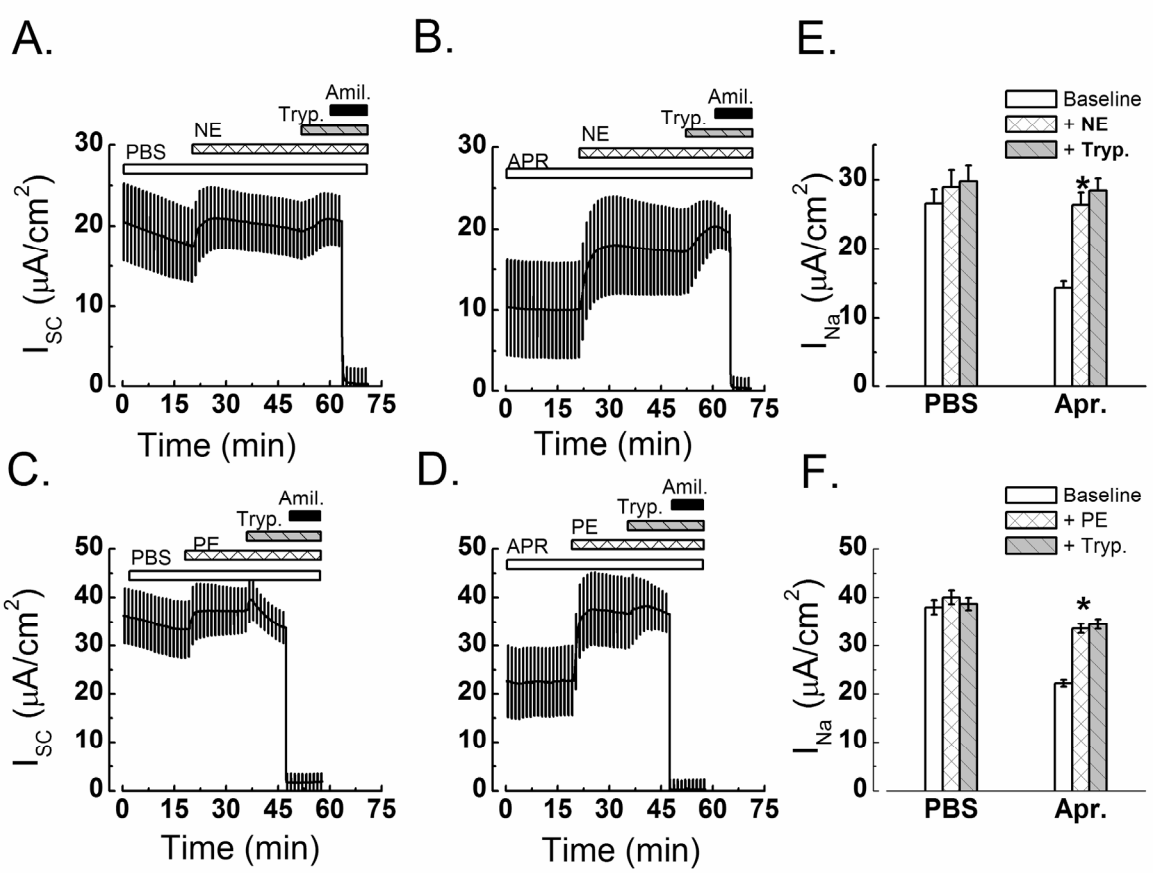

Figure 3-4 Elastase mediated activation of ENaC in FRT cells

(A, C) Representative I_{SC} in FRT cells expressing ENaC that were either pretreated with PBS. (B, D) Representative I_{SC} of cells pretreated with 10 μM aprotinin. (A, B) NE (300nM) or (C, D) PE (300 nM) was added to the apical bath of short-circuited cells. Trypsin (15 μM) and amiloride (50 μM) were subsequently added to the apical baths in all experiments as indicated (*horizontal bars*). (E) I_{Na} (mean ± SEM, N = 16-24) before (*open bars*), after 300 nM of NE or (F) PE (stripped bars) and after 15 μM trypsin (black bars). *P < 0.05 in student's t tests of baseline I_{Na} and after NE or PE addition.

3.2.3 Identification of elastase specific sites I: human neutrophil elastase

To determine whether specific sites on ENaC mediate the NE dependent activation of I_{Na}, we carried out site-directed mutagenesis of possible NE binding or hydrolytic sites in the extracellular loops of α and γ ENaC subunits. NE hydrolyzes polypeptides with a strong preference for cleavage of V-X bonds where V is at the P1 position and X is an amino acid at the P1' position. The preference is a function of both the affinity of the elastase for the cleavage site (K_M) and the rate of hydrolysis (k_{cat}). Hydrolysis by NE can also occur with other small hydrophobic amino acids at the P1 position but to a lesser degree (208). We tested the effect of mutating individual valines conservatively to glycines in the extracellular loops of α and γ ENaC because these subunits appear to be involved in activation and or processing by endogenous proteases (54, 86, 87, 105, 123). The valine mutation sites were chosen based on their proximity to previously implicated cleavage sites (86).

Table 3-1 Protease effect on I_{Na} for wild type ENaC and selected glycine substitutions

* $P < 0.05$ comparison of I_{Na} at baseline with I_{Na} at + NE
† $P < 0.05$ comparison of I_{Na} at + NE to I_{Na} at + Trypsin

PBS				
Construct	Baseline	(+) NE $I_{Na}(\mu A/cm^2)$	(+) Trypsin	N
WT	28.5 ± 1.96	30.1 ± 2.01	30.4 ± 1.84	26
α_{V171G}	23.7 ± 1.11	22.4 ± 1.67	23.6 ± 2.37	6
α_{V193G}	18.1 ± 1.25	18.2 ± 1.48	20.8 ± 0.71	6
α_{V206G}	27.5 ± 0.61	32.5 ± 2.16	31.9 ± 2.17	3
γ_{V110G}	35.7 ± 2.22	32.8 ± 2.13	30.5 ± 2.09	3
$\gamma_{V110;V146G}$	38.6 ± 1.04	40.0 ± 1.78	38.8 ± 1.24	6
γ_{V182G}	30.7 ± 1.80	30.7 ± 1.64	29.5 ± 1.28	17
γ_{V193G}	37.5 ± 4.02	37.0 ± 4.14	36.7 ± 3.12	6
$\gamma_{V182G;193G}$	32.7 ± 1.46	33.0 ± 1.50	34.8 ± 1.15	29
γ_{V202G}	32.2 ± 4.20	42.8 ± 2.77	39.7 ± 3.11	4

APR				
Construct	Baseline	(+) NE $I_{Na}(\mu A/cm^2)$	(+) Trypsin	N
WT	15.6 ± 0.86	27.8 ± 1.40*	31.3 ± 1.60	36
α_{V171G}	11.6 ± 0.37	26.0 ± 1.59*	24.9 ± 1.46	6
α_{V193G}	10.2 ± 0.61	25.6 ± 1.01*	25.3 ± 1.71	6
α_{V206G}	18.6 ± 0.95	34.2 ± 0.84*	39.5 ± 1.52	3
γ_{V110G}	22.9 ± 1.36	31.6 ± 2.02*	31.7 ± 2.74	3
$\gamma_{V110;V146G}$	21.7 ± 1.75	35.4 ± 3.47*	40.4 ± 1.54	6
γ_{V182G}	15.8 ± 0.84	28.6 ± 1.44*	32.5 ± 1.09	24
γ_{V193G}	16.6 ± 0.59	32.0 ± 2.18*	37.5 ± 2.12	13
$\gamma_{V182G;193G}$	18.3 ± 0.67	25.9 ± 1.07*	38.9 ± 1.12†	39
γ_{V202G}	22.5 ± 2.06	39.7 ± 1.92*	44.8 ± 1.35	8

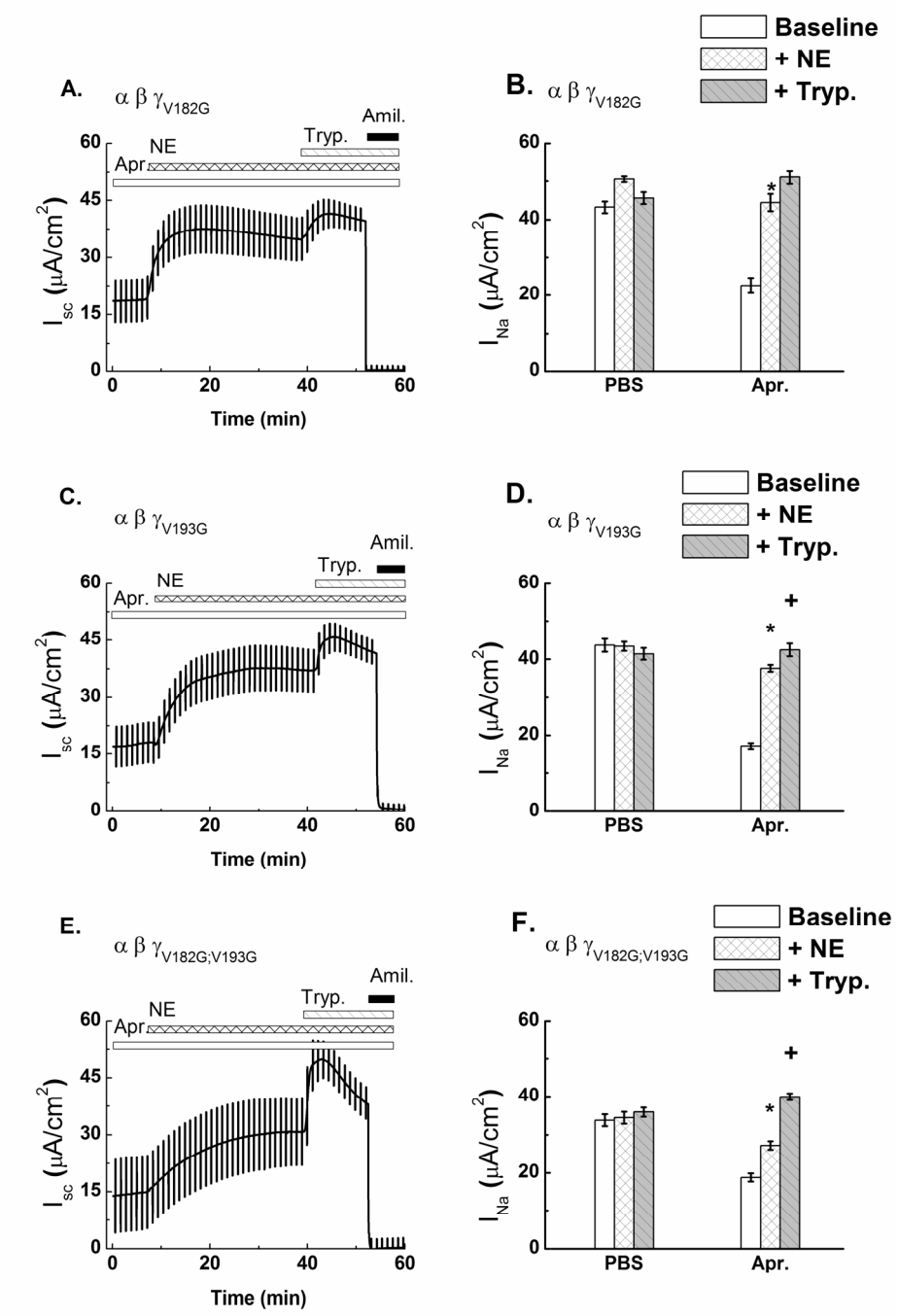

Figure 3-5 Two point mutations in γ ENaC inhibit NE activation of I_{Na} in FRT cells

(A) Representative I_{SC} of cells expressing γ_{V182G} (C) γ_{V193G} and (E) $\gamma_{V182G;V193G}$ that were pretreated with 10 μM aprotinin before short-circuiting. NE (300 nM) was added to the apical bath as indicated (*horizontal bars*). Subsequently trypsin (15 μM) and amiloride (50 μM) were added. (B) Mean (± SEM) of baseline I_{Na} (*open bars*), I_{PR} (*stripped bars*) and I_{Tryp} (*black bars*) in cells pretreated with PBS or aprotinin that were expressing $\alpha\beta\gamma_{V182G}$ (D) $\alpha\beta\gamma_{V193G}$ and (F) $\alpha\beta\gamma_{V182G;V193G}$ mutants. *$P < 0.05$ in student's t-test comparison of amiloride sensitive I_{SC} before and after NE. †$P < 0.05$ in student's t test comparison of amiloride sensitive I_{SC} after NE and after trypsin. N = 8-12.

Nine V to G mutants were evaluated; three in the α subunit and six in the γ subunits. All nine V to G mutants expressed baseline currents that were similar to wild type ENaC expressing cells. Furthermore aprotinin inhibited the baseline current to a similar degree and NE reversed this inhibition of I_{Na} (Table 3-1). Only the double mutant $\alpha\beta\gamma_{V182G;\ V193G}$ was different from wild type ENaC. Unlike wild type ENaC and several mutants where subsequent addition of trypsin had a minor further effect on I_{Na} following NE stimulation in aprotinin inhibited cells (Table 3-1), Figure 3-4, and representative mutations in Figure 3-5, $\alpha\beta\gamma_{V182G;V193G}$ could be significantly further stimulated by trypsin (Table 3-1, Figure 3-5 E and F). As shown in the figures, addition of NE to aprotinin treated FRT cells expressing wild type ENaC increased the amiloride-sensitive I_{SC} from 15.6 +/- 0.86 μA/cm^2 to 27.8 +/- 1.40 μA/cm^2 (n = 36) within 10 min. Thereafter, addition of trypsin caused only a small further increase to 31.3 ± 1.60 μA/cm^2. Thus NE caused an increase that was ~ 85% of the trypsin induced maximal protease increase in wild type ENaC expressing cells. In contrast addition of NE to aprotinin treated FRT cells expressing the $\alpha\beta\gamma_{V182G;V193G}$ mutant increased the amiloride-sensitive I_{SC} from 18.3 +/- 0.67 to 25.9 +/- 1.07 μA/cm^2 (n = 39), but the I_{SC} could be further stimulated to 39.9 +/- 1.12 μA/cm^2 after the addition of trypsin. Thus in the $\gamma_{V182G;V193G}$ cells NE only stimulated ~ 36% of the I_{Na} stimulated by trypsin.

A closer examination of the current traces revealed that the rate of activation by NE was also affected by the valine to glycine mutations and this effect was investigated in greater detail. The changes in I_{Na} following addition of NE (300 nM) to wild type and mutant ENaCs were monitored with time and reported (Figure 3-6 A) as a fraction of the maximal trypsin stimulated I_{Na}. The fractional current increase normalized to the maximum response after trypsin ($\Delta I_{PR}{}^{Norm}$) was fitted to exponentials as described in Methods to yield time constants. The $\Delta I_{PR}{}^{Norm}$ ~ 30 min after NE addition was taken as the measure of maximal NE stimulated current. The fitted parameters are summarized in Table 3-2 for αβγ and the glycine scanning mutations showing that only specific mutations in the γ subunit appreciably change the time course.

Table 3-2 Fitted parameters for Neutrophil Elastase Activation of ENaC

Values are the mean of the individual fits from N experiments. * $P < 0.05$ ANOVA-unpaired student t test comparison with WT values.

Construct	τ (+/- SEM)	ΔI_{PR}^{Norm} (+/- SEM)	N
	min		Filters
WT	3.10 +/- 0.18	0.68 +/- 0.05	10
α-V171G	1.52 +/- 0.155	0.96 +/- 0.03	6
α-V193G	1.94 +/- 0.061	0.85 +/- 0.07	6
α-V206G	2.24 +/- 0.416	0.74 +/- 0.03	3
γ-V110G	1.89 +/- 0.748	0.96 +/- 0.05	3
γ-V110/146G	1.80 +/- 0.390	0.89 +/- 0.04	5
γ-V182G	3.46 +/- 0.17	0.64 +/- 0.05	8
γ-V193G	6.32 +/- 0.36*	0.53 +/- 0.05	8
γ-V182/193G	11.82 +/- 1.49*	0.22 +/- 0.02*	8
γ-V201G	3.95 +/- 0.810	0.79 +/- 0.030	8

Representative time courses for wild type, $\alpha\beta\gamma_{V182G}$, $\alpha\beta\gamma_{V193G}$ and $\alpha\beta\gamma_{V182G;V193G}$ are shown in Figure 3-6. In wild type and $\alpha\beta\gamma_{V182G}$ expressing cells the ΔI_{PR}^{Norm} rose with identical rates and to similar plateau values with amplitudes 0.68 ± 0.05 and 0.64 ± 0.04 respectively. Therefore mutating V182 to G had no effect on NE activation of current. The cells expressing $\alpha\beta\gamma_{V193G}$ had ΔI_{PR}^{Norm} of 0.53 ± 0.05 which was not significantly decreased from wild type; but they showed a significant elongation of the time constant from the wild type value of 3.1 ± 0.18 min. (n = 10) to 6.3 ± 0.36 min. (n = 5). As noted above cells expressing the double mutant, $\alpha\beta\gamma_{V182G;V193G}$, had a marked reduction of ΔI_{PR}^{Norm} (0.22 ± 0.02) as well as a further elongation of the time constant to 11.8 ± 1.49 min (n = 8). Therefore, while mutating the V182 to G182 had no discernible effect on its own, this mutation produced a pronounced effect in the presence of the already inhibitory V193G mutation. To differentiate an effect caused by changing a V from an effect introduced specifically by the G, several amino acids were substituted at positions 182 and 193. The effect of mutating γ V182 and V193 was not specific to glycine but consistent for several amino acid substitutions (S, T, D, E, and Q). Generally, substitutions at γ182 did not result in significant differences in the τ for the residues tested (Figure 3-6 B). At residue 193, all the substitutions except E caused a significant prolongation of τ compared to wild type (Figure 3-6 B). Substitutions at both γ182 and γ193 produced significant elongation of τ for all the substitutions compared to wild type (Figure 3-6 B). The changes in ΔI_{PR}^{Norm} caused by the mutations were roughly consistent with the changes in τ. Generally, ΔI_{PR}^{Norm} was not affected by substitutions at γ 182 only, except with the S substitution (Figure 3-6 C). The ΔI_{PR}^{Norm} was reduced for substitutions at γ 193, except for the G substitution (Figure 3-6 C). All double substitutions at 182 and 193 resulted in decreased ΔI_{PR}^{Norm} compared to wild type. These results are more consistent with the conclusion that removal of a valine (as opposed to introduction of a specific residue) was responsible for both prolongation of τ and decreased ΔI_{PR}^{Norm}. Secondarily, the conserved pattern where substitutions at 182 produce no effect; substitutions at 193 increased τ and decreased ΔI_{PR}^{Norm}; and double substitutions further increasing τ and decreasing ΔI_{PR}^{Norm} suggest that the V193 is of primary importance in current activation by NE but V182 also has some effect unmasked in the absence of V193.

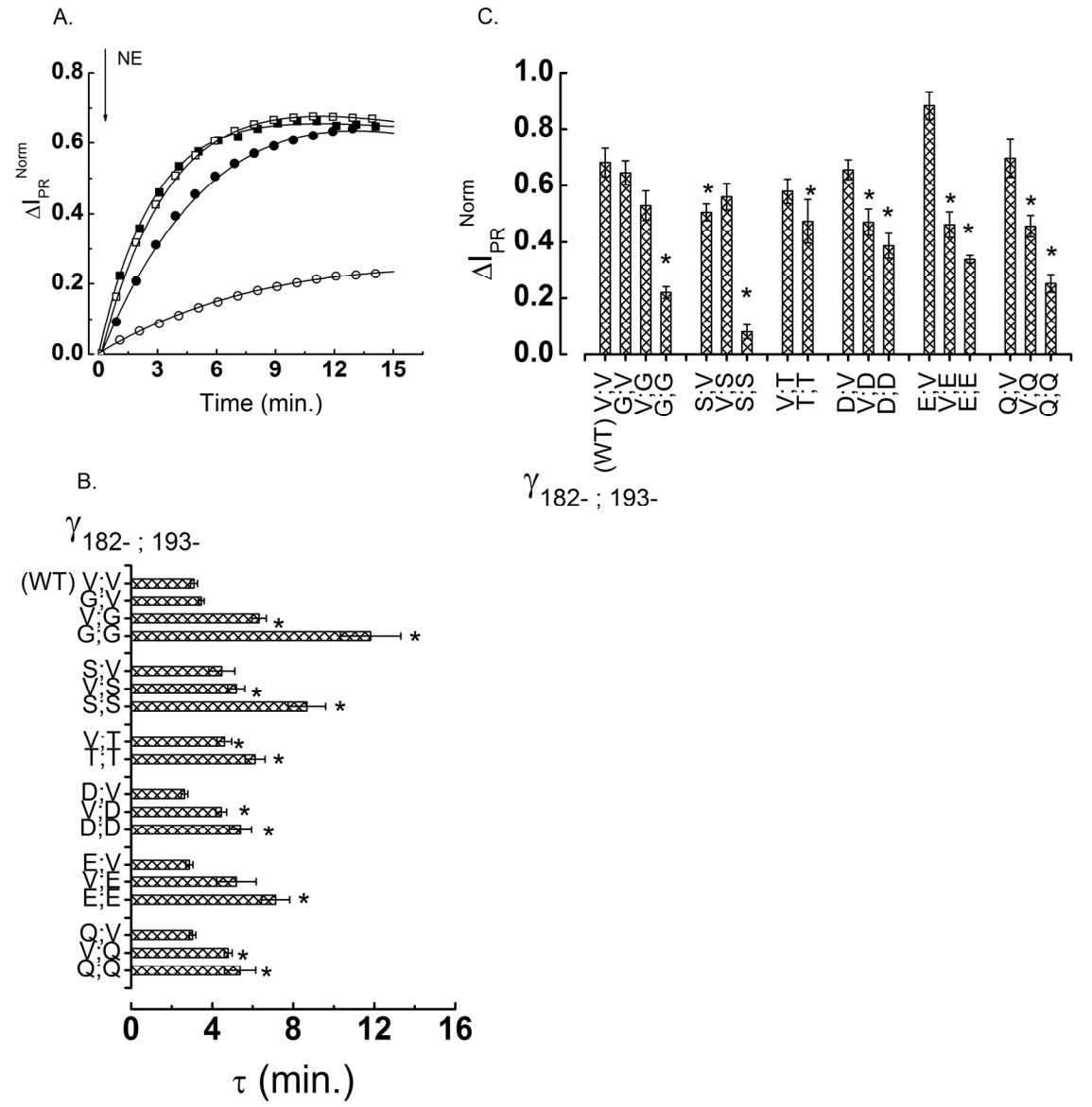

Figure 3-6 Effect of mutating residues 182 and 193 γ ENaC on NE activation of I_{Na}

NE (300 nM) was added to short-circuited FRT cells expressing the indicated γ ENaC mutants that were pre-treated with 10μM aprotinin. 30 minutes after addition of NE, Trypsin (15 μM) was added in excess over aprotinin to achieve a reference point for maximal protease stimulation. (A) Representative traces of ΔI_{PR}^{Norm} for NE activation of wild type (*solid squares*), $\alpha\beta\gamma_{V182G}$ (*open squares*), $\alpha\beta\gamma_{V193G}$ (*solid circles*) and $\alpha\beta\gamma_{V182G;V193G}$ (*open circles*) ENaCs. The solid lines are the exponential fits of the data. (B) Summary of the τ from experiments described above (mean ± SEM, N = 4- 10) for several amino acid substitutions at residues 182 and 193 in γ ENaC. $P < 0.01$, one way ANOVA (C) Steady state values of ΔI_{PR}^{Norm} for the amino acid substitution at 182 and 193 in γ ENaC (mean ± SEM, N = 6 – 36). *$P < 0.05$, one way ANOVA and t test comparison with wild type.

3.2.4 Identification of elastase specific sites II: porcine pancreatic elastase

First, we tested if the valines critical for NE were also critical for PE activation of current. I_{SC} following addition of PE (300 nM) were monitored to determine the effect of simultaneous substitutions at residues 182 and 193 on PE mediated channel activation. The effects of the double substitutions on $\Delta I_{PR}{}^{Norm}$ were small compared to the results for NE. As shown in Figure 3-7 A and B, the time courses for wild type and G substitutions were slightly prolonged. The τ was prolonged from 2.0 ± 0.14 min (N = 11) for wild type to 3.6 ± 0.27 min (N = 11) for the G substitutions. The effect on $\Delta I_{PR}{}^{Norm}$ was not different between wild type and G substitutions at ~ 0.7 for both (N = 16 and 23 respectively; Figure 3-7 C). The rest of the double substitutions examined (S, Q E and T) had small effects on τ and $\Delta I_{PR}{}^{Norm}$. These results show that the valines were not critical for increasing I_{Na} by PE.

Unlike NE, the preferential residue at P1 is A for PE (76). Therefore one explanation for minor effects of the V substitutions is that PE interacts with the channel via its preferred residue somewhere else. We reasoned that γ A190 between the two valines critical for NE was a likely target. Substitution of the γ A190 to G resulted in significant attenuation of the current response to PE (Figure 3-7 F G and H). While 1000 nM PE activated current in wild type and $\alpha\beta\gamma_{V182G;V193G}$ double mutant ENaC (Figure 3-7 F and G), with τ of 1.94 ± 0.12 and 2.17 ± 0.07 min respectively, the mutant $\alpha\beta\gamma_{A190G}$ prevented PE activation of current. Because increases in I_{Na} were small to non-existent in the $\alpha\beta\gamma_{A190G}$ mutant in response to PE, τ could not be resolved for all experiments. For those experiments where τ was resolved, it was 25.6 ± 1.09 min (Figure 3-7 H). Furthermore, the $\Delta I_{PR}{}^{Norm}$, which was 0.70 ± 0.04 and 0.89 ± 0.03 for wild type and $\alpha\beta\gamma_{V182G;V193G}$ respectively, was reduced to 0.26 ± 0.02 for $\alpha\beta\gamma_{A190G}$. These results are consistent with γ A190 being of primary significance for PE current activation, whereas the V's are more important for NE current activation. Because the results are consistent with the P1 preferences for PE and NE, they suggest that these enzymes may interact with the channel according to their substrate specificities.

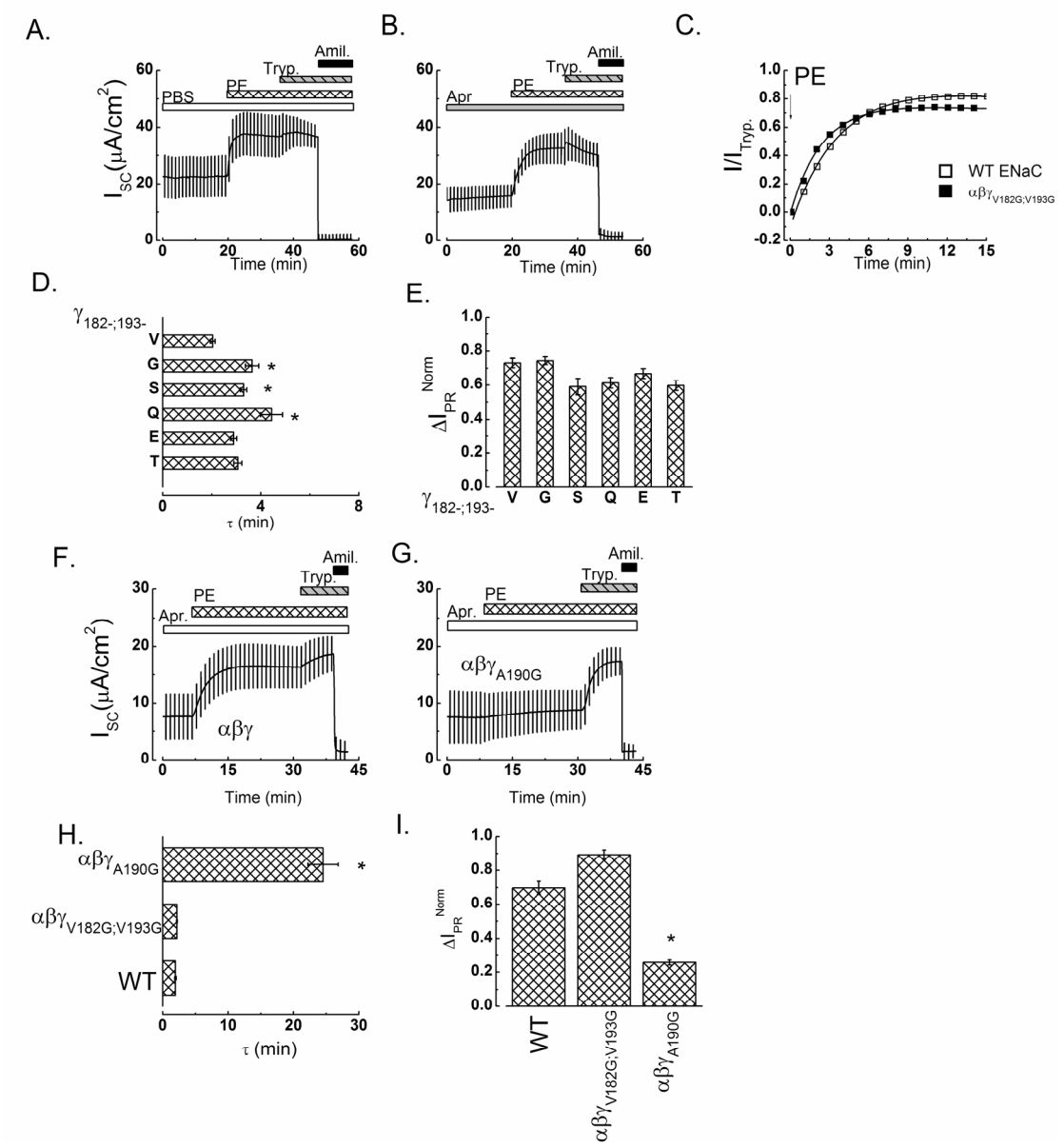

Figure 3-7 Effect of mutations at γ182 γ190 and γ193 on PE activation of ENaC

PE (300 nM) was added to short-circuited FRT cells expressing the indicated γ ENaC mutants that were pre-treated with 10μM aprotinin. 20 minutes after addition of PE, Trypsin (15 μM) was added in excess over aprotinin to achieve a reference point for maximal protease stimulation. (A) and (B) Representative I_{SC} trace of FRT cells expressing wild type or $\alpha\beta\gamma_{V182G;V193G}$ mutant. (C) Representative ΔI_{PR}^{Norm} response to PE for wild type (*solid squares*), and $\alpha\beta\gamma_{V182G;V193G}$ (*open squares*) mutant with exponential fits (*solid lines*). (D) Summary of the τ (± SEM, n = 4 - 11) from experiments described above for double substitutions at residues 182 and 193 in γ ENaC. (E) The steady state ΔI_{PR}^{Norm} (± SEM, n = 8 – 23) ratios for the double substitutions at 182 and 193 in γ ENaC. (F, G) Representative I_{SC} trace for FRT cells expressing wild type, $\alpha\beta\gamma_{V182G;V193G}$ and $\alpha\beta\gamma_{A190G}$ ENaC respectively. 1000 nM PE was used. (H and I) τ (± SEM, n = 5 - 8) and steady state ΔI_{PR}^{Norm} (± SEM, n = 5 - 8) for responses to 1000 nM PE in cells expressing wild type (*open bars*), $\alpha\beta\gamma_{V182G;V193G}$ (*light grey bars*) and $\alpha\beta\gamma_{A190G}$ (*dark grey bars*). *P < 0.05, one way ANOVA and t test comparison with wild type.

3.2.5 Concentration dependence of Protease Activation

Because the previous results suggest direct protease-ENaC interaction, a concentration dependence of activation was used to delineate two mechanistic possibilities; a) that direct binding was sufficient for channel activation or b) that a secondary step is necessary. As can be seen from the progress curves of ΔI_{PR}^{Norm} (Figure 3-8 A) the rates of current activation as well as the amplitudes of the increase were concentration dependent. Increasing NE concentration from 30 nM to 1000 nM, reduced τ for cells expressing wild type from 11.3 ± 1.5 min (N = 8) to 1.6 ± 0.04 min (N = 8). The ΔI_{PR}^{Norm} increased with increasing concentration of NE from 0.22 ± 0.02 at 30 nM to 0.75 ± 0.05 at 1000 nM (Figure 3-8 D). The τ and ΔI_{PR}^{Norm} for cells expressing the $\alpha\beta\gamma_{V182G;\ V193G}$ mutant were also concentration dependent (Figure 3-8 B and D). Time constants decreased from 13.8 ± 3.2 min (n = 8) at 30 nM NE to 5.9 ± 0.3 min (N = 8) at 1000 nM NE and ΔI_{PR}^{Norm} increased from -0.02 ± 0.04 to 0.52 ± 0.02. The concentration dependence of current activation suggests a first approximation of the mechanism of activation of current by NE and PE. Because only one exponential component was present in the fitting of the time courses, the reciprocal of the derived time constants were taken as a pseudo-first-order rate coefficient, k_{obs}. For wild type ENaC, the pseudo-first-order rate constant (k_{obs}) showed saturation behavior with respect to the added enzyme concentration (Figure 3-8 C). From the saturation at relatively slow rates, assuming that the enzyme concentration in the chamber was not altered by concentration dependent autolysis and that the enzyme concentration is in a large excess over its target ENaC, apparent kinetic parameters were derived based on 3-5 by non-linear regression of k_{obs} against the added enzyme concentration.

In cells expressing wild type ENaC the K_M was 570 ± 240 nM and the k_{cat} was 14.4 ± 2.11 • 10^{-3} s^{-1}. When the $\alpha\beta\gamma_{V182G;V193G}$ was expressed the k_{obs} showed a dependence on enzyme concentration (Figure 3-8 C). The dependence of k_{obs} on enzyme concentration, in contrast to wild type ENaC, did not show an apparent saturation; consequently the parameters k_{cat} and K_M could not be calculated. One reason why this arises may be because the concentration of NE used was well below the K_M. A linear regression was performed under the assumption that [E] << K_M. The slope of the regression, k_{cat}/K_M, was 1,300 ± 200 • $M^{-1}s^{-1}$. This quotient, represents the efficiency of NE activation of the $\gamma_{V182G;V193G}$ double mutant. This quotient for wild type

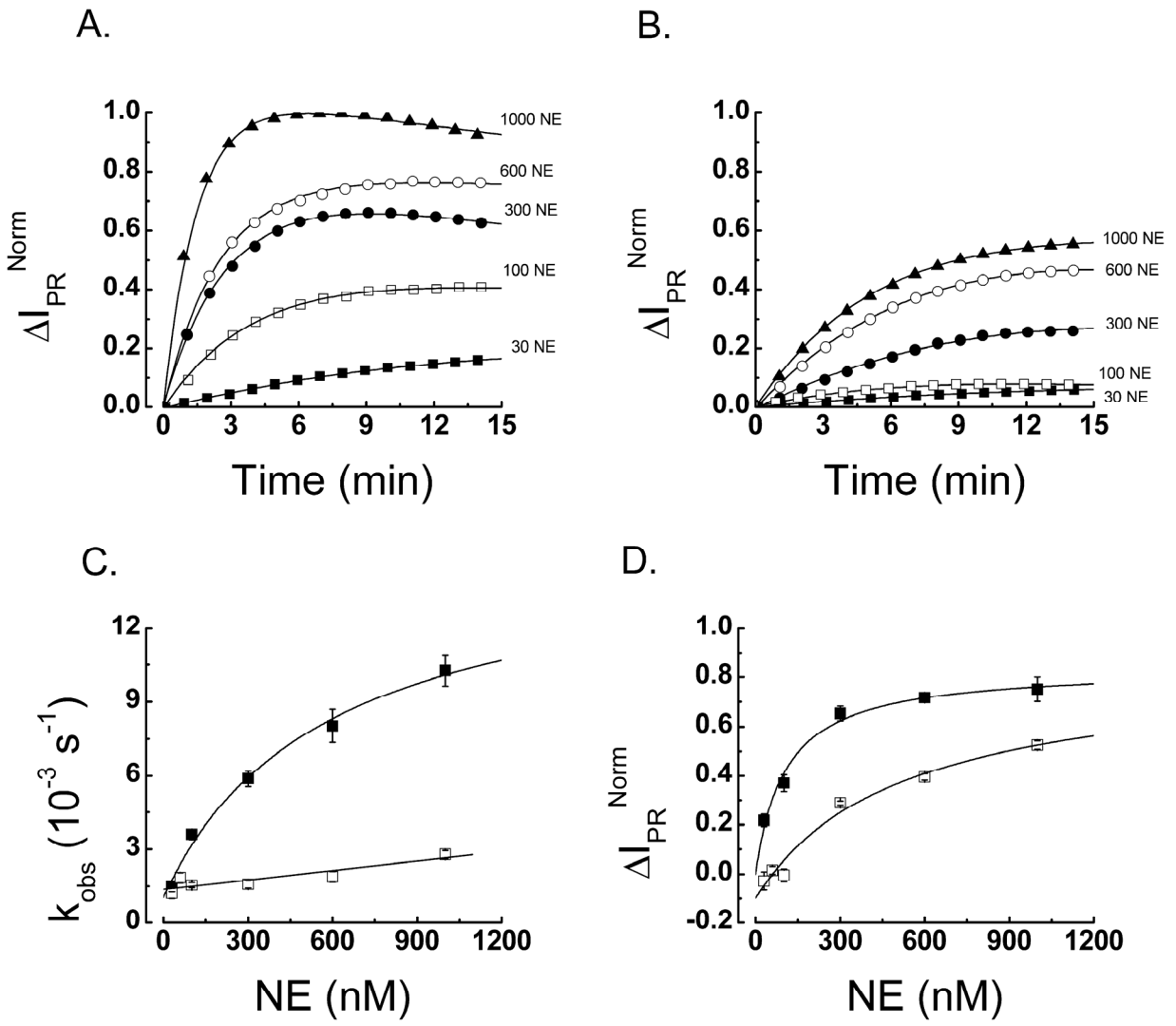

Figure 3-8 NE concentration dependence of the activation of ENaC

(A) Representative ΔI_{PR}^{Norm} responses FRT cells expressing wild type ENaC to 30 nM NE (*solid squares*), 100 nM NE (*open squares*), 300 nM NE (*solid circles*), 600 nM NE (*open circle*s) and 1000 nM NE (*solid triangles*). (B) Representative ΔI_{PR}^{Norm} responses in FRT cells expressing $\alpha\beta\gamma_{V182G;V193G}$ to 30 nM NE *(solid squares*), 100 nM NE (*open squares*), 300 nM NE (*solid circles*), 600 nM NE (*open circles*) and 1000 nM NE (*solid triangles*). (C) Mean (± SEM, n = 7-8) of k_{obs} (= $1/\tau$) with respect to the NE concentration for FRT cells expressing wild type *(solid squares*) and $\alpha\beta\gamma_{V182G;V193G}$ (*open squares*) ENaC. The solid line through the solid squares is the predicted values from a fit of the wild type data set to a kinetic model (see results) are k_{cat} = 14.2 10^{-3} s^{-1} and K_M = 570 nM. The solid line through the open squares is a linear regression of the $\alpha\beta\gamma_{V182G;V193G}$ data set with slope 1,300 M^{-1} s^{-1} ($p < 0.05$). (D) Steady state ΔI_{PR}^{Norm} (± SEM, n= 7-8) ratios for wild type (*solid squares*) and $\alpha\beta\gamma_{V182G;V193G}$ mutant (*open squares*). Solid lines are fits of the data sets to saturation kinetics. $K_{1/2}$ was 89 and 470 nM respectively.

ENaC was calculated from the fitted parameters and was ~ 24,500 $M^{-1}s^{-1}$. Thus NE efficiency for activating wild type ENaC is ~ 20 times that for activating the $\alpha\beta\gamma_{V182G;V193G}$ mutant. The $\Delta I_{PR}{}^{Norm}$ current plateau values at each NE concentration were also fitted to a saturation curve of the form $\Delta I_{PR}{}^{Norm} = \frac{(\Delta I_{PR}{}^{Norm})^{max}\,[E]}{K_{1/2} + [E]}$ where $(\Delta I_{PR}{}^{Norm})^{max}$ is the maximum increase and $K_{1/2}$ is the enzyme concentration at half maximal stimulation. For NE on wild type ENaC the $K_{1/2}$ was 100 ± 18 nM, and $(\Delta I_{PR}/I_{Tryp})^{Max}$ was 0.84 ± 0.04. For NE on the $\alpha\beta\gamma_{V182G;V193G}$ mutant, $K_{1/2}$ was 510 ± 162 nM and $(\Delta I_{PR}{}^{Norm})^{Max}$ was 0.94 ± 0.14. Consequently, the apparent affinity for NE activation of I_{Na} is ~ 5 fold weaker for the $\alpha\beta\gamma_{V182G;193G}$ mutant compared to wild type ENaC.

A concentration dependence of activation was also observed for PE activation of the I_{Na}. The same analysis as described above was carried out for the PE data sets. For wild type ENaC, the saturation behavior of the activation rate (Figure 3-9 A) had a K_M of 204± 140 nM and k_{cat} was 11.4 ± 1.34 • 10^{-3} s^{-1}. For the mutant $\alpha\beta\gamma_{V182G;193G}$, the dependence of k_{obs} on PE concentration was well defined, in contrast to what was observed for NE. Unlike NE's effect on this mutant, there was saturation with PE demonstrating a K_M of 290 ± 51 nM and a k_{cat} of 8.7 ± 0.39 • 10^{-3} s^{-1}. Therefore, unlike for NE activation of I_{Na} these mutations had a minimal effect on PE activation of I_{Na}. The parameters for the $\Delta I_{PR}{}^{Norm}$ versus concentration were $K_{1/2}$ of 77 ± 30 nM and 35 ± 9.2 nM for both wild type and $\alpha\beta\gamma_{V182G;V19G}$ respectively and $(\Delta I_{PR}{}^{Norm})^{Max}$ were 0.7 ± 0.2 and 1 ± 0.05 respectively. Clearly for both wild type and $\alpha\beta\gamma_{V182G;V193G}$ activation saturation occurred at low enzyme concentrations (Figure 3-9 B) and no difference could be discerned between the two constructs. In contrast to these minor effects the concentration dependence of PE activation of I_{Na} in the $\alpha\beta\gamma_{A190G}$ mutant was significantly impaired. The k_{obs} increased slowly with enzyme concentration showing no apparent saturation (Figure 3-9 A). Linear regression gave k_{cat}/K_M of ~ 550 M^{-1} s^{-1}. Thus PE activation of wild type ENaC was ~ 100 fold more efficient than PE activation of $\alpha\beta\gamma_{A190G}$. This loss in efficiency is accompanied by a 15-fold increase of the $K_{1/2}$ for $\Delta I_{PR}{}^{Norm}$ to 1140 nM (Figure 3-9 B).

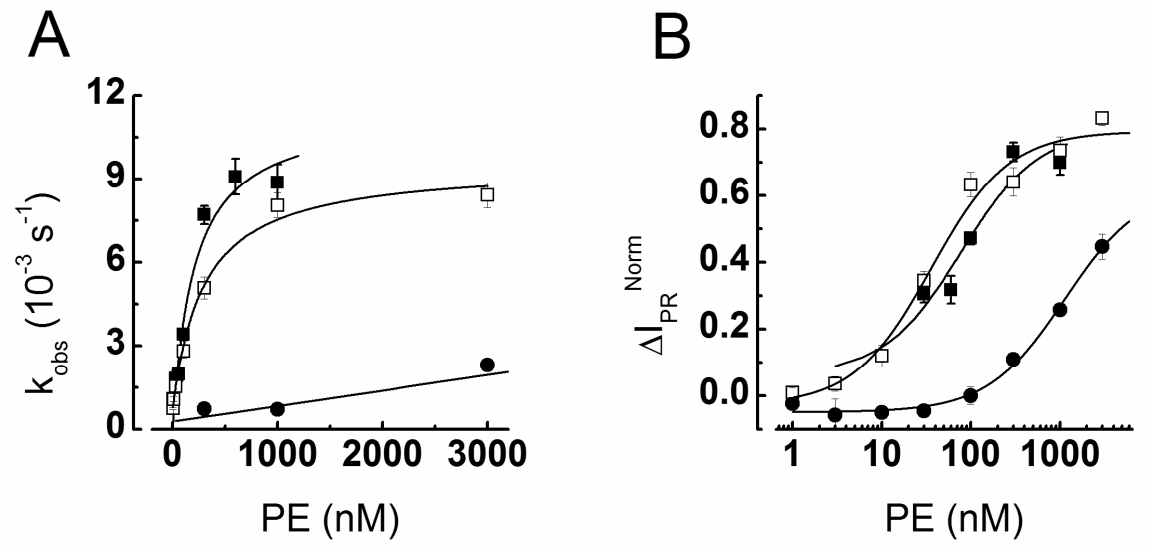

Figure 3-9 PE concentration dependence of the activation of ENaC

(A) Mean (± SEM, n = 8) of k_{obs} with respect to the PE concentration for FRT cells expressing wild type (*solid squares*) and $\alpha\beta\gamma_{V182G;V193G}$ ENaC (*open squares*) and $\alpha\beta\gamma_{A190G}$ ENaC (*solid circles*). The solid lines are the kinetic fits of the data as described in RESULTS; fitted parameters k_{cat} and K_M were 11.4 $\bullet 10^{-3}$ s^{-1} and 204 nM for wild type ENaC; 8.7 $\bullet 10^{-3}$ s^{-1} and 294 nM for $\alpha\beta\gamma_{V182G;V193G}$. Linear regression of the k_{obs} versus PE concentration for $\alpha\beta\gamma_{A190G}$ gave a slope of 550 M^{-1} s^{-1} ($p < 0.05$). (D) ΔI_{PR}^{Norm} (mean ± SEM, n = 8) ratios for wild type (*solid squares*) and $\alpha\beta\gamma_{V182G;V193G}$ (*open squares*) mutant. Solid lines are fits to saturation kinetics. $K_{1/2}$ was 77, 35 and 1140 nM respectively

3.2.6 NE and PE cleavage of the γ ENaC segment

Next NE and PE were evaluated for their ability to cleave the identified region of γ ENaC and the specific proteolytic sites were determined by MALDI-TOF mass spectrometry. The peptide T^{176}-S^{198} (200 μM), corresponding to the amino acid sequence T176 to S198 of the γ ENaC subunit, was incubated with 200 nM NE or PE in tris-acetate buffer. MALDI-TOF mass spectrometry showed the undigested peptide T^{176}-S^{198} at m/z of 2546.6. Incubation of peptide T^{176}-S^{198} with NE for 5 minutes resulted in a new peak at 1950.9 corresponding to the molecular weight of peptide T^{176}-V^{193} as well as a new peak at 615.3 corresponding to the peptide M^{194}-S^{198} along with undigested full length peptide at 2547.1 (Figure 3-10 A). Mass spectrometry of the PE digest showed the appearance of new peaks at 1650.8 and 915.2 corresponding to peptides T^{176}-A^{190} and S^{191}-S^{198} respectively (Figure 3-10 B). These fragments indicated that NE

hydrolyzed the peptide between V193 and M194 primarily whereas PE hydrolyzed the peptide between A190 and S191. Cleavages at the specific sites were detected within 1 minute of incubation. After prolonged incubation with NE (30 min), a peak at 886.0 corresponding to the peptide T^{176}-V^{182} was also evident but minor (data not shown) suggesting that cleavage by NE can occur between V182 and G183 but is not efficient. Consequently, a sequence within γ ENaC is cleaved by NE and PE and the cleavage sites correspond to the residues that mediate channel activation by the enzymes.

A

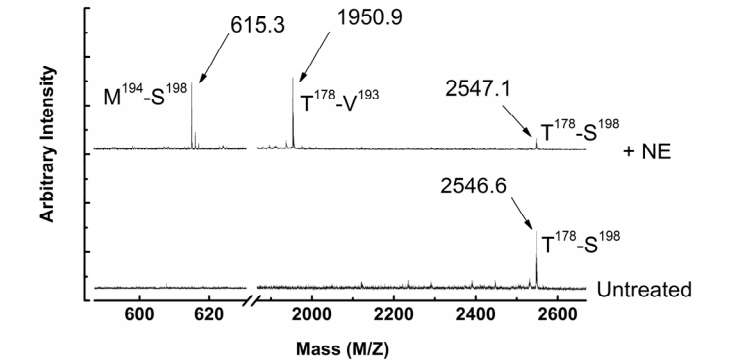

B

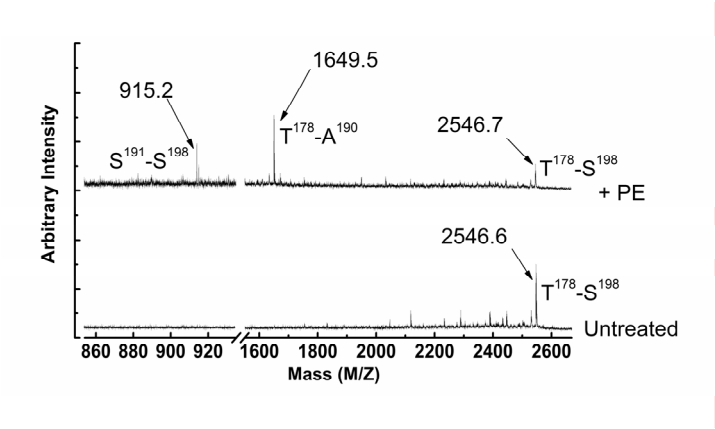

C

Figure 3-10 Localization of cleavage sites for NE and PE in a segment of the γ ENaC subunit

(A) MALDI-TOF mass spectra of the untreated peptide T^{176}-S^{198} corresponding to the amino acid sequence in γ ENaC (lower trace). Upper trace is the mass spectra of the peptides obtained after a 5 minute digestion of peptide T^{176}-S^{198} by NE at 37^0C, pH 7.4. (B) Mass spectra of untreated peptide T^{176}-S^{198} (lower trace) and peptides obtained after a 5 minute digestion with PE at 37^0C (upper trace). Tracings are representative of three independent experiments each. (C) The amino acid sequence of peptide T^{176}-S^{198} indicating the location of the deduced cleavage sites by NE and PE.

3.2.7 Thrombin Activation of ENaC

To investigate the idea that channel activation could be mediated by proteolysis at either γ182, γ193 (from NE results), or γ190 (from PE results), the γ 186 to 190 sequence (IIHKA) was changed to γ 186…LVPRG to give the mutant called $\alpha\beta\gamma_{Th}$. The lvprgs sequence, where thrombin cleaves after R, matches the specific thrombin cleavage site on bovine factor XIII (181) and is often used for cleavage of fusion proteins (93). Aprotinin is not known to inhibit thrombin (12, 146, 161). Human α thrombin (TH), in contrast to NE and PE, did not elicit significant current increases in FRT cells expressing wild type ENaC which were aprotinin pretreated (Figure 3-11 A and C). The baseline I_{Na} (9.8 ± 1.44 μA/cm^2) was unchanged after 300 nM TH (11.5 ± 0.91 μA/cm^2) but subsequent trypsin addition increased I_{Na} to 23.7 ± 0.65 μA/cm^2 (n = 8). For cells expressing $\alpha\beta\gamma_{Th}$, 300 nM TH elicited rapid current increases (Figure 3-11 B C and D) as did 300 nM NE. On average, TH increased I_{Na} from a baseline of 14.3 ± 1.32 to 23.8 ± 1.17 μA/cm^2 which was not significantly further increased by trypsin addition (24.9 ± 0.72 μA/cm^2; n = 8). A comparison of the $\Delta I_{PR}{}^{Norm}$ (Figure 3-11 D) showed that while NE and PE activated wild type ENaC (0.6 ± 0.02 and 0.7 ± 0.01, n = 8-16), TH had only a small effect (0.1 ± 0.02, n = 4). On the other hand TH activated $\alpha\beta\gamma_{Th}$ (0.9 ± 0.02, n = 8) as did NE (0.7 ± 0.04, n = 4). Interestingly, while NE also activated $\alpha\beta\gamma_{Th}$, activation of $\alpha\beta\gamma_{Th}$ by PE was significantly impaired (0.2 ± 0.04, n = 4). This result was consistent with the change of γ190A to G, which previously led to inhibited responses to PE. The activation of $\alpha\beta\gamma_{Th}$ by thrombin was similar to activation of wild type ENaC by NE and PE showing a concentration dependence of both the k_{obs} and steady-state $\Delta I_{PR}{}^{Norm}$ (Figure 3-11 E and F). The k_{cat} was 10.1 ± 0.13 10^{-3} s^{-1}, K_M was 340 ± 19.5 nM and $K_{1/2}$ was 14.8 ± 1.98 nM.

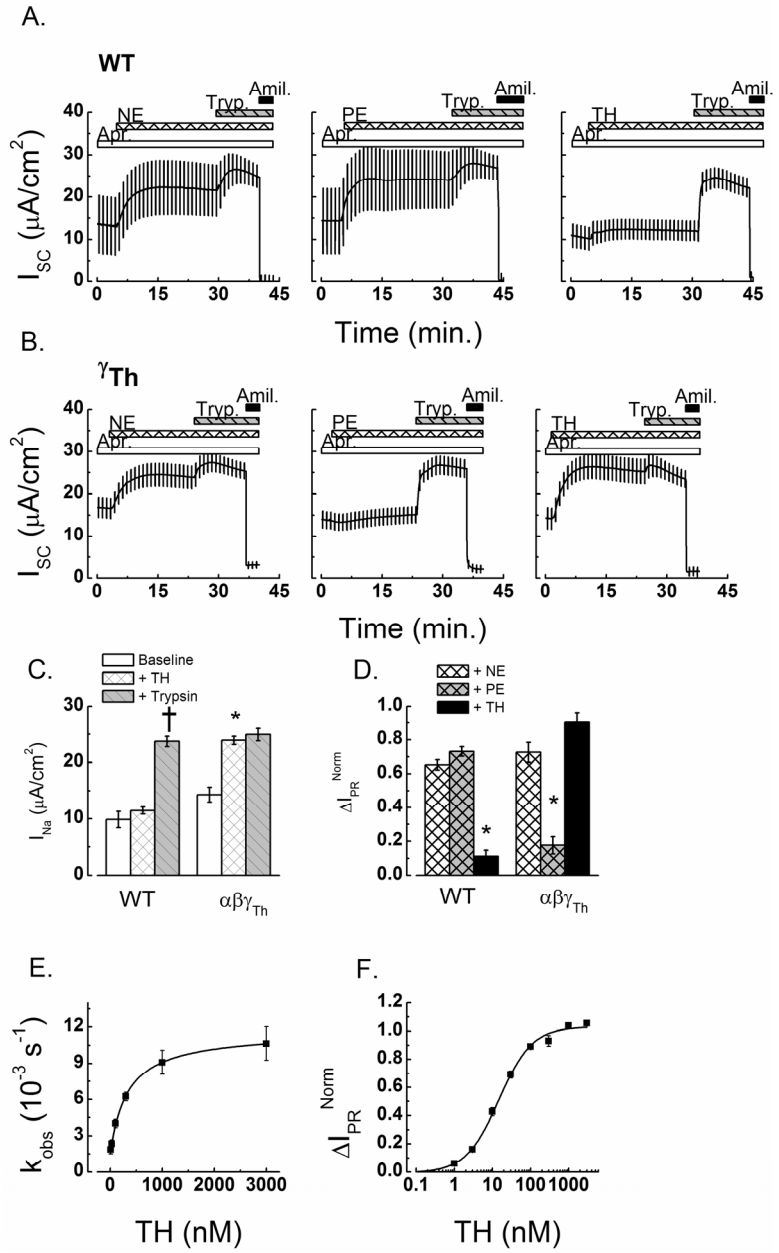

Figure 3-11 Thrombin dependent activation of ENaC via thrombin sequence insertion

(A) Addition of NE, PE and TH (300 nM) to FRT cells expressing wild type ENaC or (B) FRT cells expressing $\alpha\beta\gamma_{Th}$ (γ186…iihka → γ186…lvprg) ENaC pretreated with aprotinin (10 μM) for the indicated period. Trypsin (15 μM) and amiloride (50μM) were added as indicated. (C) I_{Na} (mean ± SEM, n = 8) in FRT cells expressing wild type and $\alpha\beta\gamma_{V182G;V193G}$ at baseline (open bars) and subsequent to 300 nM TH (*hatch bars*) and 15 μM Trypsin (*stripped bars*). * $P < 0.05$ t test comparison of I_{Na} at baseline with I_{Na} after TH and † $P < 0.01$, t test comparison of I_{Na} after TH with I_{Na} after trypsin. (D) Summary of the effect of NE (open bars), PE (grey bars) and TH (black bars) on wild type and $\alpha\beta\gamma_{Th}$ ENaC as measured by ΔI_{PR}^{Norm} (mean ± SEM, n = 8). *$P < 0.05$, one way ANOVA and t test comparison with wild type. (E) The concentration dependence of k_{obs} (mean ± SEM, n = 5) and (F) ΔI_{PR}^{Norm} (mean ± SEM, n = 5) for TH activation of current for $\alpha\beta\gamma_{Th}$. Solid lines are fits to the data as described in Methods. Parameters k_{cat} and K_M were $10.1 \cdot 10^{-3}$ s^{-1} and 340 nM. The half maximal concentration for ΔI_{PR}^{Norm} was 15 nM.

The proteolytically inactive D-phenylalanyl-L-prolyl-arginine-chloromethyl ketone-thrombin (FPRCK-TH) has its active site blocked (94) and shows no ability to activate I_{Na} in aprotinin inhibited FRT cells expressing the $\alpha\beta\gamma_{TH}$ construct (Figure 3-12). The I_{Na} before addition of FPRCK-TH was 19.6 ± 1.56 μA/cm^2, 17.9 ± 1.65 μA/cm^2 after a twenty minute exposure to 1 μM FPRCK-TH and increased to 32.2 ± 2.39 μA/cm^2 after addition of trypsin (n = 4).

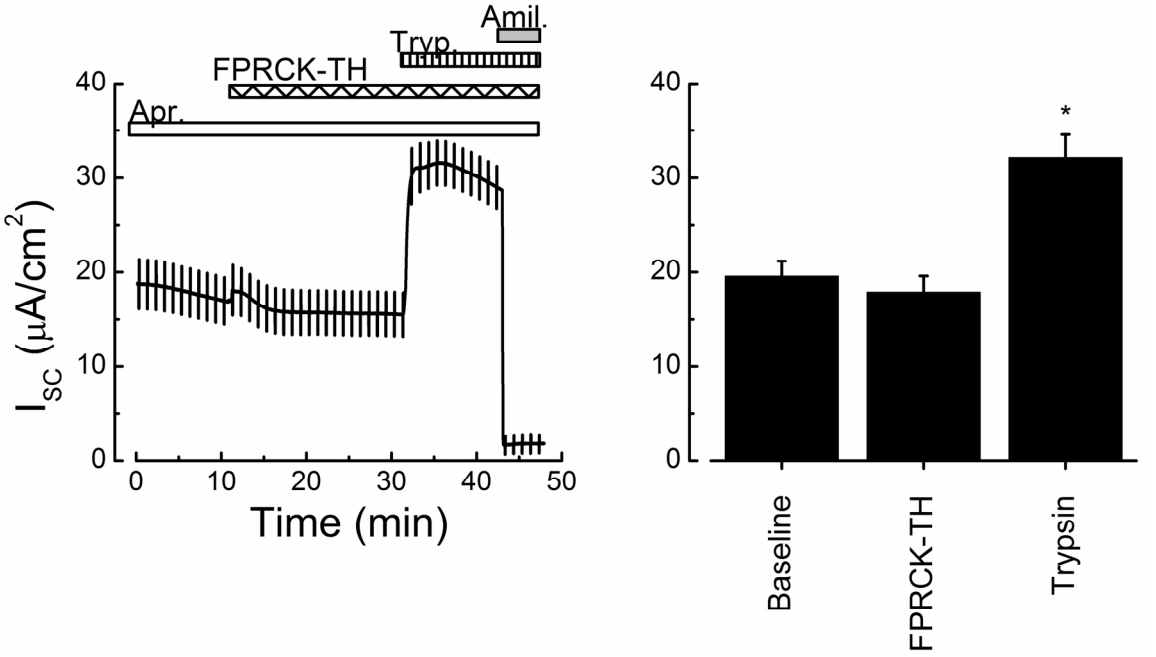

Figure 3-12 Inactivated thrombin does not active I_{Na}

A) Representative short-circuit current tracing of FRT cells expressing $\alpha\beta\gamma_{TH}$ pre-incubated with aprotinin. Addition of 1 μM FPRCK-TH where indicated showed no stimulatory effect on I_{SC}. B) I_{Na} (mean ± SEM, n = 4) before addition of FPRCK-TH, 20 minutes after addition of 1 μM FPRCK and the maximum value observed after addition of trypsin. * $p < 0.01$

3.3 DISCUSSION

The studies reported here were made possible by the development of a tricistronic plasmid (hENaC) expressing all three human ENaC subunits. Cell lines stably expressing wild type and mutant ENaC could be selected using a single antibiotic. FRT cells were chosen because they are readily transfected, do not express any native rat ENaC and form a moderately tight epithelium (1 to 2 k Ωcm^2). Previous studies in FRT cells using three separate ENaC subunit plasmids have shown ENaC is targeted to the apical membrane allowing one to use standard transepithelial short circuit current (I_{SC}) measurements to study channel activity (105, 171, 175). Our studies reveal hENaC-FRT cells respond to aldosterone and dexamethasone treatment in a manner similar to native ENaC expressing epithelia (65). Since the expression of the ENaC subunits in the hENaC-FRT cells is driven by separate CMV promoters the stimulatory effects of the steroids on sodium transport must be mediated by other steroid responsive effectors such as enhanced Na^+K^+-ATPase activity, up-regulation of SGK (serum and glucocorticoid regulated kinase) and/or down regulation of Nedd 4-2. Thus, the hENaC tricistronic plasmid and stably transfected FRT cells offer an additional model to study steroid stimulation of sodium transport.

3.3.1 Aprotinin Sensitivity of FRT Cells

Approximately 50% of the I_{Na} in the hENaC-FRT cells was inhibited by the serine protease inhibitor aprotinin. A similar aprotinin inhibitory effect on I_{Na} of 50 to 80% has been observed in a number of epithelia that natively express ENaC and includes: toad urinary bladder (118, 137) amphibian (4, 191) and murine (116, 132) renal epithelia and human bronchial (25) nasal (49) and alveolar (147) epithelia. One may infer from these observations that there exists an aprotinin sensitive protease responsible for ENaC activation. Support for this notion comes from the cloning of several membrane proteases that when co-expressed with ENaC cause channel activation (8, 191, 200). The inhibitory effects of aprotinin on I_{Na} can be reversed by aprotinin washout or by the addition of excess exogenous proteases such as trypsin and elastase and this too was observed in the hENaC-FRT cells. The aprotinin effect is consistent with the notion that activation of channels by proteases at the apical membrane is blocked by aprotinin producing a time-dependent reduction of the number of active channels (4) that results from internalization or

degradation of already activated channels. Channels newly arriving at the apical membrane then form a pool that can be activated by exogenous proteases. In the studies reported here we used the hENaC-FRT cells and site-directed mutagenesis of hENaC together with the amino acid preferences of human neutrophil (NE) and porcine pancreatic (PE) elastase to determine whether there is a direct interaction between ENaC and proteases in the channel activating process. The activation of ENaC by extracellular proteases may result from protease interaction with a protease responsive receptor which subsequently activates ENaC or from a direct protease interaction with ENaC. A requirement for a diffusible 2nd messenger has not yet been identified for the protease dependent activation and in particular signaling through G proteins via protease activated receptors is not implicated (29, 37). Since it is possible that non-aqueous lipids or localized protein-protein interactions may transduce the protease signal, direct and indirect mechanisms remain distinct possibilities explaining channel activation by proteases. The results presented here suggest that the inhibition of current by the serine protease inhibitor aprotinin can be reversed by direct protease interactions with ENaC and point to a protease interaction domain in a segment of the γ subunit of the channel encompassing residues 182 to 193.

3.3.2 Direct interaction of protease and ENaC

There are several possible mechanisms whereby the aprotinin inhibition of I_{Na} can be reversed by exogenous proteases in FRT cells. The binding of aprotinin by the proteases can be ruled out since the concentrations of proteases that activate I_{Na} are much less than the aprotinin concentration and insufficient to form an aprotinin sink. In other systems, such as Xenopus oocytes and fibroblasts, activation by trypsin and NE can be seen in the absence of aprotinin. Protease dependent effects on trafficking is possible but unlikely given the observations that trypsin did not increase cell surface quantities of channel subunits (37) and is able to activate current in excised outside-out membrane patches (29). A role for trafficking is also unlikely based on the mutational studies reported here and discussed below indicating that the activation requires binding. The activation of ENaC by extracellular proteases may result from protease interaction with a protease responsive receptor which subsequently activates ENaC or from a direct protease interaction with ENaC.

There are several lines of evidence suggesting a direct protease interaction with the channel. The large extracellular domain (70%) of the ENaC/DEG family of ion channels suggests that extracellular ligand and protein-protein interactions may play a role in the physiology of these channels. Such interactions have been identified for the degenerin members of the family (184). In this report we identified a segment in the γ subunit that is involved in elastase dependent activation of the channel. This segment is in the extracellular domain just after the first membrane spanning domain (M1). The post-M1 region has been implicated in endogenous furin cleavage of γ ENaC and exogenous trypsin cleavage of ASIC1a, a member of the ENaC super family of ion channels (86, 202). The idea that the post-M1 region of γ ENaC is accessible is supported by the ability to label cell surface ENaC with antibodies directed against this region (58). Cleavage of ASIC1a changes the pH dependence of channel gating (150). Furin cleavage and trypsin activation of ENaC appear to modulate Na^+ dependence of channel gating (36, 163). The segment identified is therefore in an accessible part of the channel that is involved in channel regulation. Based on the P1 specificity of NE, a scanning mutagenesis was performed substituting glycine for the native valines that identified two residues in γ ENaC critical for NE dependent activation of ENaC. Substitutions at γV182 and γV192 specifically inhibited the activation of ENaC by NE; because neither PE, a similar protease, nor trypsin activation was significantly affected. Since the substitutions did not inhibit activation by PE and trypsin and did not affect endogenous protease activation (implied by the equivalent control currents and aprotinin sensitivity for wild type and mutant ENaC) the substitutions did not impinge upon a common protease activation pathway. The specificity provides evidence that NE interacts directly with ENaC since interaction of proteases with a different receptor that subsequently activates ENaC would result in significant cross-interaction by virtue of ENaC being the final common step in such a pathway. The results show that one residue, γA190, in the vicinity of the residues critical for NE is important for PE dependent activation of ENaC. As observed for NE, the effect is also specific since trypsin activated the γA190G mutant channels. Furthermore, in the context of the $\alpha\beta\gamma_{Th}$ construct the specificity of γA190 for PE was evident since this construct with intact γV182 and γV193 residues but with a γA190G mutation was activated by NE and TH but PE activation was impaired. The presence of a sequence recognized by the thrombin active site creates a gain of function whereby the channel, not naturally activated by thrombin, becomes a thrombin activated channel. When the thrombin active site is blocked

by FPR-chloromethyl ketone, thrombin no longer activates the channel. The substitutions that impair NE and PE dependent activation result from changing of residues that are most likely to be good substrates based on the known primary amino acid specificities of the proteases to less preferred residues. These observations concur to implicate direct protease-ENaC interactions in channel activation.

3.3.3 Dependence of activation on Binding or Hydrolysis

Inferences about the nature of the protease-ENaC interaction can be drawn from the protease activated current trajectories. From the analysis of the progress curves for current activation, the k_{obs} dependence on enzyme concentration naturally suggests that activation requires at least two steps; an initial reversible step and a secondary rate limiting activation step. If proteases interact directly with the channel, then the first step is $C + E \leftrightarrow C{\bullet}E$, a rapid equilibrium from the association of channel (C) and enzyme (E). If the reaction is limited to one step where species C•E is the activated channel, the current trajectory would contain relaxation rate constants or k_{obs} according to $k_{on}{\bullet}[E]$ + koff which represents a linear dependence of k_{obs} on enzyme concentration. Since the measured k_{obs} was not linear but hyperbolic, C•E is not the activated channel. At least one additional concentration independent step is rate limiting which may correspond to one or more possible physical states that represent the activated channel. One parsimonious interpretation is that the rate limiting step includes hydrolysis. We found that the efficiency parameter k_{cat}/K_M for NE is on the order of the k_{cat}/K_M for the highest efficiencies of NE hydrolysis of its best extended synthetic substrates (i.e. substrates encompassing amino and carboxyl ends of the scissile bond (107)). It is noteworthy that the ratio of k_{cat}/K_M for the change of V residues to G residues for NE, and A residue to G residue for PE were also consistent with k_{cat}/K_M ratios for the same P1 residue changes in synthetic substrates (107, 131, 208). In fact, the K_M determined for NE is remarkably similar to the dissociation constant for the NE alpha proteinase inhibitor complex (128). There are also examples of TH cleavage of its synthetic peptide substrates such as the protease activated receptor 1 peptides (199) and natural substrates such as protein C (44) with similar k_{cat}/K_M as observed for TH activation of current in the results presented. Hydrolysis is further suggested by the MALDI-TOF mass spectrometry performed on

the synthetic peptide which confirmed that NE cleavage is located between V193 and M194 while PE cleavage is located between A190 and S191 in the γ subunit.

The results of the kinetic analysis of the progress curves and peptide T^{176}-S^{198} digestions are consistent with hydrolysis dependent activation but cannot exclude other possibilities. These include the possibility that the k_{cat} represents a rate limiting intramolecular rearrangement occurring long after cleavage, perhaps related to the Na^+ self inhibition of the channel (36, 163) or removal of an inhibitory domain (32). Secondarily, protease binding to the channel is sufficient to create a rate limiting step including binding dependent prevention of tonic inhibition by an ENaC cofactor or binding induced conformational changes that directly activates the channel. Experiments so far do not rule out the latter two as it can be imagined that a binding induced conformational change is sufficient to activate the channel; and an accompanying hydrolysis ensues but has no significance. That the results are consistent with hydrolysis is in line with other studies showing that ENaC expressed at the apical membrane can be cleaved by furin and this cleavage correlates with channel activity (87). Also, the extent of channel cleavage correlates inversely with the trypsin activation of current (105) suggesting that once cleaved by endogenous proteases, channels may no longer be activated by trypsin. There is however evidence suggesting that the aprotinin-sensitive, trypsin-activated current may not be related to the cleavage patterns observed. In alveolar epithelial cells expressing CAP1, and ENaC-mediated I_{Na} sensitive to aprotinin inhibition and trypsin reversal, a presumably cleaved fragment of the α subunit is expressed at the apical membrane (147). The abundance of this fragment was not affected by aprotinin. In A6 cells, aprotinin inhibition of I_{Na} did not change the relative abundance of the low molecular weight species of the α subunit, nor have any effect on the γ subunit (4). These results are not entirely irreconcilable with cleavage mediated activation. If there is endogenous cleavage of the γ subunit at γ138R (86), it appears this cleavage is not sensitive to aprotinin. Nevertheless, it was recently shown that mouse CAP1 lacking a catalytic triad retained the ability to activate ENaC (8). Therefore, furin independent catalytic and non catalytic mechanisms remain likely possibilities in channel activation by proteases. Further experiments are needed to determine if the catalytic activity of the exogenous proteases is required or if binding is sufficient for activation.

3.3.4 Relevance to physiological regulation of ENaC

These results of this study have important implications for ENaC regulation by proteases. First, extracellular proteases can produce a graded Na^+ transport response over a short time scale. If hydrolysis is irreversible, then eventual activation of all channels should occur over extended periods. From the results, the plateau current elicited by NE, PE and TH correlates with the rate of activation. The plateau values may result from a steady-state between protease activation and channel inactivation. The turnover time for ENaC in the membrane varies considerably from biochemical measurements from a few minutes to several hours (6, 75, 204). However, functional experiments in FRT cells suggest a turnover time for channels of ~ 30 min (171). If the NE and PE activated channels in FRT cells in the present study have the same turnover time as channels in the baseline condition, then the steady-state current would depend on the rate of protease activation. By changing the rate of protease activation, up- and down-regulation of epithelial Na^+ transport can be achieved within a 30 min window. Alternatively, the extent of protease activation could be altered by reducing the deactivation of channels. Recent studies showed that protease activation of ENaC could be up-regulated by maneuvers known to impair channel internalization (105). A graded response may also result from an equilibrium association of channel and protease. This association would not be a Michealis-Menten complex but involve further complex rearrangements typical of tight binding proteinase-inhibitor complexes (17). Second, predictably from the turnover times and k_{cat}, the concentration of protease needed to achieve channel activation can be quite low. This is clearly evident for the thrombin case where the half maximal concentration was ~ 15 nM. Consequently, inadvertent activation of ENaC in inflammatory states such as chronic obstructive pulmonary disease could result from the increased proteases in the local environment (180) and may be involved in exacerbation of obstructive airways disease. Thirdly, it is noteworthy that only one region was found to be critical for NE mediated activation. However, multiple furin cleavage sequences were found to be important in the α subunit and in the γ subunit (86, 163). Because of a lack of strict adherence of NE to valines at the P1 position in its substrate, the valine substitution approach may miss other important P1 positions for NE interaction. Therefore, under aprotinin-treated conditions, it cannot be ruled out that NE/PE interacts also at the α subunit. On the other hand, with TH there is reduced likelihood of such an interaction and the results would suggest

that interaction at one site in the γ subunit was sufficient for activation. Perhaps, under the aprotinin-treated conditions the α subunits are already cleaved and do not require further cleavage for channel activation. It is emphasized that these conclusions arise in the context of an aprotinin inhibited state which does not represent the nascent channel state. As a result, ENaC may be acted upon by intra- and extracellular proteases, possibly in a serial fashion, and the segment investigated in this study may represent the site of action of an endogenous protease at the apical membrane.

4.0 ENDOGENOUS PROTEASE SITES IN ENAC

In chapter 2, it was shown that the protease inhibitor aprotinin can inhibit Na^+ transport in native Na^+ transporting cells by down regulating the number of active channels. In chapter 3, the aprotinin inhibitable ENaC-mediated Na^+ transport was reconstituted in FRT cells by stable co-expression of α β and γ ENaC subunits. The heterologous system showed that protease reversal of aprotinin inhibition was accomplished through direct interactions at least at one site in the γ subunit. These findings suggest that there may be one or more endogenous proteases constitutively activating ENaC by direct interaction at one or more sites on the channel. There are a number of candidate proteases. The first is prostasin or CAP1. Prostasin is a GPI-anchored plasma membrane bound serine protease first isolated from the prostate (206). Prostasin is found in native Na^+ transporting cells such as the human airway epithelial cells (49), its mouse and amphibian homologues have been isolated in renal Na^+ transporting epithelial cells (191, 201). Prostasin can up-regulate ENaC activity in Xenopus oocytes, a phenomenon that can be inhibited by aprotinin. Cells with reduced prostasin expression show reduced Na^+ transport (188). Two other membrane associated proteases, CAP2 and CAP3, are transmembrane proteins with serine protease activity that can also up-regulate ENaC activity in Xenopus oocytes (200). The up-regulation mediated by CAP3 can be inhibited by aprotinin. A fourth candidate is furin which is a transmembrane member of the subtilisin-like serine protease family called pro-protein convertases (PCs) that cycles between the plasma membrane and the trans golgi network. PC family members are involved in processing of proteins on the secretory pathway such as hormones (e.g. insulin) and receptors as well as modifying bacterial and viral toxins. The furin directed serine protease inhibitor α1 antitrypsin Pittsburgh (α1PDX) inhibited Na^+ transport in renal CCD cells while furin deficient Chinese hamster ovary cells had reduced Na^+ transport (86).

A commonality amongst the proteases is their substrate sequence specificities. Prostasin, CAP3 and PCs hydrolyze after arginine residues but they also have extended substrate sequence preferences. Minimally, the proteases can cleave $RXXR^{\downarrow}$ residues, where X is any amino acid. Prostasin, in addition to cleaving RXXR (167), also cleaves $RXR^{\downarrow}$ according to a peptide substrate screen by Dr. Yi Cheng in our laboratory (personal communication); as does CAP3 (182). The PCs cleave at sequences $R(X_n)R^{\downarrow}$ where n = 0, 2, 4, or 6 (101). These sequences, heretofore referred to as polybasic sequences, are present in the α and γ ENaC subunits and some have been shown to mediate the activation of Na^+ transport when ENaC is expressed in Xenopus oocytes (86). The fact that several proteases implicated in ENaC regulation share specificities for arginine rich polybasic sequences increases the likelihood of redundancy. Such redundancy has been noted in the processing of several proteins by the PC family members furin, paired basic amino acid cleaving enzyme 4 (PACE4) and PC7 or PC8 (185). The protease inhibitor aprotinin, shown to inhibit Na^+ transport in chapter 1 inhibits prostasin and prevents its ability to up-regulate Na^+ transport (191, 206), but may also inhibit other serine proteases. Furin is however not inhibited by aprotinin (Yi Cheng, personal communication) and the effect of aprotinin on other members of the PC family has not been reported. Similarly, α1PDX inhibits other PCs in addition to furin (60). These inhibitors do not allow for distinguishing the specific proteases mediating channel activation in a given cell. Thus depending on the cell type, different proteases may cleave the same sites to activate the channel. Therefore the mutations carried out only test the idea that ENaC could be activated by an endogenous protease but cannot distinguish among the endogenous proteases.

In this chapter some preliminary findings on the effect of the polybasic sequences in α and γ ENaC subunits on activation of ENaC currents in FRT cells are presented. The experiments were carried out to investigate which sequences were important for the spontaneous Na^+ transport rate and which sequences were important for the aprotinin regulated component of the Na^+ transport rate. Furthermore, the possible importance of the polybasic sequences in the activation of ENaC by exogenous NE and PE were also tested to determine if multiple proteases are required to act sequentially for activation of ENaC-mediated current. The findings suggest several future experiments that may elucidate the mechanism of activation by different proteases.

Site-directed mutagenesis, cell culture and transfection, evaluation of I_{Na} and statistical analysis were carried out as described in section 3.1. Dexamethasone pre-stimulated cells were used throughout the experiments.

4.1 RESULTS

4.1.1 Effect of mutations at putative protease sites on expression of spontaneous I_{Na}

The sequences α_RSR[177], α_RSRR[178], α_RDLR[181], α_RRAR[204] and γ_RKRR[138] represent minimal recognition sequences for one or more of the putative proteases that could activate ENaC-mediated Na^+ transport. The final residue in each sequence represents the P1 position; hydrolysis can be expected at the peptide bond immediately after this residue. Mutation of the P1 position from R to a non-basic amino acid should prevent hydrolysis by the putative ENaC activating proteases at that point. The Na^+ current was measured in cells expressing wild type ENaC (αβγ) and the mutant constructs $\alpha_{R177A}\beta\gamma$, $\alpha_{R178A}\beta\gamma$, $\alpha_{R181A}\beta\gamma$, $\alpha_{R204}\beta\gamma$, $\alpha_{R178A;R204A}$, and $\alpha\beta\gamma_{R138A}$. The average I_{Na} is shown in Table 4-1 for each construct.

Table 4-1 The spontaneous I_{Na} in cells expressing αβγ and selected mutant ENaCs

[a] The difference in currents before and after addition of trypsin
* $P < 0.05$, student's t test versus αβγ.

Construct	I_{Na} (± SEM)		[a]ΔI_{Na} (± SEM)	N
	Baseline	+ Trypsin		
		$\mu A/cm^2$	$\mu A/cm^2$	
αβγ	27.6 ±0.93	28.4 ± 0.90	0.8 ± 0.34	119
$\alpha_{R177A}\beta\gamma$	25.7 ± 1.56	28.9 ± 0.77	3.3 ± 1.27*	12
$\alpha_{R178A}\beta\gamma$	29.9 ± 2.77	35.6 ± 2.70*	5.8 ± 3.00*	9
$\alpha_{R181A}\beta\gamma$	38.7 ± 1.21*	41.3 ± 0.80*	2.6 ± 0.69	12
$\alpha_{R204A}\beta\gamma$	35.3 ± 1.35	38.2 ± 1.40*	2.85 ± 0.80	12
$\alpha_{R178A;R204A}\beta\gamma$	24.7 ± 2.57	34.7 ± 1.94*	10.0 ± 1.55*	20
$\alpha_{R138A}\beta\gamma$	19.9 ± 1.77	31.3 ± 2.31	11.5 ± 1.24*	55

The baseline I_{Na} of αβγ and several mutants were ~ 30 μA/cm^2. The $\alpha_{181A}\beta\gamma$ demonstrated significantly higher baseline current (38.7 ± 1.21 μA/cm^2) whereas $\alpha\beta\gamma_{R138A}$ demonstrated significantly reduced baseline current (19.9 ± 1.77 μA/cm^2) at the $p < 0.05$ level (unpaired students t test). To demonstrate if the differences in baseline I_{Na} result from different levels of protease activation, trypsin was added to the apical chamber of short-circuited FRT cells as indicated in Figure 4-1. In αβγ expressing cells trypsin induces small current increases suggesting that the baseline I_{Na} in wild type cells cannot be further significantly increased by trypsin. The I_{SC} trace for the $\alpha_{R177A}\beta\gamma$ mutant was similar to wild type showing a characteristic small increase following trypsin addition. On average I_{Na} increased by 0.8 ± 0.34 μA/cm^2 for αβγ. The increase in current (3.3 ± 1.27 μA/cm^2) for the $\alpha_{R177A}\beta\gamma$ was significantly greater than the increase in αβγ. Similarly $\alpha_{R178A}\beta\gamma$ showed significant increases in I_{Na} following addition of trypsin. The increase in I_{Na} upon trypsin addition for $\alpha_{R181A}\beta\gamma$ and $\alpha_{R204A}\beta\gamma$ was not significantly different from the increase seen with αβγ (Table 4-1). The mutants $\alpha_{R178A;R204A}\beta\gamma$ and $\alpha\beta\gamma_{R138A}$

had the most significant increase in I_{Na}, 10 ± 1.55 and 11.5 ± 1.25 μA/cm^2 respectively, following addition of trypsin.

The I_{Na} after trypsin addition averaged ~ 30 μA/cm^2 for wild type αβγ. However the mutants $\alpha_{R178A}\beta\gamma$, $\alpha_{R181A}\beta\gamma$, $\alpha_{R204A}\beta\gamma$ and $\alpha_{R178A;R204A}\beta\gamma$ had slightly elevated post trypsin I_{Na}. The other mutants did not demonstrate a trypsin activated current significantly different from αβγ. The ratio of I_{Na} at baseline to I_{Na} after addition of trypsin I_{PR}, shown in Figure **4-2**, was used to factor the possible different levels of ENaC expression for the mutant constructs. The I_{PR} for $\alpha_{R177A}\beta\gamma$ and $\alpha_{R178A}\beta\gamma$ were moderately depressed at 0.88 ± 0.05 and 0.86 ± 0.08 respectively versus 0.97 ± 0.01 for αβγ. The $\alpha_{R181A}\beta\gamma$ and $\alpha_{R204A}\beta\gamma$ were not significantly depressed at 0.94 ± 0.02 and 0.92 ± 0.02 respectively. The I_{PR} ratios were most significantly depressed at ~ 0.6 for $\alpha_{R178A;R204A}\beta\gamma$ and $\alpha\beta\gamma_{R138A}$. These results suggest that removal of the R at possible P1 positions simultaneously at α178 and α204, or at γ138 could result in a channel that is only partially activated. These partially activated channels can then respond to trypsin stimulation.

A

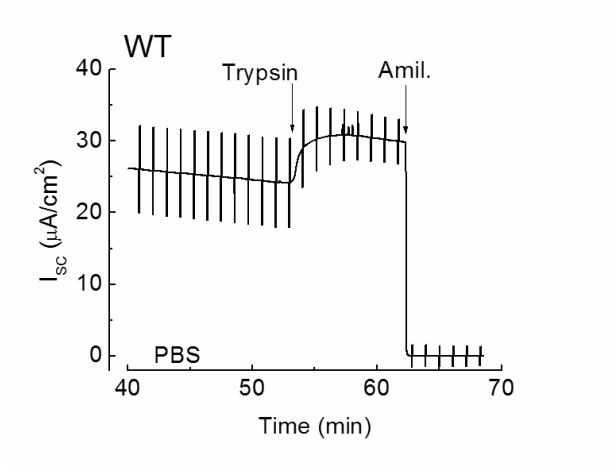
WT
Trypsin
Amil.
PBS
I_{SC} (μA/cm^2)
Time (min)

B

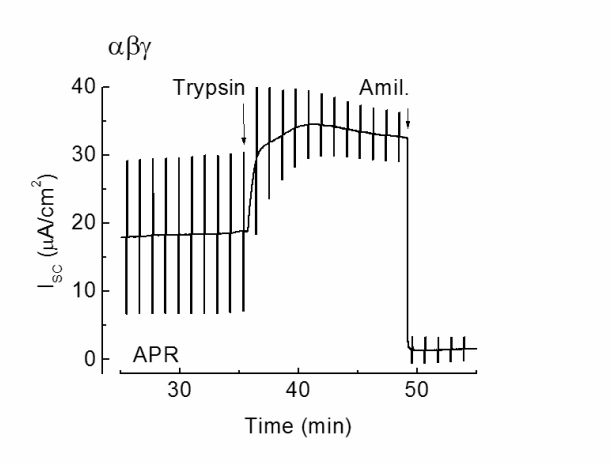
αβγ
Trypsin
Amil.
APR
I_{SC} (μA/cm^2)
Time (min)

C

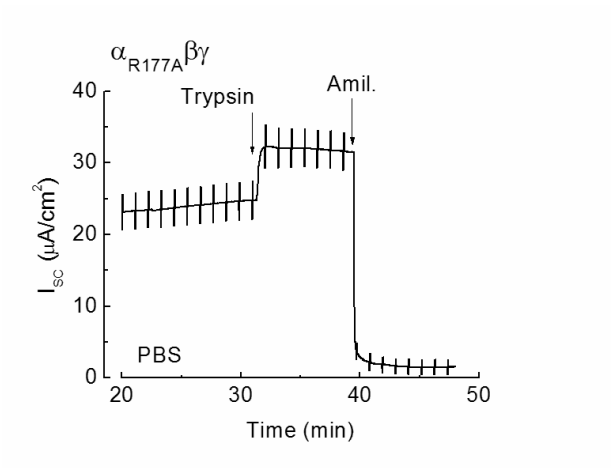
$\alpha_{R177A}\beta\gamma$
Trypsin
Amil.
PBS
I_{SC} (μA/cm^2)
Time (min)

D

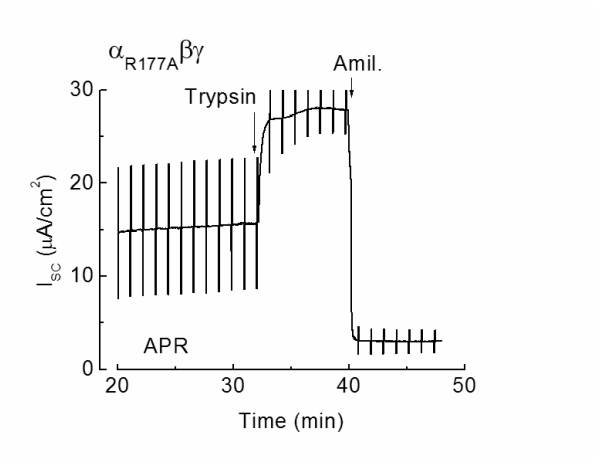
$\alpha_{R177A}\beta\gamma$
Trypsin
Amil.
APR
I_{SC} (μA/cm^2)
Time (min)

E

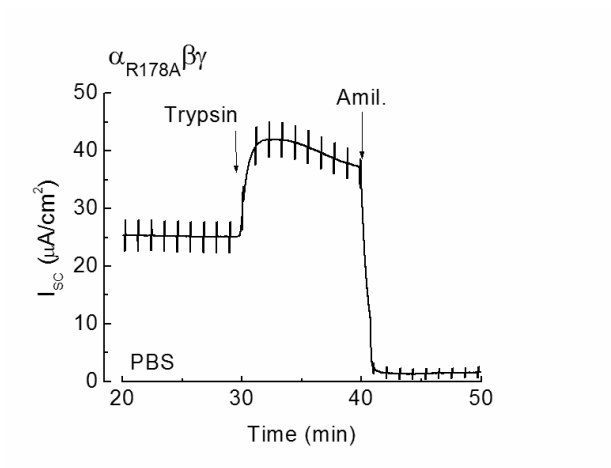
$\alpha_{R178A}\beta\gamma$
Trypsin
Amil.
PBS
I_{SC} (μA/cm^2)
Time (min)

F

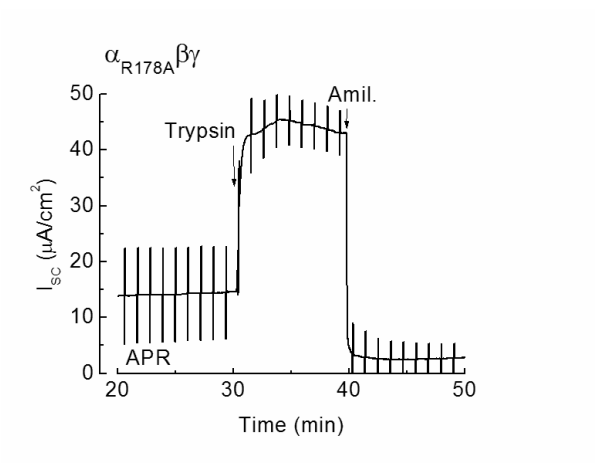
$\alpha_{R178A}\beta\gamma$
Trypsin
Amil.
APR
I_{SC} (μA/cm^2)
Time (min)

Figure 4-1 continued

G

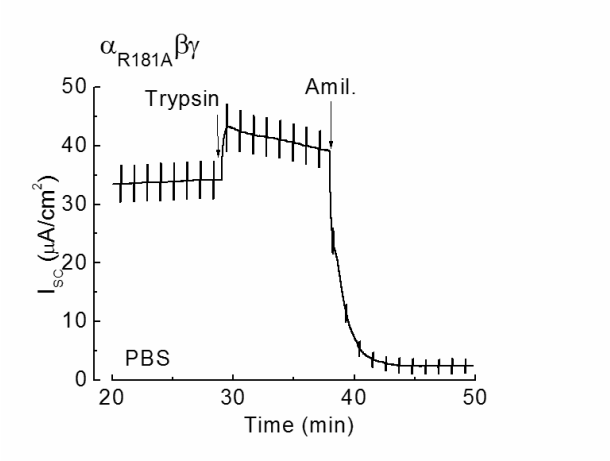

H

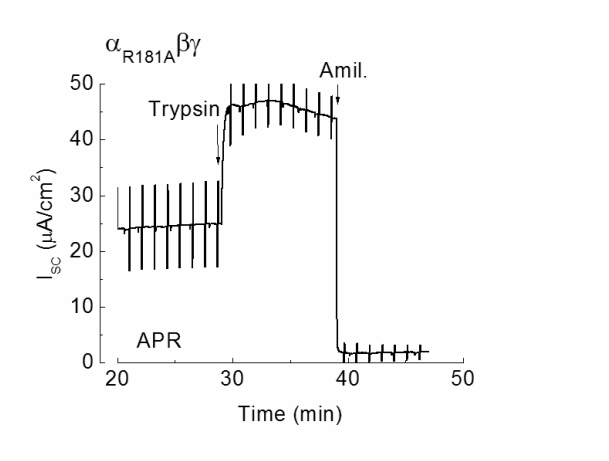

I

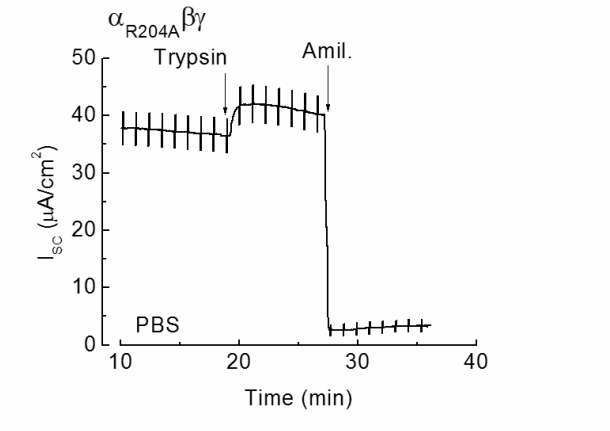

J

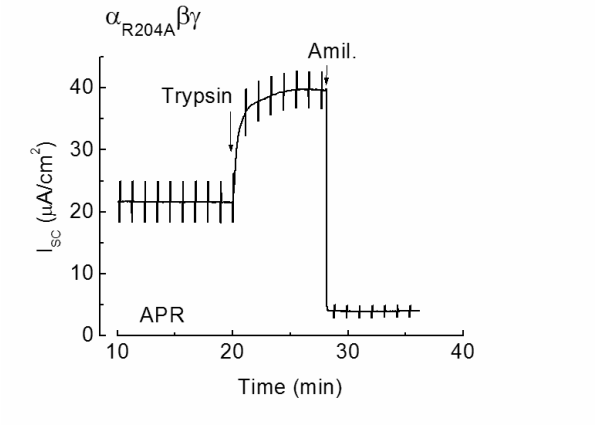

K

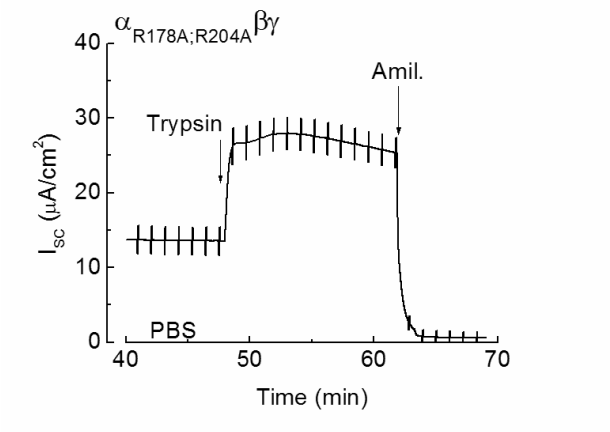

L

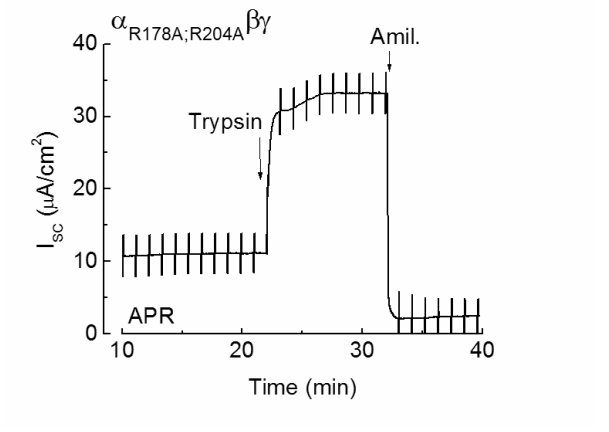

Figure 4-1 continued

M

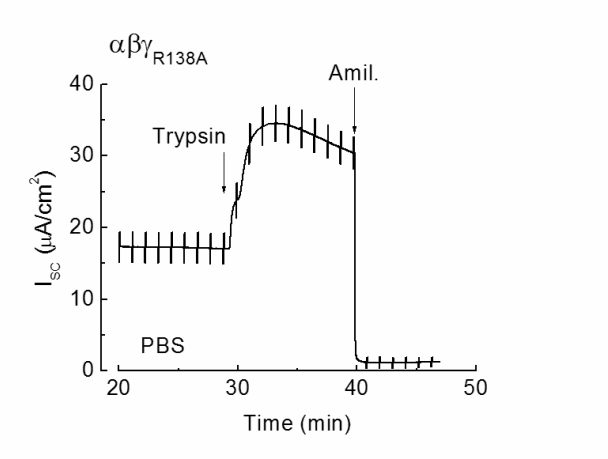

N

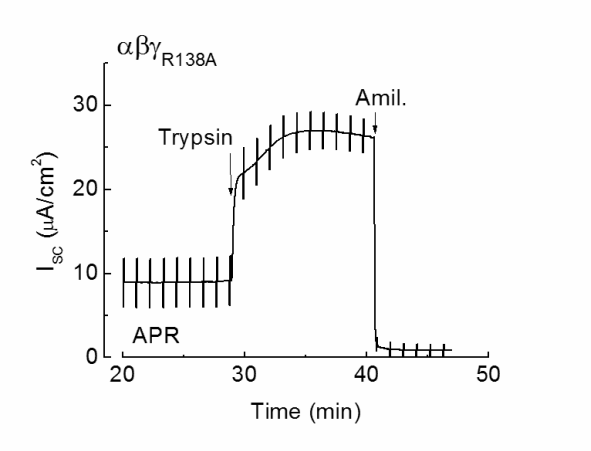

Figure 4-1 Representative ISC traces of αβγ and selected endogenous protease site mutants

Shown are the baseline current in PBS and aprotinin (10 μM) pre-treated cells and the responses to 15 μM Trypsin added to the apical side. Amiloride was added at the indicated time.

4.1.2 Effect of mutations on aprotinin inhibition of I_{Na}

The mutated sites may represent potential sites of action of an aprotinin sensitive protease therefore, the sensitivities of the mutant channels to aprotinin were measured. Shown in Table 4-2 are the I_{Na} values for aprotinin treated FRT cells expressing αβγ and the mutant ENaCs. As previously observed, aprotinin caused a significant reduction in the I_{Na} for all constructs. The I_{Na} averaged ~ 14 to 16.0 μA/cm^2 for αβγ, $\alpha_{R177A}\beta\gamma$ and $\alpha_{R204A}\beta\gamma$; and a significantly higher 19 μA/cm^2 for $\alpha_{R181A}\beta\gamma$. Unlike in the control conditions, where the cells were not treated with aprotinin, both $\alpha_{R178A}\beta\gamma$ and $\alpha_{R178A;R204A}\beta\gamma$ had significantly lower I_{Na} compared to αβγ at 9.0 ± 0.77 and 7.9 ± 0.69 μA/cm^2 respectively. The $\alpha\beta\gamma_{R138A}$ also demonstrated significantly lower I_{Na}. Consequently, aprotinin reduced the I_{Na} for αβγ and $\alpha_{R177A}\beta\gamma$, $\alpha_{R204A}\beta\gamma$, and $\alpha\beta\gamma_{R138A}$ to half of their control values whereas $\alpha_{R178A}\beta\gamma$ and $\alpha_{R178A;R204A}\beta\gamma$ I_{Na} values were reduced to a third of their control values. The trypsin activation of current in aprotinin treated FRT cells was also measured. The trypsin addition as shown in the representative traces (Figure 4-1) caused significant increases in the I_{Na} for all the mutants. The I_{Na} values after addition of trypsin to aprotinin treated cells (Table 4-2) reached the same values as the I_{Na} of control cells after addition of trypsin. That is, the maximal activated current in control and aprotinin treated cells were the equal. In aprotinin treated cells, trypsin increased I_{Na} for αβγ and $\alpha_{R177A}\beta\gamma$ by 13.0 μA/cm^2. However, significantly higher increases were observed for $\alpha_{R178A}\beta\gamma$, $\alpha_{R181A}\beta\gamma$, $\alpha_{R204A}\beta\gamma$ and $\alpha_{R178A;R204A}\beta\gamma$ as well as $\alpha_{R138A}\beta\gamma$ suggesting that these mutants have a more significant protease activation deficit in the aprotinin treated cells compared to αβγ. To factor in differences that could arise from different levels of expression, the currents in aprotinin treated cells were normalized to the maximal trypsin response as I_{PR} as shown in Figure 4-3. Here, αβγ had I_{PR} of 0.56 ± 0.01, $\alpha_{R177A}\beta\gamma$ 0.52 ± 0.02, α_{R181A} 0.50 ± 0.02 and α_{R204A} 0.48 ± 0.02. The significant differences were found with $\alpha_{R178A}\beta\gamma$, $\alpha_{R178A;R204A}$ and $\alpha\beta\gamma_{R138A}$ at 0.25 ± 0.01, 0.26 ± 0.01 and 0.34 ± 0.02 respectively. Continued inhibition of the mutants by aprotinin suggests that neither the α polybasic sequences nor the γ polybasic sequence are solely responsible for the aprotinin inhibitable pathway.

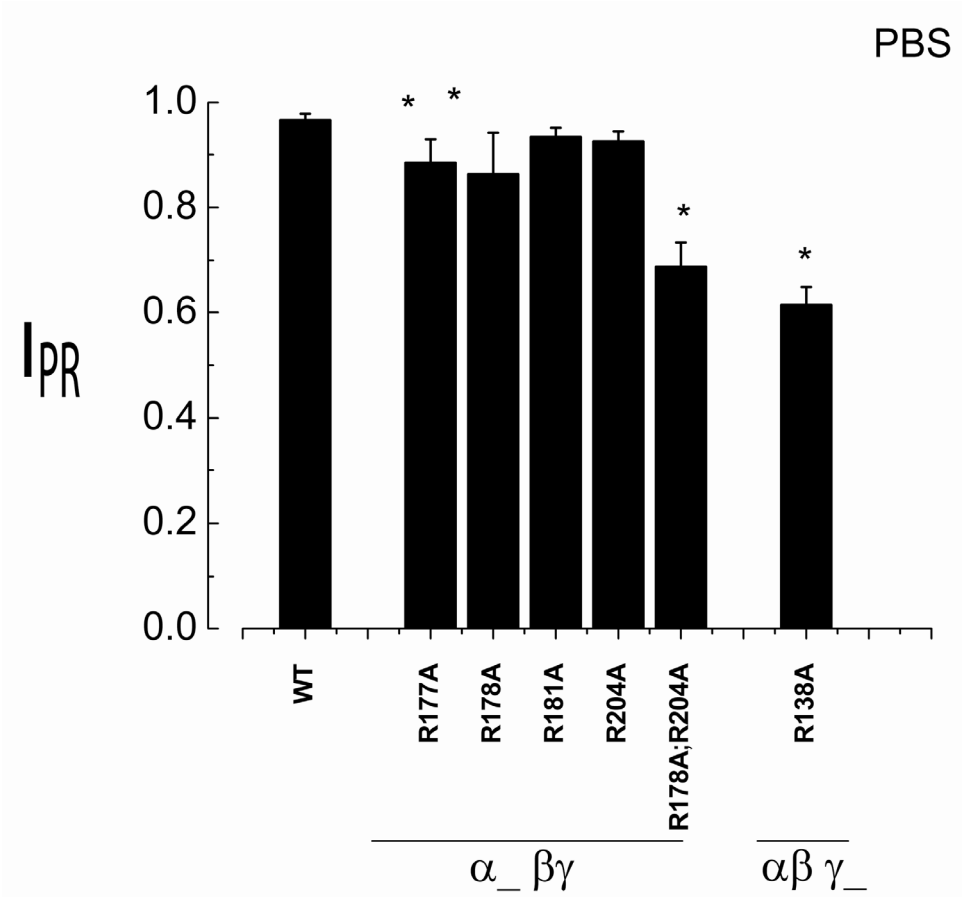

Figure 4-2 Summary of the baseline current as a fraction of the trypsin stimulated current

The I_{Na} before trypsin addition was normalized to the I_{Na} after addition of trypsin to give I_{PR} plotted for mutations that should eliminate putative furin consensus sequences in the α and γ subunits by changing the P1 position from R to A. *P < 0.05 ANOVA, student t test comparison with αβγ.

Table 4-2 Activation of I_{Na} by trypsin in aprotinin inhibited cells

The aprotinin pretreated I_{Na} in cells expressing αβγ and selected mutant ENaCs and the effect of trypsin addition. *P < 0.05 by ANOVA t test compared to αβγ

Construct	I_{Na} (± SEM)		ΔI_{Na} (± SEM)	N
	Baseline(Aprotinin)	+ Trypsin		
	$\mu A/cm^2$		$\mu A/cm^2$	
αβγ	16.0 ± 0.38	29.2 ± 0.65	13.2 ± 0.39	181
$\alpha_{R177A}\beta\gamma$	14.7 ± 0.76	28.0 ± 0.67	13.3 ± 0.44	11
$\alpha_{R178A}\beta\gamma$	9.0 ± 0.77*	35.8 ± 1.86	26.9 ± 1.14*	8
$\alpha_{R181A}\beta\gamma$	19.2 ± 0.78*	38.6 ± 0.93	19.3 ± 0.84*	3
$\alpha_{R204A}\beta\gamma$	16.7 ± 0.67	34.8 ± 0.76	18.2 ± 1.08*	11
$\alpha_{R178A;R204A}\beta\gamma$	7.9 ± 0.69*	30.4 ± 1.76	22.5 ± 1.24*	16
$\alpha_{R138A}\beta\gamma$	11.7 ± 1.02*	32.0 ± 2.03	20.3 ± 1.31*	36

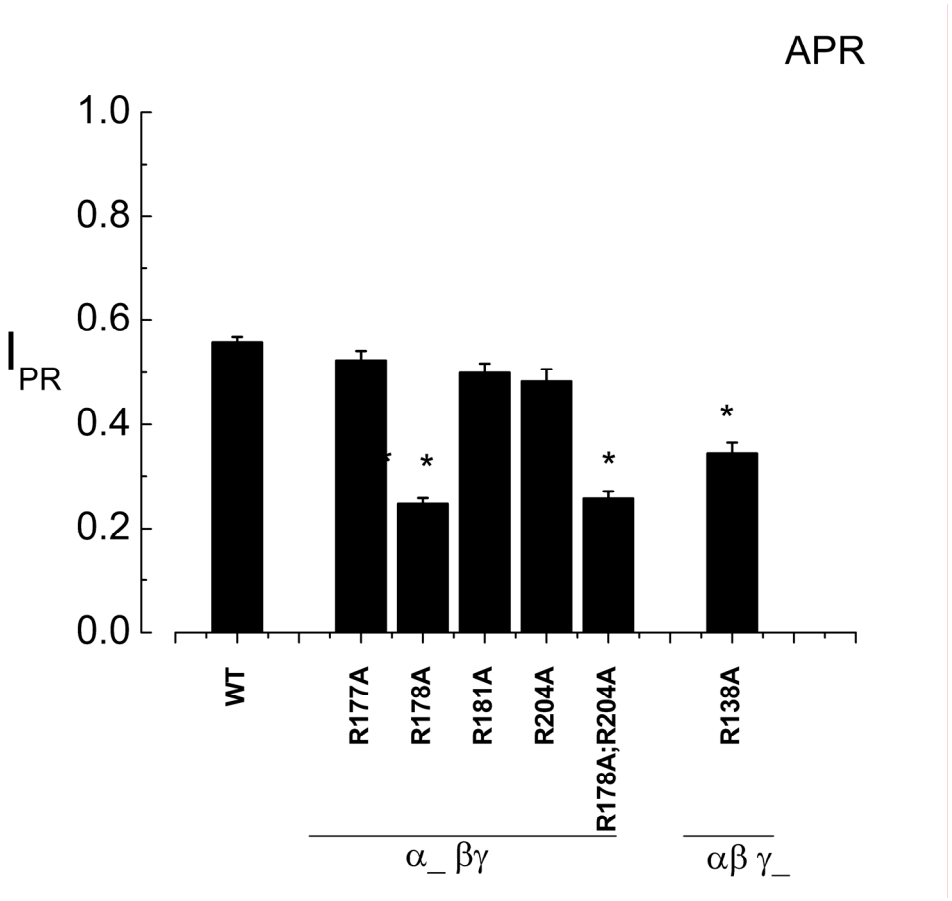

Figure 4-3 The aprotinin inhibited I_{Na} as a fraction of the trypsin stimulated I_{Na}

The I_{Na} before trypsin addition was normalized to the I_{Na} after addition of trypsin to give I_{PR} plotted for mutations that should eliminate putative furin consensus sequences in the α and γ subunits by changing the P1 position from R to A. *P < 0.05 ANOVA, student t test comparison with αβγ.

4.1.3 Effect of mutations on Elastase activation of I_{Na}

An elastase responsive region in the γ subunit of ENaC was identified in chapter 3. To further characterize the properties of the mutants found to affect spontaneous ENaC expression and aprotinin inhibition of I_{Na}, elastase mediated activation of current was measured in the $\alpha_{R178A;R204A}\beta\gamma$ and $\alpha\beta\gamma_{R138A}$ constructs. Shown in Figure 4-4 A are representative current traces depicting the effect of NE and trypsin on I_{Na} for αβγ and $\alpha_{R178A;R204A}\beta\gamma$. As previously observed, neither NE (300 nM) nor subsequent trypsin causes a significant increase in I_{Na} for αβγ. The I_{Na} averaged 26 to 28 μA/cm^2 at baseline, after NE and after trypsin. In contrast, for $\alpha_{R178A;R204A}\beta\gamma$ NE caused a significant current increase from ~12 μA/cm^2 to ~23 μA/cm^2 after which trypsin no longer increased current. Consequently, the impaired protease activation arising from the mutation could be completely reversed by the addition of NE. In aprotinin treated cells NE activated current in both αβγ and $\alpha_{R178A;R204A}\beta\gamma$ (Figure 4-4 B). For αβγ NE increased I_{Na} from 14 to 26 μA/cm^2, which was slightly further increased to 28 μA/cm^2 by trypsin. As previously shown, the I_{Na} for $\alpha_{R178A;R204A}\beta\gamma$ in cells treated with aprotinin was markedly low averaging 4.1 ± 0.30 μA/cm^2. Addition of NE caused a large increase of I_{Na} to 19.4 ± 0.83 μA/cm^2. Subsequent trypsin addition increased I_{Na} to 25.4 ± 0.96 μA/cm^2. Clearly this mutant responds to NE in the absence or presence of aprotinin providing further evidence that $\alpha_{R178A;R204A}\beta\gamma$ is only partially activated by endogenous proteases. A summary is shown in Figure 4-5. Similar results were obtained with PE (300nM) on the $\alpha_{R178A;R204A}\beta\gamma$ construct with representative traces shown in Figure 4-6 and results summarized in Figure 4-7. Thus the partial activation of $\alpha_{R178A;R204A}\beta\gamma$ was overcome with exogenous trypsin, NE and PE. Shown in Figure 4-8 are representative current traces for $\alpha\beta\gamma_{R138A}$. Compared to αβγ, the baseline I_{Na} for $\alpha\beta\gamma_{R138A}$ is seen to be reduced as previously observed. Addition of NE, unlike in the case for $\alpha_{R178A;R204A}\beta\gamma$, did not significantly increase I_{Na}. Finally, addition of trypsin, as previously observed, increased I_{Na}. In aprotinin treated cells, NE increased I_{Na} from 14.9 ± 1.12 to 20.5 ± 1.12 μA/cm^2. However, addition of trypsin doubled I_{Na} to 39.3 μA/cm^2. Similar results were obtained with PE (Figure 4-11). Thus, unlike $\alpha_{R178A;R204A}\beta\gamma$, the response to NE and PE is significantly impaired for $\alpha\beta\gamma_{R138A}$.

A

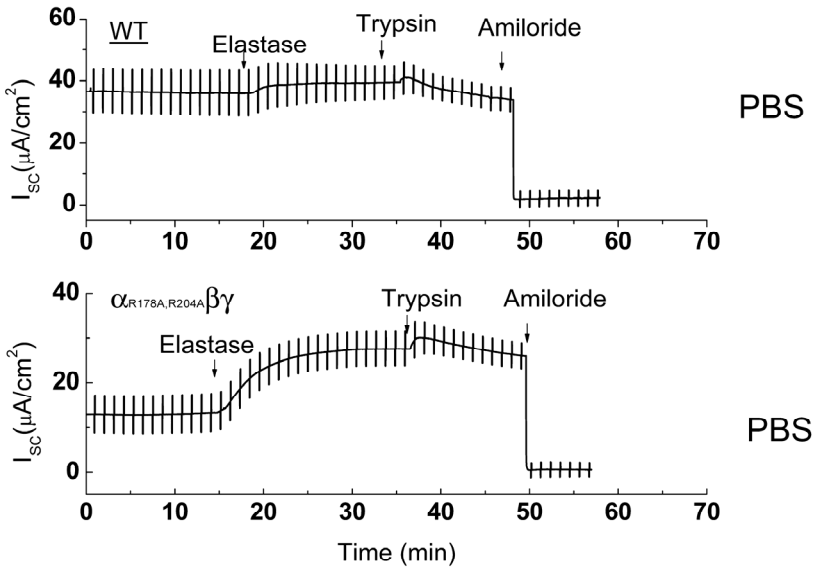

B

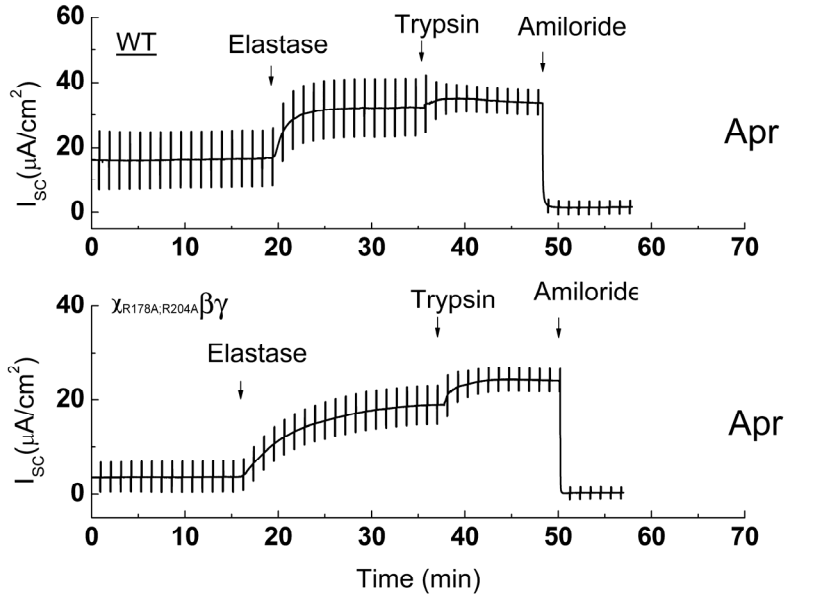

Figure 4-4 Representative traces for NE activation of $\alpha_{R178A;R204A}\beta\gamma$

A) Representative current trace of NE activation of αβγ (upper trace) and $\alpha_{R178A;R204A}\beta\gamma$ (lower trace) in the absence of aprotinin (PBS = vehicle). B) Representative current trace of NE activation of αβγ (upper trace) and $\alpha_{R178A;R204A}\beta\gamma$ (lower trace) in the presence of aprotinin (Apr).

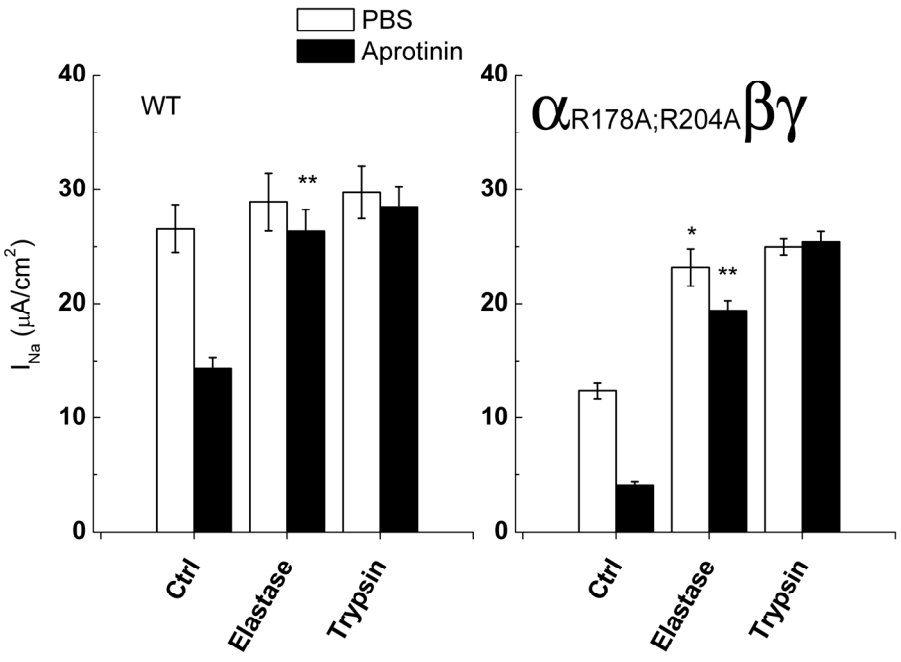

Figure 4-5 Summary of NE activation of $\alpha_{R178A;R204A}\beta\gamma$

The mean values of I_{Na} (± SEM) in PBS and aprotinin treated cells before protease addition (ctrl), after addition of 300 nM NE and after addition of trypsin. *P < 0.05 and **P < 0.05 student's t test comparison of elastase I_{Na} to control I_{Na} in PBS and in aprotinin treated cells respectively.

A

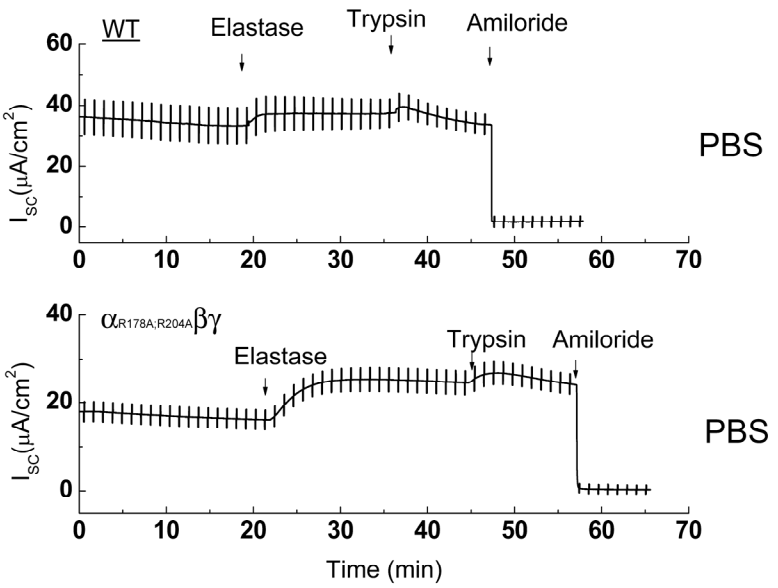

B

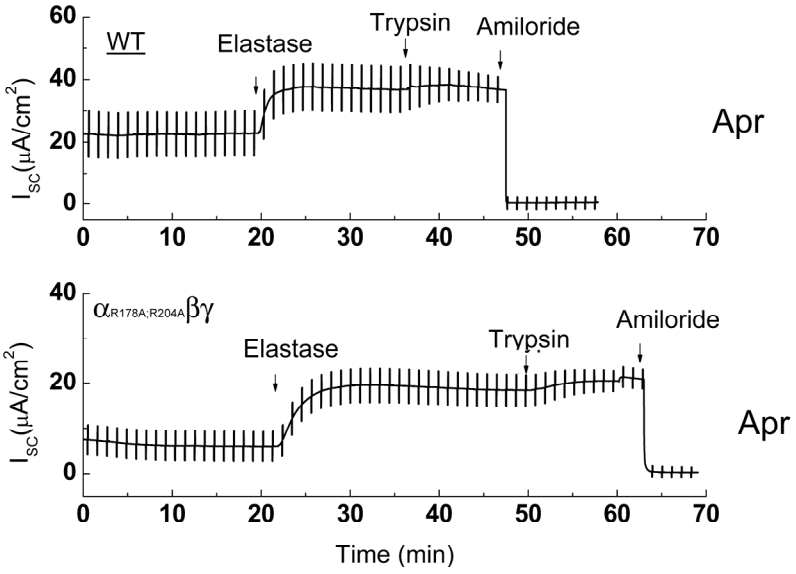

Figure 4-6 Representative traces of PE activation of $\alpha_{R178A;R204A}\beta\gamma$

A) Representative current trace of PE activation of αβγ (upper trace) and $\alpha_{R178A;R204A}\beta\gamma$ (lower trace) in the absence of aprotinin (PBS = vehicle). B) Representative current trace of PE activation of αβγ (upper trace) and $\alpha_{R178A;R204A}\beta\gamma$ (lower trace) in the presence of aprotinin (Apr).

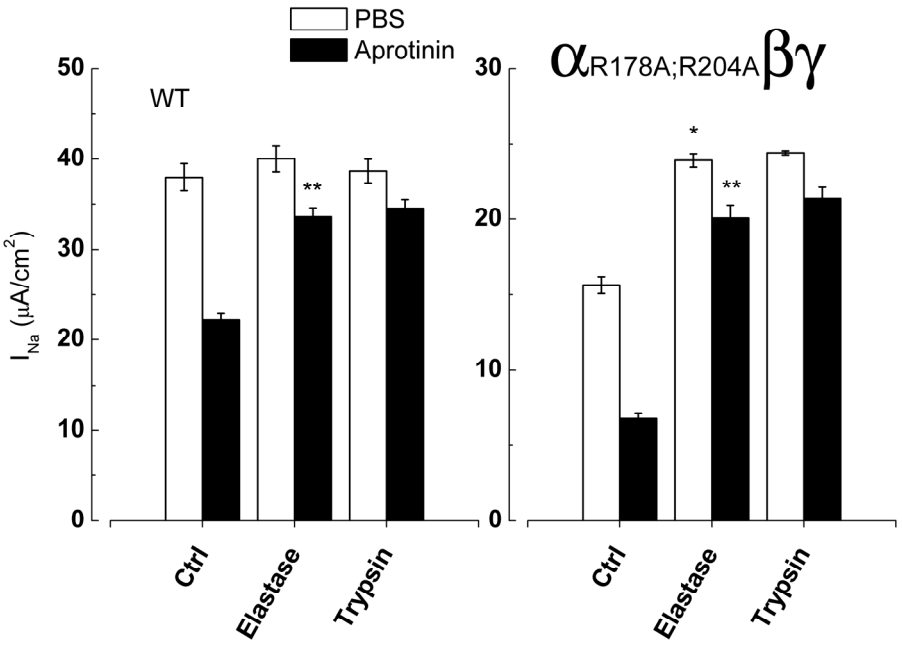

Figure 4-7 Summary of PE activation of WT (αβγ) and $\alpha_{R178A;R204A}\beta\gamma$

The mean values of I_{Na} (± SEM) in PBS and aprotinin treated cells before protease addition (ctrl), after addition of PE and after addition of trypsin. *P < 0.05 and **P < 0.05 student's t test comparison of elastase I_{Na} to control I_{Na} in PBS and in aprotinin treated cells respectively.

A

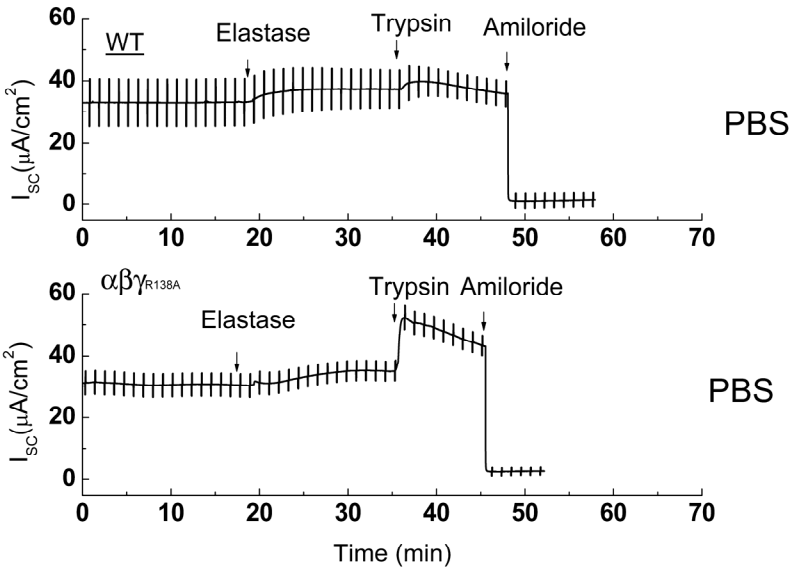

B

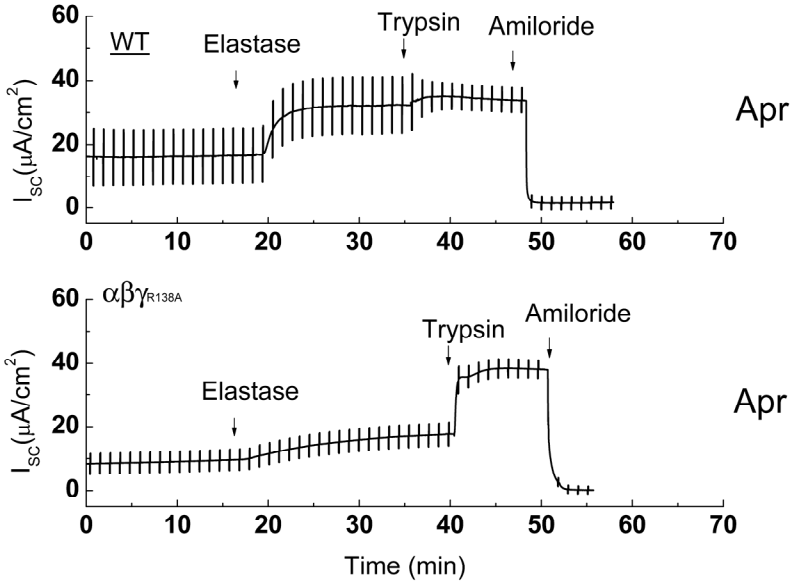

Figure 4-8 Representative current traces of NE activation of WT (αβγ) and $\alpha\beta\gamma_{138A}$

A) Representative current trace of NE activation of αβγ (upper trace) and $\alpha\beta\gamma_{R138A}$ (lower trace) in the absence of aprotinin (PBS = vehicle). B) Representative current trace of NE activation of αβγ (upper trace) and $\alpha\beta\gamma_{R138A}$ (lower trace) in the presence of aprotinin (Apr).

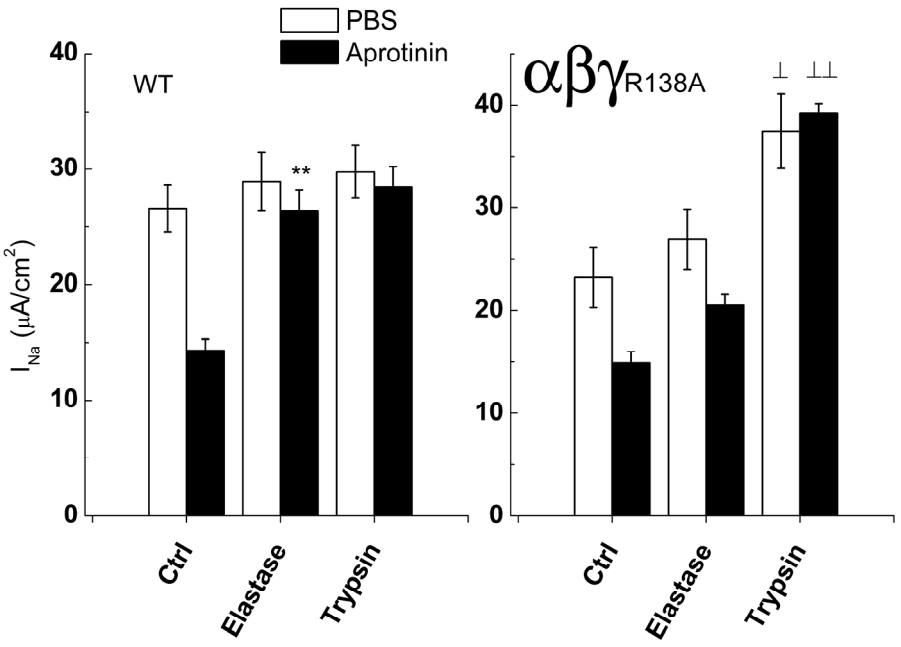

Figure 4-9 Summary of NE activation of wild type ENaC (αβγ) and the $\alpha\beta\gamma_{R138A}$

The mean values of I_{Na} (± SEM) in PBS and aprotinin treated cells before protease addition (ctrl), after addition of NE and after addition of trypsin. *P < 0.05 and **P < 0.05 student's t test comparison of elastase I_{Na} to control I_{Na} in PBS and in aprotinin treated cells respectively. †P < 0.05 and ††P < 0.05 student's t test comparison of I_{Na} after trypsin to I_{Na} after elastase.

A

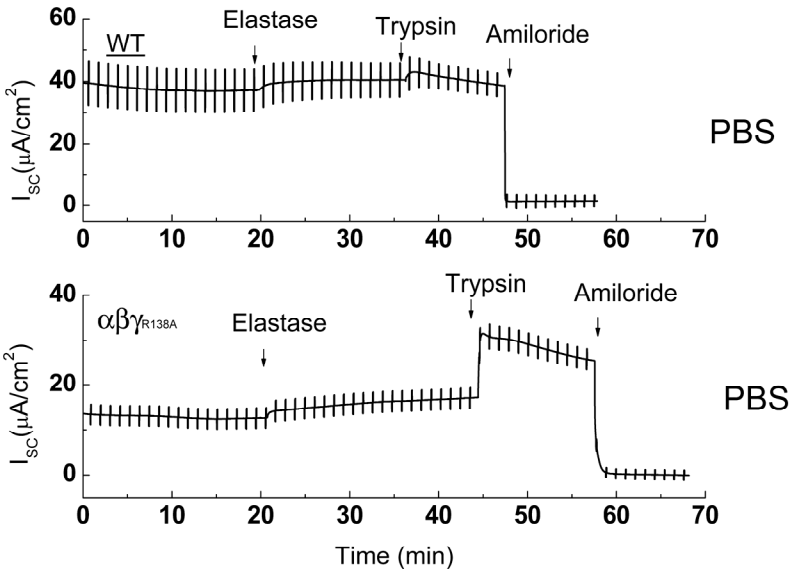

B

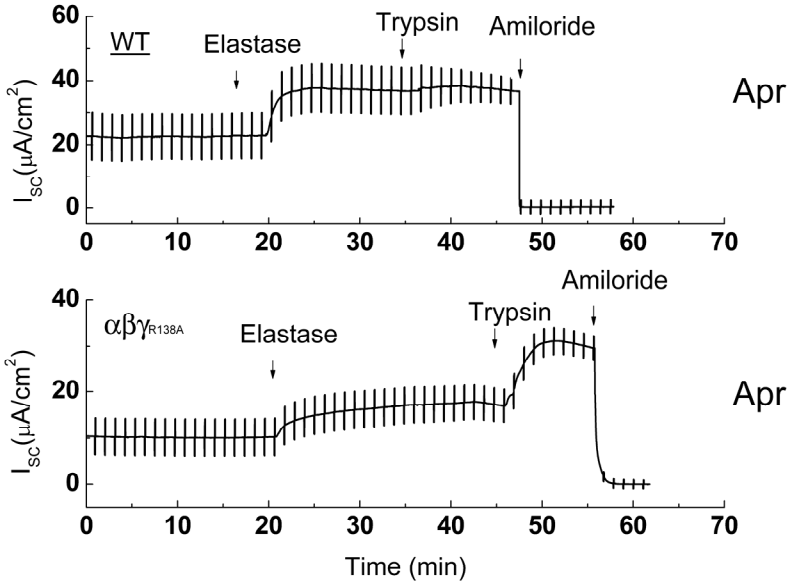

Figure 4-10 Representative current traces of PE activation of WT (αβγ) and αβγ138A

A) Representative current trace of PE activation of αβγ (upper trace) and $\alpha\beta\gamma_{R138A}$ (lower trace) in the absence of aprotinin (PBS = vehicle). B) Representative current trace of PE activation of αβγ (upper trace) and $\alpha\beta\gamma_{138A}$ (lower trace) in the presence of aprotinin (Apr).

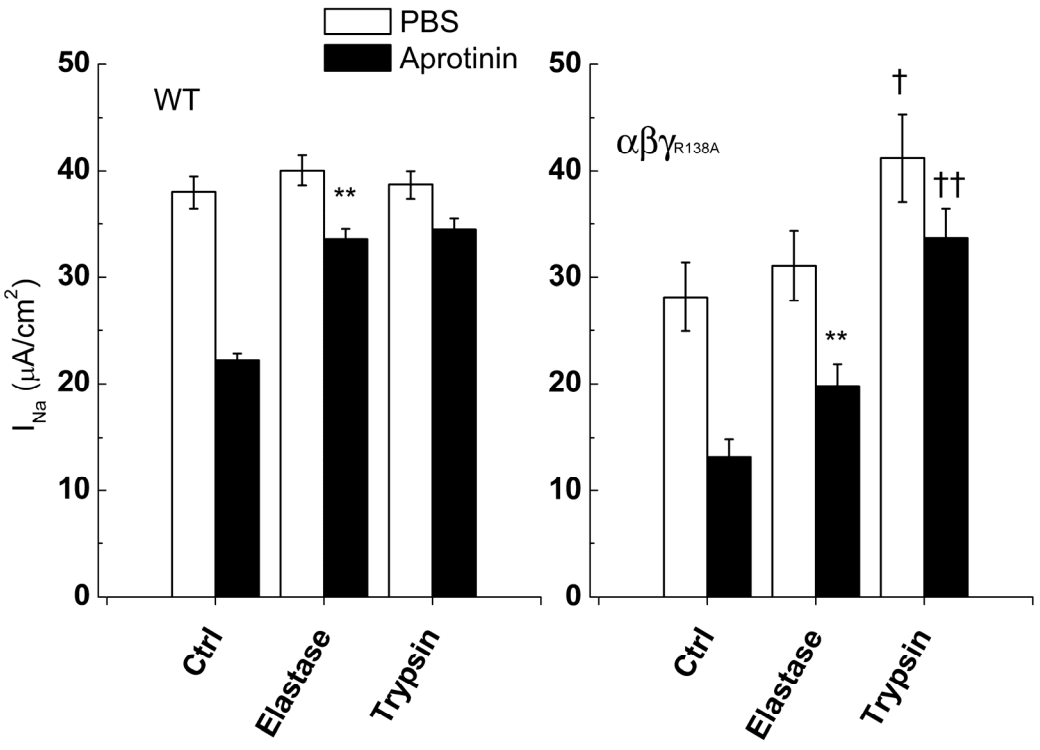

Figure4-11 Summary of PE activation of WT (αβγ) and the $\alpha\beta\gamma_{R138A}$

The mean values of I_{Na} (± SEM) in PBS and aprotinin treated cells before protease addition (ctrl), after addition of PE and after addition of trypsin. **P < 0.05 student's t test comparison of elastase I_{Na} to control I_{Na} in aprotinin treated cells. †P < 0.05 and ††P < 0.05 student's t test comparison of I_{Na} after trypsin to I_{Na} after elastase in control and aprotinin treated cells respectively.

Table 4-3 Time course of NE and PE Activation of ENaC-mediated Na+ Current

The τ are time constants obtained from fitting the change in I_{Na}, following addition of Porcine elastase as a fraction of the maximal I_{Na} obtained after subsequent trypsin addition to a single exponential curve. I_{PR} represents the predicted maximal I_{Na} following elastase stimulation as a fraction of maximal trypsin stimulated I_{Na} observed. ΔI_{PR} represents the maximal elastase stimulated increase in I_{Na} as fraction of the maximal trypsin stimulated I_{Na} observed. The values are obtained from a fitting the mean of (n) experiments and the 95 % confidence interval (95% CI) on the parameters are reported.

	Construct	τ (+/- 95% CI)	I_{PR} (+/- 95% CI)	ΔI_{PR} (+/- 95% CI)	n
NE		*min*			
	αβγ	2.59 ± 0.080	0.87 ± 0.003	0.43 ± 0.006	8
	$\alpha\beta\gamma_{R138A}$	12.4 ± 0.741	0.53 ± 0.011	0.29 ± 0.010	4
	$\alpha_{R178A;R204A}\beta\gamma$	6.44 ± 0.675	0.80 ± 0.028	0.63 ±0.025	6
PE	αβγ	2.01 +/- 0.320	0.97 ± 0.010	0.34 ± 0.024	16
	$\alpha\beta\gamma_{R138A}$	2.03 ± 0.462	0.57 ± 0.008	0.18 ± 0.032	15
	$\alpha_{R178A;R204A}\beta\gamma$	3.86 +/- 0.764	0.95 ± 0.040	0.68 ± 0.049	8

Further differences were found by characterizing the time course of current activation. As previously described, the time course of current activation fits a single exponential component. The time courses for NE and PE activation of current in aprotinin pre-treated FRT cells expressing αβγ and $\alpha_{R178A;R204A}\beta\gamma$ were plotted in Figure 4-12. Prior to protease addition the effect of the mutation $\alpha_{R178A;R204}\beta\gamma$ was evident. In the NE set of experiments the I_{PR} for aprotinin treated cells expressing αβγ was 0.48 ± 0.004 while that for cells expressing $\alpha_{R178A;R204}\beta\gamma$ was 0.18 ± 0.002. Addition of NE caused an increase in current to 0.87 ± 0.003 for αβγ and 0.7 ± 0.028 for $\alpha_{R178A;R204A}\beta\gamma$. The increases were characterized by time constants of 2.59 ± 0.08 and 6.44 ± 0.675 min respectively. The final values extrapolated from the exponential fits were 0.87 ± 0.003 and 0.80 ± 0.028 respectively. Thus as previously observed, NE reverses the aprotinin inhibition of cells expressing αβγ as shown in chapter 3. NE also reversed the aprotinin inhibition in cells expressing $\alpha_{R178A;R204A}\beta\gamma$ as well as reversing the inhibitory effect attributable to the mutation itself. However, the activation by NE in cells expressing the $\alpha_{R178A;R204A}\beta\gamma$

mutant had a prolonged time constant relative to cells expressing αβγ and points to a slower rate limiting step in the activation process. In the PE set of experiments, the normalized values for aprotinin treated FRT cells expressing αβγ was 0.62 while that for cells expressing the $\alpha_{R178A;R204A}\beta\gamma$ mutant was 0.3. Addition of PE caused an increase in the current to an I_{PR} of 0.97 ± 0.01 and 0.95 ± 0.04 for αβγ and $\alpha_{R178A;R204A}\beta\gamma$ expressing cells respectively. The time courses were characterized by time constants of 2.01 ± 0.32 and 3.86 ± 0.76 respectively. Clearly PE reversed the aprotinin inhibition as well as the inhibition caused by the $\alpha_{R178A;R204A}\beta\gamma$ mutation and it did so with a slightly prolonged time course. The time course for the activation of current in cells expressing the $\alpha\beta\gamma_{R138A}$ mutant was different as shown in Figure 4-13. As was true for $\alpha_{R178A;R204A}\beta\gamma$, the $\alpha\beta\gamma_{R138A}$ mutant had a reduced I_{PR} (0.22 ± 0.008). Addition of NE caused an increase to 0.4 ± 0.01 with a time constant of 12.4 ± 0.74 min. Extrapolation of the fit indicates a final steady-state value of 0.53 ± 0.01. NE appeared to reverse the aprotinin inhibition of current only and not the inhibitory effect of the $\alpha\beta\gamma_{R138A}$ mutation. Secondarily, the reversal of aprotinin inhibition of current by NE is characterized by a prolonged time course suggesting a much slower rate limiting step for the $\alpha\beta\gamma_{R138A}$ mutant compared to $\alpha_{R178A;R204A}\beta\gamma$ or αβγ. Addition of PE to cells expressing the $\alpha\beta\gamma_{R138A}$ mutant increased I_{PR} from 0.38 ± 0.006 to 0.57 ± 0.008 with a time constant of 2.03 ± 0.462 min. PE also reversed the aprotinin inhibition and it did this with a time constant that is the same as that observed for αβγ (2.01 ± 0.32). However it did not reverse the inhibitory effect due to the $\alpha\beta\gamma_{R138A}$ mutation.

A

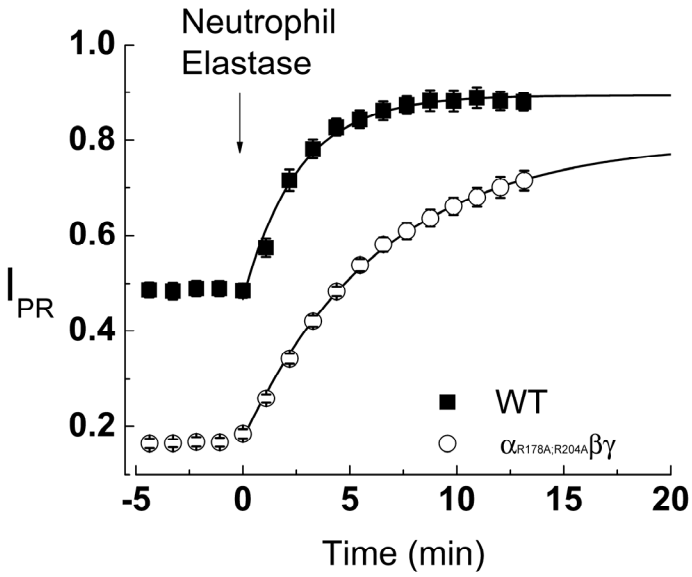

B

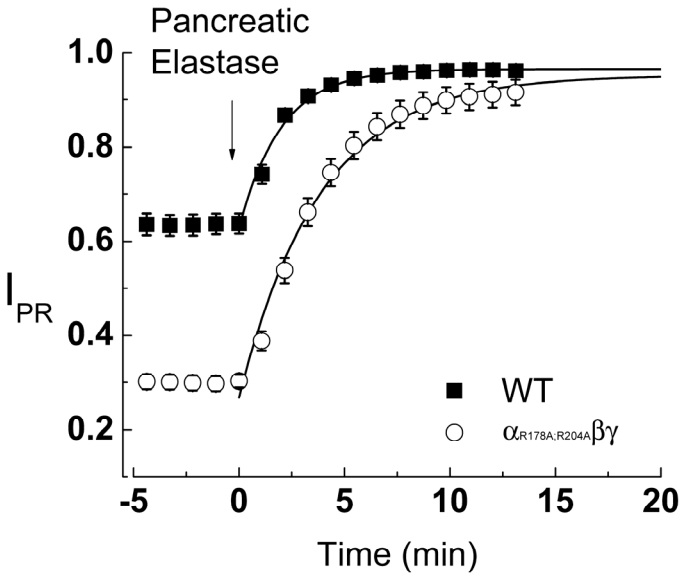

Figure 4-12 Time course of NE and PE activation of $\alpha_{R178A;R204A}\beta\gamma$

Time-dependent increase in current following 300 nM NE (A) and 300 nM PE (B) addition to aprotinin treated FRT cells expressing WT (solid squares) and $\alpha_{R178A;R204A}\beta\gamma$ as a fraction of the trypsin stimulated maximum. Solid lines are single exponential fits of the data.

A

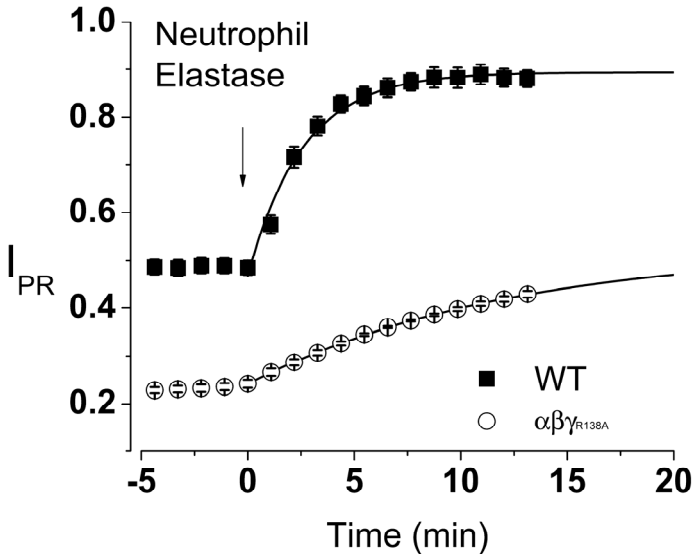

B

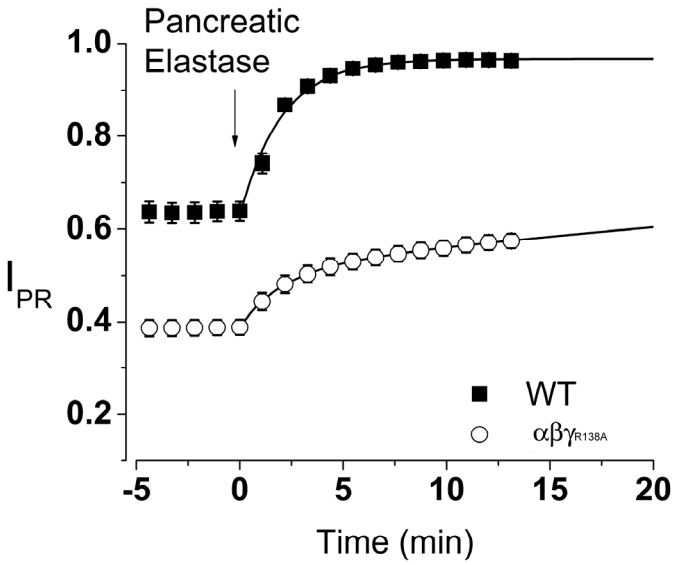

Figure 4-13 Time course of NE and PE activation of $\alpha\beta\gamma_{R138A}$

Time-dependent increase in current following 300 nM NE (A) and 300 nM PE (B) addition to aprotinin treated FRT cells expressing WT (solid squares) and $\alpha\beta\gamma_{R138A}$ as a fraction of the trypsin stimulated maximum. Solid lines are single exponential fits of the data.

4.2 DISCUSSION

In this chapter it was investigated whether potential endogenous protease consensus polybasic sequences mediate expression of Na^+ current in Na^+ transporting epithelial cells by carrying out amino acid substitutions of the polybasic sequences. The results are preliminary and the conclusions tentative; they primarily provide questions for future studies. The results showed that mutations of polybasic sequences in the α and γ subunits indeed caused significant decreases in the current. The decreases were protease sensitive because they were reversible by addition of exogenous trypsin, and in the case of the $\alpha_{R178A;R204A}\beta\gamma$ reversible by the elastases NE and PE. The results were therefore broadly consistent with previous reports that concluded that mutation of the particular arginines of the polybasic sequences reduced ENaC-mediated current in Xenopus oocytes and prevented α and γ subunit cleavages in the Madine-Darby canine kidney (MDCK) model epithelial cell (86). The mutations did not result in complete channel inhibition which could be explained by at least two different hypotheses. First, the partial inhibition may be attributed to a reduced P_o of uncleaved channels caused by an enhanced Na^+ self inhibition effect (163). Alternatively, the single point mutations may not completely abolish hydrolysis by endogenous proteases but instead reduce the rate of hydrolysis. As discussed in section 3.3.4, low rates of activation could result in a reduced current steady-state level because of the balance between proteolytic activation and endocytic retrieval. Activation by exogenous trypsin could be mediated by possible cleavage at several residues within or surrounding the polybasic sequences (the trypsin primary specificity is R/K) thereby substituting for the endogenous protease cleavage. This is reminiscent of the activation of the fusogenic property of a viral protein which is inhibited by mutation of a polybasic residue and activated by exogenous trypsin (117). Because several proteases such as CAP1, CAP3, and many members of the PC family can cleave polybasic sequences the results do not indicate a particular protease as being of primary importance but highlight a general possibility of ENaC cleavage by endogenous proteases. To further investigate the dependence of channel activity on cleavage, polybasic sequences could be changed by substitutions of all the basic residues to completely eliminate the sites rather than the use of single point mutations as we have done. In this way we could mutate all the putative

endogenous sequences and then carryout the replacement of the polybasic sequences with the thrombin sequence, as described in our studies in chapter 3. Thrombin could then be used to show that cleavage at those sequences indeed mediate channel activation.

The attempt to investigate the mechanism of aprotinin (a serine proteases inhibitor) inhibition of I_{Na} did not yield conclusive results. The results show that serine protease inhibition by aprotinin continues to inhibit I_{Na} in cells expressing the polybasic sequence mutants therefore the mutations did not prevent activation by an aprotinin sensitive pathway. The only conclusion that may be drawn is that an aprotinin-sensitive protease does not cleave at sites corresponding to $RSRR^{178}$ and $RRAR^{204}$ in the α subunit alone or a site corresponding to $RKRR^{138}$ in the γ subunit alone. In other words, we cannot rule out an aprotinin sensitive simultaneous cleavage at the polybasic sequences in both subunits as well as at other sites not yet identified.

Perhaps, the most interesting finding is that the mutations of the polybasic sequences in the α and γ subunit have different consequences for elastase mediated activation of current. We first consider the observation that in cells expressing the $\alpha_{R178A;R204A}\beta\gamma$ mutant and untreated with aprotinin NE and PE increased the I_{Na} reversing the inhibitory effect of the mutation. This activation seen in the absence of aprotinin treatment may arise from the elastases essentially mimicking a polybasic sequence dependent endogenous protease cleavage of the α subunit by utilizing several of the valines and alanines in the α178-204 span as possible cleavage sites. When the cells expressing the $\alpha_{R178A;R204A}\beta\gamma$ were inhibited by aprotinin, the increase in I_{Na} mediated by NE/PE had a prolonged time course relative to cells expressing wild type ENaC. This prolongation may arise from the possibility that the rate-limiting step has been shifted to elastase interactions with less susceptible α subunit valines/alanines instead of the γ sites which would be rate limiting for wild type ENaC. Alternatively, multiple pathways may lead to channel activation. In other words, the NE/PE mediated cleavage of the γ subunit at γV182, γV193 or γA190 described in results from chapter 3 may be an independent path for channel activation that could reverse inhibition of I_{Na} caused by the $\alpha_{R178A;R204A}\beta\gamma$ mutation just as it reversed the inhibition of I_{Na} caused by aprotinin treatment. To test the latter alternative hypothesis the $\alpha\beta\gamma_{V182G;V193G}$ (for NE) or $\alpha\beta\gamma_{A190G}$ (for PE) could be evaluated in the context of the $\alpha_{R178A;R204A}\beta\gamma$ mutant. Inhibited responses to NE/PE in cells expressing the resultant mutant construct will confirm the latter hypothesis but continued responses will indicate that activation inducing cleavage sites for NE/PE could be present in the α subunit. Heterologous expression of

the $\alpha_{R178A;R204A}\beta\gamma$ construct in a model epithelial cell such as the human embryonic kidney (HEK) or MDCK cell could be used to biochemically determine if elastases cause cleavage of the α subunit. The actual cleavage site could be searched with MALDI-TOF on the appropriate representative peptide sequence and the functional significance of the cleaved site verified by site-directed mutagenesis and measurement of NE/PE dependent I_{Na} increase in FRT cells.

Unlike the $\alpha_{R178A;R204A}\beta\gamma$ mutant, cells expressing the $\alpha\beta\gamma_{R138A}$ mutant displayed remarkable resistance to activation by NE and by PE in cells without aprotinin treatment. In this case the cleavage at γV182, γV193 and γA190 by NE and PE is expected yet activation is impaired. It is possible that mutating γR138, and preventing cleavage there, blocks a conformational transition that would facilitate elastase hydrolysis at the down stream residues. Alternatively, cleavage at the down stream residues may occur but be insufficient to activate the channel. This conclusion cannot be definitely ascertained without showing that cleavage by NE/PE persists although activation is impaired. Again expression of ENaC in the HEK/MDCK model cells and biochemical characterization of subunit fragmentation could be evaluated. Clearly, NE/PE activation via the γ subunit (as discussed in chapter 3) does not simply mimic the endogenous protease cleavage of the polybasic sequence at γR138. The idea that multiple cleavage sites and possibly multiple proteases could be involved necessarily in the regulation of channel activity is intriguing in light of the fact that NE and PE appear to mediate small I_{Na} increases for the $\alpha\beta\gamma_{R138A}$ mutant only in cells that were aprotinin inhibited. Activation by PE appears to return the current to the pre-aprotinin treatment values but not to trypsin activated values as was found for wild type and $\alpha_{R178A;R204A}$. Similar results were apparent for NE although the time constants differ considerably. In the case of PE, the results were consistent with PE mediated reversal of aprotinin inhibition but not reversal of the effect of the $\alpha\beta\gamma_{R138A}$ mutation. The results show the following: 1) NE/PE fully (with respect to trypsin activation) activates I_{Na} in aprotinin inhibited cells expressing wild type ENaC; 2) NE/PE did not increase I_{Na} in cells that express the $\alpha\beta\gamma_{R138A}$ mutant without aprotinin treatment; 3) NE/PE partially (with respect to trypsin) increased I_{Na} in aprotinin inhibited cells expressing the $\alpha\beta\gamma_{R138A}$ mutant. Including the report that $\alpha\beta\gamma_{R138A}$ prevents cleavage of the γ subunit (86), it follows from 1, 2 and 3 that aprotinin did not cause inhibition by preventing cleavage at γR138. Otherwise, NE/PE would not increase I_{Na} in aprotinin inhibited cells. We speculate that NE/PE cleavage of the γ subunit mimics an aprotinin sensitive protease that cleaves the γ subunit down stream of

γR138A, close to the identified NE/PE sites; perhaps likely at the polybasic sequence KRKR[181] in the γ subunit. In addition, the notion that activation by cleavage of the α subunit requires two cleavage sites is mirrored (32) in the γ subunit but here two different endogenously expressed proteases may play a role, one of which is sensitive to aprotinin.

Many questions are left unanswered by these experiments. First, what is the target of aprotinin? A leading candidate in mammalian cells is CAP1/prostasin, which activates ENaC in heterologous expression systems (49). Prostasin and other CAPs are likely to mediate the aprotinin effect because both their protease activity (167, 206) and their capacity for increasing Na^+ transport (201) are inhibitable by aprotinin. It is not yet known if prostasin cleaves ENaC, which subunits are cleaved or what cleavage sites are utilized. It was shown that CAP1 lacking a catalytic triad that is required for serine protease activity increased the I_{Na} in Xenopus oocytes, but other similar proteases (CAP2 and CAP3) require an intact catalytic triad to activate the channel (8). If a secondary endogenous protease that does not use the PC consensus sequences plays a role in channel activation it is not evident from biochemical studies in MDCK cells expressing the polybasic sequence mutants, which showed a lack of subunit cleavage (86). However, it is not known whether other proteases that can activate the channel (e.g. prostasin/CAP2/CAP3) are expressed in the MDCK cells and the formation of functional channels were not assessed in the MDCK cells. A search for aprotinin interacting proteins would significantly enhance complete elucidation of the aprotinin sensitive pathway.

Second, the contribution of each cleavage to channel activation remains to be resolved because the experiments herein do not show that the mutation completely eliminated channel cleavage. Therefore biochemical measurements of protein cleavage in the same epithelial cells as measurement of the I_{Na} is a necessary step in determining the extent to which cleavage is inhibited by mutations of the putative endogenous protease sites. Assuming cleavage is completely prevented by the mutations, the significance of cleavage in multiple subunits and perhaps by multiple proteases is not yet clearly understood. Indeed the mechanism whereby cleavage leads to channel activation is not yet clear. Cleavage appears to involve both changes in the number of active channels as well as the open probability. It is possible that some cleavage steps set the open probability of the channels whereas others determine whether the channels are open or not. One might speculate that channels reaching the surface are already primed by proteases in the biosynthetic pathway; once at the surface the channels are then

activated by a final proteolytic step/s which allows for channel opening or uncapping. The channels that have been properly primed are uncapped to the set open probability and uncapping of unprimed channels results in inactive or low P_o channels. It is also possible that incremental cleavage steps lead to incremental changes of the channel's open probability. Accordingly, some proteases which can cleave at all proteolytic sites (e.g. trypsin) can lead to activation of channels from very low open probability (essentially inactive) to high open probabilities whereas proteases that cleave one site alone can only effect step increases in channel opening. A third layer of complexity involves the possibility that some proteases may require a prior cleavage of the channel before they can act on it. These possibilities can be delineated by careful simultaneous measurements of channel P_o, N_T and cleavage starting with a system where no cleavage occurs.

Studies towards understanding the effects of proteases, protease inhibitors and mutations of putative cleavage sites on channel subunit cleavage, P_o and N_T are currently underway. Antibodies against several epitopes on the α and γ subunits have been recently obtained and may be useful as primary tools for examining the fragmentation of the subunits under different experimental conditions. Initial studies on the utility of blocker induced noise analysis to study the single channel properties of ENaC expressed in FRT cells have been performed using analogs of two classical Na^+ channel inhibitors; amiloride and triameterene. With these analogs, we demonstrated that blocker induced Lorentzians can be measured in short-circuited FRT cells providing estimates of the single channel current that is consistent across the blockers. Two problems prevent utilization of this approach at present. First, increased accuracy on the estimates of the blocker dissociation constants and hence the spontaneous channel P_o requires optimization of the blocker off-rates. Secondarily, the nature of blocker interactions with human ENaC needs to be elucidated before blocker induced noise analysis can be routinely used to measure single channel properties. Our studies on human and mouse ENaC suggest a blocking mechanism other than the open channel blocked observed with Xenopus ENaC in A6 cells. A cell based high-throughput screening assay is currently being used to identify different classes of human ENaC blockers for the purposes of optimizing the blocker characteristics. Expression of functional ENaC at the plasma membrane of FRT cells grown on non-porous substrates has been confirmed by immunoflorescence and amiloride-sensitive membrane potential measurements. The excised, outside-out patch clamp configuration could be used on the FRT cells to study the

P_o of individual channels as well as the mechanism of blockade of the blockers identified from the high-throughput screening. It is expected that in the near future, the combination of patch clamp analysis and noise analysis of the short-circuit current will yield a clearer picture of the mechanism of activation by endogenous and exogenous proteases.

5.0 SUMMARY

In this dissertation the hypothesis that apical surface activation of ENaC occurs in epithelial cells by protease dependent conversion of inactive channels to active channels was examined. Direct extracellular protease activation of surface receptors can be found in trypsin activation of the G-protein coupled, protease activated receptors (138) and insulin (168) as well as tissue type plasminogen activator regulation of the N-methyl D-aspartate receptor (56). In these cases, protease cleavage leads to intrinsically active receptors or potentiation of the receptor activity. It is suggested by the results presented in this thesis that the same is true for ENaC.

The experiments from chapter 2 demonstrate several properties of the protease pathway. It was shown in cultured epithelial cells that protease activation may be a constitutive phenomenon which can be potently and reversibly inhibited by apical administration of serine protease inhibitors. The time course of inhibition was no faster than the rate at which channel subunits are removed from the apical membrane. The decrease in current results from a decrease in the number of active channels whereas compensatory increases occur in the single channel current and channel open probability. With removal of protease inhibition, the changes in single channel properties abruptly reverse. These studies suggest that in the presence of protease inhibition active channels are continually deactivated, perhaps by continuous endocytic withdrawal, whereas channels in the biosynthetic pathway remain inactive until removal of the protease inhibitor or exogenous addition of proteases. Because noise analysis, as carried out in chapter 2, treats the apical membrane channels as an ensemble, small heterogeneities will be missed and ensemble properties will reflect the properties of the most active channels; in this case, high P_o channels which may co-exist with low P_o channels. Thus, the remainder current after aprotinin inhibition represents high P_o active channels either selectively not internalized, resulting from compensatory up regulation or the new equilibrium established at low but significant levels of remaining proteolytic activity. Alternatively, these may represent the

channels arriving at the apical membrane already activated. The protease activation as presented in this dissertation suggests the possibility that in the apical membrane of epithelial cells the channels are not homogenous. It has long been known that ENaC gating varies widely and that at least a low P_o and a high P_o mode can be observed (141, 142). Studies on ENaC regulation looking at single channel parameters tend to implicate either very large changes in P_o or changes in the number of channels for the same stimulus depending on whether one chooses to look at individual channels or calculate single channel properties from a population (82, 100). If heterogeneities exist, then single channel data may not be extrapolated to the entire population and population statistics may not represent single channel properties with fidelity. New techniques will be needed to measure the distribution of single channel properties of multiple channels.

Many studies suggest that ENaC at the apical membrane exists in a cleaved form resulting from the action of endogenous proteases such as PCs and the presence of the cleaved forms correlate with channel activity. It may thus be concluded that PCs and perhaps other proteases such as CAPs 1-3 may play a role in cleavage-mediated conversion. In chapter 3, it was shown that ENaC expressed heterologously in FRT epithelial cells also have similar protease regulation as previously observed in many epithelial cells. Steroid up-regulation of Na^+ transport in transfected cells did not change the pattern of aprotinin inhibition and protease activation. Using the heterologous system, it was shown that direct interaction of proteases occurs with the ENaC γ subunit resulting in activation of current from aprotinin inhibited states. This was demonstrated by the dependence of protease activation of current on the presence of specific residues within the γ182-193 segment. The correspondence of activation by the elastases NE and PE with the presence of their preferred P1 substrate residue at γV193 and γ190 respectively combined with novel thrombin activation of current induced by engineering into the γ subunit a thrombin cleavage sequence demonstrated the dependence of activation directly on protease interaction with the γ subunit. Upon binding there is a rate limiting step in channel activation which is consistent with hydrolysis at the specific residue but can also result from hydrolysis independent steps. The correlation of activation time constants and steady-state values suggest a limited life time of the active channel at the apical membrane. This is in line with measurements of subunit lifetimes in the apical membrane (6) and the dependence of Na^+ transport and cleavage on endocytic mechanisms (105).

The preliminary studies in chapter 4 indicated the importance of polybasic sequences within the α and γ subunit for channel activity. Mutating putative P1 positions resulted in partial activity of ENaC. These sequences are consensus sequences for several trypsin-like proteases including prostasin, CAP3 and several PC family members. Thus the mutations do not indicate a particular protease as being involved. Interestingly, the effect of the mutations on elastase activation of ENaC were different depending on whether the α subunit or the γ subunit was investigated. The α subunit mutant ($\alpha_{R178A;R204A}\beta\gamma$) was activated by the elastases NE and PE whereas the γ subunit mutant ($\alpha\beta\gamma_{R138A}$) was not. Further, aprotinin inhibition showed that the γ subunit mutant was not entirely unresponsive since some activation was observed in the context of an aprotinin inhibited epithelial cells. However this activation by the elastases was minimal relative to activation by trypsin and appears only to reverse the extent of aprotinin inhibition. The results highlight some complexities of the protease regulatory pathway indicating that more than one type of protease may be involved in activation of the channel in a series of sequential steps.

In conclusion, our results show that protease activities at the apical membrane regulate Na^+ transport by partitioning the channels into active and inactive populations. These populations could be held in a steady-state by continuous insertion into the membrane from the biosynthetic pathway and retrieval from the membrane for degradation. The inactive channels hence form a reserve pool that could be rapidly activated by a protease dependent process or by other means. Thus in addition to the ability to change the open probability of channels already in the membrane, the ability to change their numbers as well increases the dynamic range of regulation of Na^+ transport.

APPENDIX

After aprotinin treatment we assume that there exists an inactive channel population (C) that can be converted to active channels (A) by the enzyme (E). For direct enzyme channel interactions we considered two schemes; 1) Single step enzyme binding and 2) a enzyme binding followed by a secondary conformational change, possibly catalysis. The first reaction consists of the enzyme binding to the channel as shown in equation A 1.

$$C + E \leftarrow \frac{k_{on}}{k_{off}} \rightarrow A$$

A 1

Since A is measured as the increase in current in response to protease (ΔI_{PR}^{Norm}), we write the differential equation for A as

$$\frac{d}{dt}(A) = k_{on} E \cdot C - k_{off} A$$

A 2

Then assume that the number of activable channels (C_0) is fixed so that

$$C_0 = C + A$$

A 3

to yield:

$$\frac{d}{dt}(A) = k_{on}E \cdot C_0 - (k_{off} + k_{on}E)A$$

A 4

In the reaction, E is in excess relative to C so that its concentration does not change and a pseudo-first order kinetic is evident. Equation A 4 is immediately solved as a linear differential equation to give the typical binding exponential curve as in equation A 5.

$$A(t) = \frac{k_{on}E \cdot C_0}{k_{off} + k_{on}E}\left(1 - e^{-\lambda t}\right)$$

A 5

where

$$\lambda = 1/\tau = k_{off} + k_{on}E$$

A 6

Since A represents active channels, equation A 4 can thus be written as equation A 7

$$\Delta I_{PR}{}^{Norm}(t) = \Delta I_{PR}{}^{Norm}(\infty)\left(1 - e^{-t/\tau}\right)$$

A 7

for the increase in current with time. The relaxation rate constant λ increases linearly with E and the plateau value ($\Delta I_{PR}{}^{Norm}(\infty)$) is the typical ligand binding hyperbolic expression.

$$C + E \leftarrow \frac{k_{on}}{k_{off}} \rightarrow CE \xrightarrow{k_{cat}} A$$

A 8

The second reaction, as indicated in equation A8, consists of enzyme binding and a secondary step which we call catalysis for the sake of argument but could represent any rate limiting step (e.g. conformational change leading to channel opening). With fixed number of activable channels there reaction is defined by the differential equations

$$\frac{d}{dt}(CE) = k_{on}E \cdot C_0 - (k_{cat} + k_{off} + k_{on}E) \cdot CE - k_{on}E \cdot A$$

A 9

$$\frac{d}{dt}(A) = k_{cat} \cdot CE$$

A 10

With assumption of excess E, these become linear differential equations that are solved conveniently using the eigenvalue-eigenvector method. In vector notation these differential equations become:

$$\frac{d}{dt}\begin{pmatrix} CE \\ A \end{pmatrix} = \begin{pmatrix} k_{on}E \cdot C_0 \\ 0 \end{pmatrix} - \begin{bmatrix} k_{cat} + k_{off} + k_{on}E & k_{on}E \\ -k_{cat} & 0 \end{bmatrix} \cdot \begin{pmatrix} CE \\ A \end{pmatrix}$$

A 11

Using the substitutions

$$\hat{v} = \begin{pmatrix} CE \\ A \end{pmatrix},\ \hat{r} = \begin{pmatrix} k_{on}E \cdot C_0 \\ 0 \end{pmatrix} \text{ and } M = \begin{bmatrix} k_{cat} + k_{off} + k_{on}E & k_{on}E \\ -k_{cat} & 0 \end{bmatrix}$$

The differential equation is written as

$$\frac{d}{dt}(\hat{v}) = \hat{r} - M\hat{v}$$

A 12

which is solved analogously (with vector algebra conventions) to equation A 4 to give

$$\hat{v}(t) = M^{-1}(I - e^{-Mt})\hat{r}$$

A 13

where,

$$e^{-Mt} = \sum_{i=1}^{2} A_i e^{-\lambda_i t}$$

A 14

I is the identity matrix, A_i are the spectral matrices (not the active channels) and λ_i the eigenvalues of M (38). The eigenvalues and eigenvectors of M are obtained in the usual way and the spectral matrices A_i can be calculated from them (38). Therefore CE(t) and A(t) are sums of a constant and two exponentials with rate constants λ_1 and λ_2 and substituting ΔI_{PR}^{Norm} for A(t) we get

$$\Lambda I_{PR}^{Norm}(t) = \Delta I_{PR}^{Norm}(\infty) + \alpha_1 e^{-\lambda_1 t} + \alpha_2 e^{-\lambda_2 t}$$

A 15

As previously indicated we are interested in the relaxation rate constants obtained by fitting the current traces to equation A 15. The eigenvalues are given by equation A 16 below

$$\lambda = 1/2(b \pm b\sqrt{1 - a/b^2})$$

A 16

where,

$$b = k_{cat} + k_{off} + k_{on}E$$

$$a = 4k_{cat}k_{on}E$$

Using the Taylor series expansion

$$f(x_0 + a) = f(x_0) + a\frac{df}{dx}(x_0) + \frac{a}{2!}^2 \frac{d^2 f}{dx^2}(x_0) + \cdots$$

the square root term becomes

$$\sqrt{1 - a/b^2} = 1 - \frac{a}{2b^2} + \frac{1}{2}\left(\frac{a}{2b^2}\right)^2 - \cdots$$

At infinite enzyme concentration the maximal rate of formation of A is limited by k_{cat}. The maximal rate is small in our experiments. We assume that k_{off} and k_{on} are much larger than k_{cat} so that $a/b^2 << 1$ and the higher order terms in the Taylor series go to 0. The rate constants in equation A15 are now given by

$$\lambda_1 = b - a/4b$$

A 17

and

$$\lambda_2 = a / 4b$$

A 18

Substituting equations A18 and A 18 into equations A 13 and A 14, it can be shown that α_1 vanishes in equation A10 and α_2 becomes C_0 so that rate constant λ_2 is the slower saturable rate and represents the exponential component observed in our experiments. Substituting the expressions for a and b gives:

$$\lambda_2 = \frac{k_{cat} E}{K_M + E}$$

A 19

where

$$K_M = \frac{k_{cat} + k_{off}}{k_{on}}$$

To obtain the values for k_{off} and k_{on} we need to observe the fast exponential. The time resolution in our experiment is however limited by the solution exchange rate with a variable rise time averaging ~ 5-10 s as estimated from amiloride inhibition of current. This is may explain why a fast rate was never observed, however solution exchange remained fast enough not to be rate limiting for the slow exponential component.

BIBLIOGRAPHY

1. **Abramcheck FJ, Van Driessche W, and Helman SI.** Autoregulation of apical membrane Na+ permeability of tight epithelia. Noise analysis with amiloride and CGS 4270. *J Gen Physiol* 85: 555-582, 1985.

2. **Aceves J and Erlij D.** Sodium transport across the isolated epithelium of the frog skin. *J Physiol* 212: 195-210, 1971.

3. **Adachi M, Kitamura K, Miyoshi T, Narikiyo T, Iwashita K, Shiraishi N, Nonoguchi H, and Tomita K.** Activation of epithelial sodium channels by prostasin in Xenopus oocytes. *J Am Soc Nephrol* 12: 1114-1121, 2001.

4. **Adebamiro A, Cheng Y, Johnson JP, and Bridges RJ.** Endogenous protease activation of ENaC: effect of serine protease inhibition on ENaC single channel properties. *J Gen Physiol* 126: 339-352, 2005.

5. **Alvarez de la Rosa D, Canessa CM, Fyfe GK, and Zhang P.** Structure and regulation of amiloride-sensitive sodium channels. *Annu Rev Physiol* 62: 573-594, 2000.

6. **Alvarez de la Rosa D, Li H, and Canessa CM.** Effects of aldosterone on biosynthesis, traffic, and functional expression of epithelial sodium channels in A6 cells. *J Gen Physiol* 119: 427-442, 2002.

7. **Alvarez de la Rosa D, Paunescu TG, Els WJ, Helman SI, and Canessa CM.** Mechanisms of regulation of epithelial sodium channel by SGK1 in A6 cells. *J Gen Physiol* 124: 395-407, 2004.

8. **Andreasen D, Vuagniaux G, Fowler-Jaeger N, Hummler E, and Rossier BC.** Activation of Epithelial Sodium Channels by Mouse Channel Activating Proteases (mCAP) Expressed in Xenopus Oocytes Requires Catalytic Activity of mCAP3 and mCAP2 but not mCAP1. *J Am Soc Nephrol*, 2006.

9. **Asher C, Eren R, Kahn L, Yeger O, and Garty H.** Expression of the amiloride-blockable Na+ channel by RNA from control versus aldosterone-stimulated tissue. *J Biol Chem* 267: 16061-16065, 1992.

10. **Asher C and Garty H.** Aldosterone increases the apical Na+ permeability of toad bladder by two different mechanisms. *Proc Natl Acad Sci U S A* 85: 7413-7417, 1988.

11. **Asher C, Wald H, Rossier BC, and Garty H.** Aldosterone-induced increase in the abundance of Na+ channel subunits. *Am J Physiol* 271: C605-611, 1996.

12. **Auerswald EA, Horlein D, Reinhardt G, Schroder W, and Schnabel E.** Expression, isolation and characterization of recombinant [Arg15,Glu52]aprotinin. *Biol Chem Hoppe Seyler* 369 Suppl: 27-35, 1988.

13. **Baugh RJ and Travis J.** Human leukocyte granule elastase: rapid isolation and characterization. *Biochemistry* 15: 836-841, 1976.

14. **Baxendale-Cox LM, Duncan RL, Liu X, Baldwin K, Els WJ, and Helman SI.** Steroid hormone-dependent expression of blocker-sensitive ENaCs in apical membranes of A6 epithelia. *Am J Physiol* 273: C1650-1656, 1997.

15. **Becchetti A, Malik B, Yue G, Duchatelle P, Al-Khalili O, Kleyman TR, and Eaton DC.** Phosphatase inhibitors increase the open probability of ENaC in A6 cells. *Am J Physiol Renal Physiol* 283: F1030-1045, 2002.

16. **Benos DJ, Awayda MS, Berdiev BK, Bradford AL, Fuller CM, Senyk O, and Ismailov, II.** Diversity and regulation of amiloride-sensitive Na+ channels. *Kidney Int* 49: 1632-1637, 1996.

17. **Beynon RJ and Bond JS.** *Proteolytic Enzymes*. New York: Oxford University Press, 1996.

18. **Biber TU, Chez RA, and Curran PF.** Na transport across frog skin at low external Na concentrations. *J Gen Physiol* 49: 1161-1176, 1966.

19. **Biber TU and Curran PF.** Direct measurement of uptake of sodium at the outer surface of the frog skin. *J Gen Physiol* 56: 83-99, 1970.

20. **Blazer-Yost BL and Helman SI.** The amiloride-sensitive epithelial Na+ channel: binding sites and channel densities. *Am J Physiol* 272: C761-769, 1997.

21. **Boucher RC.** New concepts of the pathogenesis of cystic fibrosis lung disease. *Eur Respir J* 23: 146-158, 2004.

22. **Boucher RC, Cotton CU, Gatzy JT, Knowles MR, and Yankaskas JR.** Evidence for reduced Cl- and increased Na+ permeability in cystic fibrosis human primary cell cultures. *J Physiol* 405: 77-103, 1988.

23. **Boucher RC, Stutts MJ, Knowles MR, Cantley L, and Gatzy JT.** Na+ transport in cystic fibrosis respiratory epithelia. Abnormal basal rate and response to adenylate cyclase activation. *J Clin Invest* 78: 1245-1252, 1986.

24. **Bourdeau JE and Lau K.** Basolateral cell membrane Ca-Na exchange in single rabbit connecting tubules. *Am J Physiol* 258: F1497-1503, 1990.

25. **Bridges RJ, Newton BB, Pilewski JM, Devor DC, Poll CT, and Hall RL.** Na+ transport in normal and CF human bronchial epithelial cells is inhibited by BAY 39-9437. *Am J Physiol Lung Cell Mol Physiol* 281: L16-23, 2001.

26. **Brochiero E, Raschi C, and Ehrenfeld J.** Na/Ca exchange in the basolateral membrane of the A6 cell monolayer: role in Cai homeostasis. *Pflugers Arch* 430: 105-114, 1995.

27. **Butterworth MB, Edinger RS, Johnson JP, and Frizzell RA.** Acute ENaC stimulation by cAMP in a kidney cell line is mediated by exocytic insertion from a recycling channel pool. *J Gen Physiol* 125: 81-101, 2005.

28. **Caldwell RA, Boucher RC, and Stutts MJ.** Neutrophil elastase activates near-silent epithelial Na+ channels and increases airway epithelial Na+ transport. *Am J Physiol Lung Cell Mol Physiol* 288: L813-819, 2005.

29. **Caldwell RA, Boucher RC, and Stutts MJ.** Serine protease activation of near-silent epithelial Na+ channels. *Am J Physiol Cell Physiol* 286: C190-194, 2004.

30. **Canessa CM, Merillat AM, and Rossier BC.** Membrane topology of the epithelial sodium channel in intact cells. *Am J Physiol* 267: C1682-1690, 1994.

31. **Canessa CM, Schild L, Buell G, Thorens B, Gautschi I, Horisberger JD, and Rossier BC.** Amiloride-sensitive epithelial Na+ channel is made of three homologous subunits. *a* 367: 463-467, 1994.

32. **Carattino MD, Sheng S, Bruns JB, Pilewski JM, Hughey RP, and Kleyman TR.** The epithelial Na+ channel is inhibited by a peptide derived from proteolytic processing of its alpha subunit. *J Biol Chem*, 2006.

33. **Cereijido M, Herrera FC, Flanigan WJ, and Curran PF.** The Influence Of Na Concentration On Na Transport Across Frog Skin. *J Gen Physiol* 47: 879-893, 1964.

34. **Chang D and Dawson DC.** Digitonin-permeabilized colonic cell layers. Demonstration of calcium-activated basolateral K+ and Cl- conductances. *J Gen Physiol* 92: 281-306, 1988.

35. **Chao J and Margolius HS.** Studies on rat renal cortical cell kallikrein. II. Identification of kallikrein as an ecto-enzyme. *Biochim Biophys Acta* 570: 330-340, 1979.

36. **Chraibi A and Horisberger JD.** Na self inhibition of human epithelial Na channel: temperature dependence and effect of extracellular proteases. *J Gen Physiol* 120: 133-145, 2002.

37. **Chraibi A, Vallet V, Firsov D, Hess SK, and Horisberger JD.** Protease modulation of the activity of the epithelial sodium channel expressed in Xenopus oocytes. *J Gen Physiol* 111: 127-138, 1998.

38. **Colquhoun D and Hawks AG.** *Single-Channel Recording*. New York: Plenum Press, 1995.

39. **Cox TC and Helman SI.** Na+ and K+ transport at basolateral membranes of epithelial cells. III. Voltage independence of basolateral membrane Na+ efflux. *J Gen Physiol* 87: 503-509, 1986.

40. **Cuthbert AW.** An upper limit to the number of sodium channels in frog skin epithelium. *J Physiol* 228: 681-692, 1973.

41. **Danahay H, Withey L, Poll CT, van de Graaf SF, and Bridges RJ.** Protease-activated receptor-2-mediated inhibition of ion transport in human bronchial epithelial cells. *Am J Physiol Cell Physiol* 280: C1455-1464, 2001.

42. **Davis CW and Finn AL.** Sodium transport effects on the basolateral membrane in toad urinary bladder. *J Gen Physiol* 80: 733-751, 1982.

43. **Davis CW and Finn AL.** Sodium transport inhibition by amiloride reduces basolateral membrane potassium conductance in tight epithelia. *Science* 216: 525-527, 1982.

44. **De Cristofaro R and Landolfi R.** Allosteric modulation of BPTI interaction with human alpha- and zeta-thrombin. *Eur J Biochem* 260: 97-102, 1999.

45. **Debonneville C, Flores SY, Kamynina E, Plant PJ, Tauxe C, Thomas MA, Munster C, Chraibi A, Pratt JH, Horisberger JD, Pearce D, Loffing J, and Staub O.** Phosphorylation of Nedd4-2 by Sgk1 regulates epithelial Na(+) channel cell surface expression. *Embo J* 20: 7052-7059, 2001.

46. **DeFelice LJ.** *Introduction to membrane noise*. New York: Plenum Press, 1981.

47. **Devor DC and Pilewski JM.** UTP inhibits Na+ absorption in wild-type and DeltaF508 CFTR-expressing human bronchial epithelia. *Am J Physiol* 276: C827-837, 1999.

48. **Donaldson SH, Bennett WD, Zeman KL, Knowles MR, Tarran R, and Boucher RC.** Mucus clearance and lung function in cystic fibrosis with hypertonic saline. *N Engl J Med* 354: 241-250, 2006.

49. **Donaldson SH, Hirsh A, Li DC, Holloway G, Chao J, Boucher RC, and Gabriel SE.** Regulation of the epithelial sodium channel by serine proteases in human airways. *J Biol Chem* 277: 8338-8345, 2002.

50. **Edinger RS, Yospin J, Perry C, Kleyman TR, and Johnson JP.** Regulation of Epithelial Na+ Channels (ENaC) by Methylation: A NOVEL METHYLTRANSFERASE STIMULATES ENaC ACTIVITY. *J Biol Chem* 281: 9110-9117, 2006.

51. **Els WJ and Helman SI.** Dual role of prostaglandins (PGE2) in regulation of channel density and open probability of epithelial Na+ channels in frog skin (R. pipiens). *J Membr Biol* 155: 75-87, 1997.

52. **Els WJ and Helman SI.** Regulation of epithelial sodium channel densities by vasopressin signalling. *Cell Signal* 1: 533-539, 1989.

53. **Els WJ, Helman SI, and Mencio T.** Activation of epithelial Na channels by hormonal and autoregulatory mechanisms of action. *J Gen Physiol* 98: 1197-1220, 1991.

54. **Ergonul Z, Frindt G, and Palmer LG.** Regulation of Maturation and Processing of ENaC subunits in the Rat Kidney. *Am J Physiol Renal Physiol*, 2006.

55. **Faletti CJ, Perrotti N, Taylor SI, and Blazer-Yost BL.** sgk: an essential convergence point for peptide and steroid hormone regulation of ENaC-mediated Na+ transport. *Am J Physiol Cell Physiol* 282: C494-500, 2002.

56. **Fernandez-Monreal M, Lopez-Atalaya JP, Benchenane K, Cacquevel M, Dulin F, Le Caer JP, Rossier J, Jarrige AC, Mackenzie ET, Colloc'h N, Ali C, and Vivien D.** Arginine 260 of the amino-terminal domain of NR1 subunit is critical for tissue-type plasminogen activator-mediated enhancement of N-methyl-D-aspartate receptor signaling. *J Biol Chem* 279: 50850-50856, 2004.

57. **Firsov D, Gautschi I, Merillat AM, Rossier BC, and Schild L.** The heterotetrameric architecture of the epithelial sodium channel (ENaC). *Embo J* 17: 344-352, 1998.

58. **Firsov D, Schild L, Gautschi I, Merillat AM, Schneeberger E, and Rossier BC.** Cell surface expression of the epithelial Na channel and a mutant causing Liddle syndrome: a quantitative approach. *Proc Natl Acad Sci U S A* 93: 15370-15375, 1996.

59. **Fisher RS, Erlij D, and Helman SI.** Intracellular voltage of isolated epithelia of frog skin: apical and basolateral cell punctures. *J Gen Physiol* 76: 447-453, 1980.

60. **Fugere M and Day R.** Cutting back on pro-protein convertases: the latest approaches to pharmacological inhibition. *Trends Pharmacol Sci* 26: 294-301, 2005.

61. **Fyfe GK and Canessa CM.** Subunit composition determines the single channel kinetics of the epithelial sodium channel. *J Gen Physiol* 112: 423-432, 1998.

62. **Garty H.** Mechanisms of aldosterone action in tight epithelia. *J Membr Biol* 90: 193-205, 1986.

63. **Garty H.** Regulation of the epithelial Na+ channel by aldosterone: open questions and emerging answers. *Kidney Int* 57: 1270-1276, 2000.

64. **Garty H and Edelman IS.** Amiloride-sensitive trypsinization of apical sodium channels. Analysis of hormonal regulation of sodium transport in toad bladder. *J Gen Physiol* 81: 785-803, 1983.

65. **Garty H and Palmer LG.** Epithelial sodium channels: function, structure, and regulation. *Physiol Rev* 77: 359-396, 1997.

66. **Garty H, Peterson-Yantorno K, Asher C, and Civian MM.** Effects of corticoid agonists and antagonists on apical Na+ permeability of toad urinary bladder. *Am J Physiol* 266: F108-116, 1994.

67. **Geller RG, Margolius HS, Pisano JJ, and Keiser HR.** Effects of mineralocorticoids, altered sodium intake, and adrenalectomy on urinary kallikrein in rats. *Circ Res* 31: 857-861, 1972.

68. **Gottardi CJ, Dunbar LA, and Caplan MJ.** Biotinylation and assessment of membrane polarity: caveats and methodological concerns. *Am J Physiol* 268: F285-295, 1995.

69. **Goulet CC, Volk KA, Adams CM, Prince LS, Stokes JB, and Snyder PM.** Inhibition of the epithelial Na+ channel by interaction of Nedd4 with a PY motif deleted in Liddle's syndrome. *J Biol Chem* 273: 30012-30017, 1998.

70. **Granitzer M, Leal T, Nagel W, and Crabbe J.** Apical and basolateral conductance in cultured A6 cells. *Pflugers Arch* 417: 463-468, 1991.

71. **Granitzer M, Nagel W, and Crabbe J.** Basolateral membrane conductance in A6 cells: effect of high sodium transport rate. *Pflugers Arch* 420: 559-565, 1992.

72. **Grunder S, Firsov D, Chang SS, Jaeger NF, Gautschi I, Schild L, Lifton RP, and Rossier BC.** A mutation causing pseudohypoaldosteronism type 1 identifies a conserved glycine that is involved in the gating of the epithelial sodium channel. *Embo J* 16: 899-907, 1997.

73. **Grunder S, Jaeger NF, Gautschi I, Schild L, and Rossier BC.** Identification of a highly conserved sequence at the N-terminus of the epithelial Na+ channel alpha subunit involved in gating. *Pflugers Arch* 438: 709-715, 1999.

74. **Hamilton KL and Eaton DC.** Single-channel recordings from amiloride-sensitive epithelial sodium channel. *Am J Physiol* 249: C200-207, 1985.

75. **Hanwell D, Ishikawa T, Saleki R, and Rotin D.** Trafficking and cell surface stability of the epithelial Na+ channel expressed in epithelial Madin-Darby canine kidney cells. *J Biol Chem* 277: 9772-9779, 2002.

76. **Hartley BS and Shotton DM.** *The Enzymes*: Academic Press, 1971.

77. **Harvey BJ, Thomas SR, and Ehrenfeld J.** Intracellular pH controls cell membrane Na+ and K+ conductances and transport in frog skin epithelium. *J Gen Physiol* 92: 767-791, 1988.

78. **Helman SI and Baxendale LM.** Blocker-related changes of channel density. Analysis of a three-state model for apical Na channels of frog skin. *J Gen Physiol* 95: 647-678, 1990.

79. **Helman SI and Fisher RS.** Microelectrode studies of the active Na transport pathway of frog skin. *J Gen Physiol* 69: 571-604, 1977.

80. **Helman SI and Kizer NL.** *Channels and Noise in Epithelial Tissues*. San Diego [etc.]: Academic Press, 1990.

81. **Helman SI and Liu X.** Substrate-dependent expression of Na+ transport and shunt conductance in A6 epithelia. *Am J Physiol* 273: C434-441, 1997.

82. **Helman SI, Liu X, Baldwin K, Blazer-Yost BL, and Els WJ.** Time-dependent stimulation by aldosterone of blocker-sensitive ENaCs in A6 epithelia. *Am J Physiol* 274: C947-957, 1998.

83. **Hille B.** *Ionic Channels of Excitable Membranes*. Sunderland, Massachusetts: Sinauer, 1984.

84. **Horwitz D, Margolius HS, and Keiser HR.** Effects of dietary potassium and race on urinary excretion of kallikrein and aldosterone in man. *J Clin Endocrinol Metab* 47: 296-299, 1978.

85. **Huf EG and Wills J.** Influence of some inorganic cations on active salt and water uptake by isolated frog skin. *Am J Physiol* 167: 255-260, 1951.

86. **Hughey RP, Bruns JB, Kinlough CL, Harkleroad KL, Tong Q, Carattino MD, Johnson JP, Stockand JD, and Kleyman TR.** Epithelial sodium channels are activated by furin-dependent proteolysis. *J Biol Chem* 279: 18111-18114, 2004.

87. **Hughey RP, Bruns JB, Kinlough CL, and Kleyman TR.** Distinct pools of epithelial sodium channels are expressed at the plasma membrane. *J Biol Chem*, 2004.

88. **Hughey RP, Mueller GM, Bruns JB, Kinlough CL, Poland PA, Harkleroad KL, Carattino MD, and Kleyman TR.** Maturation of the epithelial Na+ channel involves proteolytic processing of the alpha- and gamma-subunits. *J Biol Chem* 278: 37073-37082, 2003.

89. **Hummler E, Barker P, Beermann F, Gatzy J, Verdumo C, Boucher R, and Rossier BC.** Role of the epithelial sodium channel in lung liquid clearance. *Chest* 111: 113S, 1997.

90. **Hummler E, Barker P, Gatzy J, Beermann F, Verdumo C, Schmidt A, Boucher R, and Rossier BC.** Early death due to defective neonatal lung liquid clearance in alpha-ENaC-deficient mice. *Nat Genet* 12: 325-328, 1996.

91. **Hummler E, Barker P, Talbot C, Wang Q, Verdumo C, Grubb B, Gatzy J, Burnier M, Horisberger JD, Beermann F, Boucher R, and Rossier BC.** A mouse model for the renal salt-wasting syndrome pseudohypoaldosteronism. *Proc Natl Acad Sci U S A* 94: 11710-11715, 1997.

92. **Ismailov, II, Kieber-Emmons T, Lin C, Berdiev BK, Shlyonsky VG, Patton HK, Fuller CM, Worrell R, Zuckerman JB, Sun W, Eaton DC, Benos DJ, and Kleyman TR.** Identification of an amiloride binding domain within the alpha-subunit of the epithelial Na+ channel. *J Biol Chem* 272: 21075-21083, 1997.

93. **Jenny RJ, Mann KG, and Lundblad RL.** A critical review of the methods for cleavage of fusion proteins with thrombin and factor Xa. *Protein Expr Purif* 31: 1-11, 2003.

94. **Jones LG, McDonough PM, and Brown JH.** Thrombin and trypsin act at the same site to stimulate phosphoinositide hydrolysis and calcium mobilization. *Mol Pharmacol* 36: 142-149, 1989.

95. **Jovov B, Wills NK, Donaldson PJ, and Lewis SA.** Vectorial secretion of a kallikrein-like enzyme by cultured renal cells. I. General properties. *Am J Physiol* 259: C869-882, 1990.

96. **Kellenberger S, Auberson M, Gautschi I, Schneeberger E, and Schild L.** Permeability properties of ENaC selectivity filter mutants. *J Gen Physiol* 118: 679-692, 2001.

97. **Kellenberger S, Gautschi I, and Schild L.** An external site controls closing of the epithelial Na+ channel ENaC. *J Physiol* 543: 413-424, 2002.

98. **Kellenberger S, Gautschi I, and Schild L.** A single point mutation in the pore region of the epithelial Na+ channel changes ion selectivity by modifying molecular sieving. *Proc Natl Acad Sci U S A* 96: 4170-4175, 1999.

99. **Kellenberger S and Schild L.** Epithelial sodium channel/degenerin family of ion channels: a variety of functions for a shared structure. *Physiol Rev* 82: 735-767, 2002.

100. **Kemendy AE, Kleyman TR, and Eaton DC.** Aldosterone alters the open probability of amiloride-blockable sodium channels in A6 epithelia. *Am J Physiol* 263: C825-837, 1992.

101. **Khatib AM, Bassi D, Siegfried G, Klein-Szanto AJ, and Ouafik L.** Endo/exo-proteolysis in neoplastic progression and metastasis. *J Mol Med* 83: 856-864, 2005.

102. **Kirschner LB.** Sodium chloride absorption across the body surface: frog skins and other epithelia. *Am J Physiol* 244: R429-443, 1983.

103. **Kleyman TR and Cragoe EJ, Jr.** Amiloride and its analogs as tools in the study of ion transport. *J Membr Biol* 105: 1-21, 1988.

104. **Kleyman TR, Zuckerman JB, Middleton P, McNulty KA, Hu B, Su X, An B, Eaton DC, and Smith PR.** Cell surface expression and turnover of the alpha-subunit of the epithelial sodium channel. *Am J Physiol Renal Physiol* 281: F213-221, 2001.

105. **Knight KK, Olson DR, Zhou R, and Snyder PM.** Liddle's syndrome mutations increase Na+ transport through dual effects on epithelial Na+ channel surface expression and proteolytic cleavage. *Proc Natl Acad Sci U S A*, 2006.

106. **Koefoed-Johnsen V and Ussing HH.** The nature of the frog skin potential. *Acta Physiol Scand* 42: 298-308, 1958.

107. **Koehl C, Knight CG, and Bieth JG.** Compared action of neutrophil proteinase 3 and elastase on model substrates. Favorable effect of S'-P' interactions on proteinase 3 catalysts. *J Biol Chem* 278: 12609-12612, 2003.

108. **Kosari F, Sheng S, Li J, Mak DO, Foskett JK, and Kleyman TR.** Subunit stoichiometry of the epithelial sodium channel. *J Biol Chem* 273: 13469-13474, 1998.

109. **Kunzelmann K, Schreiber R, and Boucherot A.** Mechanisms of the inhibition of epithelial Na(+) channels by CFTR and purinergic stimulation. *Kidney Int* 60: 455-461, 2001.

110. **Lewis SA and Alles WP.** Urinary kallikrein: a physiological regulator of epithelial Na+ absorption. *Proc Natl Acad Sci U S A* 83: 5345-5348, 1986.

111. **Li JH, Cragoe EJ, Jr., and Lindemann B.** Structure-activity relationship of amiloride analogs as blockers of epithelial Na channels: II. Side-chain modifications. *J Membr Biol* 95: 171-185, 1987.

112. **Li JH and Lindemann B.** Competitive blocking of epithelial sodium channels by organic cations: the relationship between macroscopic and microscopic inhibition constants. *J Membr Biol* 76: 235-251, 1983.

113. **Lindemann B.** Taste reception. *Physiol Rev* 76: 718-766, 1996.

114. **Lindemann B and Van Driessche W.** The Mechanism of Na Uptake Through Na-Selective Channels in the Epithelium of Frog Skin. *Membrane Transport Processes* 1: 155-179, 1978.

115. **Lindemann B and Van Driessche W.** Sodium-specific membrane channels of frog skin are pores: current fluctuations reveal high turnover. *Science* 195: 292-294, 1977.

116. **Liu L, Hering-Smith KS, Schiro FR, and Hamm LL.** Serine protease activity in m-1 cortical collecting duct cells. *Hypertension* 39: 860-864, 2002.

117. **Maisner A, Mrkic B, Herrler G, Moll M, Billeter MA, Cattaneo R, and Klenk HD.** Recombinant measles virus requiring an exogenous protease for activation of infectivity. *J Gen Virol* 81: 441-449, 2000.

118. **Margolius HS and Chao J.** Amiloride inhibits mammalian renal kallikrein and a kallikrein-like enzyme from toad bladder and skin. *J Clin Invest* 65: 1343-1350, 1980.

119. **Margolius HS, Chao J, and Kaizu T.** The effects of aldosterone and spironolactone on renal kallikrein in the rat. *Clin Sci Mol Med Suppl* 3: 279s-282s, 1976.

120. **Margolius HS, Horwitz D, Pisano JJ, and Keiser HR.** Relationships among urinary kallikrein, mineralocorticoids and human hypertensive disease. *Fed Proc* 35: 203-206, 1976.

121. **Markadieu N, Blero D, Boom A, Erneux C, and Beauwens R.** Phosphatidylinositol 3,4,5-trisphosphate: an early mediator of insulin-stimulated sodium transport in A6 cells. *Am J Physiol Renal Physiol* 287: F319-328, 2004.

122. **Marunaka Y and Eaton DC.** Effects of vasopressin and cAMP on single amiloride-blockable Na channels. *Am J Physiol* 260: C1071-1084, 1991.

123. **Masilamani S, Kim GH, Mitchell C, Wade JB, and Knepper MA.** Aldosterone-mediated regulation of ENaC alpha, beta, and gamma subunit proteins in rat kidney. *J Clin Invest* 104: R19-23, 1999.

124. **Matsui H, Grubb BR, Tarran R, Randell SH, Gatzy JT, Davis CW, and Boucher RC.** Evidence for periciliary liquid layer depletion, not abnormal ion composition, in the pathogenesis of cystic fibrosis airways disease. *Cell* 95: 1005-1015, 1998.

125. **McDonald FJ, Price MP, Snyder PM, and Welsh MJ.** Cloning and expression of the beta- and gamma-subunits of the human epithelial sodium channel. *Am J Physiol* 268: C1157-1163, 1995.

126. **McDonald FJ, Snyder PM, McCray PB, Jr., and Welsh MJ.** Cloning, expression, and tissue distribution of a human amiloride-sensitive Na+ channel. *Am J Physiol* 266: L728-734, 1994.

127. **McDonald FJ, Yang B, Hrstka RF, Drummond HA, Tarr DE, McCray PB, Jr., Stokes JB, Welsh MJ, and Williamson RA.** Disruption of the beta subunit of the epithelial Na+ channel in mice: hyperkalemia and neonatal death associated with a pseudohypoaldosteronism phenotype. *Proc Natl Acad Sci U S A* 96: 1727-1731, 1999.

128. **Mellet P, Boudier C, Mely Y, and Bieth JG.** Stopped flow fluorescence energy transfer measurement of the rate constants describing the reversible formation and the irreversible rearrangement of the elastase-alpha1-proteinase inhibitor complex. *J Biol Chem* 273: 9119-9123, 1998.

129. **Nadal MS, Ozaita A, Amarillo Y, Vega-Saenz de Miera E, Ma Y, Mo W, Goldberg EM, Misumi Y, Ikehara Y, Neubert TA, and Rudy B.** The CD26-related dipeptidyl aminopeptidase-like protein DPPX is a critical component of neuronal A-type K+ channels. *Neuron* 37: 449-461, 2003.

130. **Nagel W.** The dependence of the electrical potentials across the membranes of the frog skin upon the concentration of sodium in the mucosal solution. *J Physiol* 269: 777-796, 1977.

131. **Nakajima K, Powers JC, Ashe BM, and Zimmerman M.** Mapping the extended substrate binding site of cathepsin G and human leukocyte elastase. Studies with peptide substrates related to the alpha 1-protease inhibitor reactive site. *J Biol Chem* 254: 4027-4032, 1979.

132. **Nakhoul NL, Hering-Smith KS, Gambala CT, and Hamm LL.** Regulation of sodium transport in M-1 cells. *Am J Physiol* 275: F998-F1007, 1998.

133. **Narikiyo T, Kitamura K, Adachi M, Miyoshi T, Iwashita K, Shiraishi N, Nonoguchi H, Chen LM, Chai KX, Chao J, and Tomita K.** Regulation of prostasin by aldosterone in the kidney. *J Clin Invest* 109: 401-408, 2002.

134. **Narvarte J and Finn AL.** Microelectrode studies in toad urinary bladder epithelium. effects of Na concentration changes in the mucosal solution on equivalent electromotive forces. *J Gen Physiol* 75: 323-344, 1980.

135. **Nguyen TD, Moody MW, Steinhoff M, Okolo C, Koh DS, and Bunnett NW.** Trypsin activates pancreatic duct epithelial cell ion channels through proteinase-activated receptor-2. *J Clin Invest* 103: 261-269, 1999.

136. **Ohlsson K and Olsson AS.** Purification and partial characterization of human pancreatic elastase. *Hoppe Seylers Z Physiol Chem* 357: 1153-1161, 1976.

137. **Orce GG, Castillo GA, and Margolius HS.** Inhibition of short-circuit current in toad urinary bladder by inhibitors of glandular kallikrein. *Am J Physiol* 239: F459-465, 1980.

138. **Ossovskaya VS and Bunnett NW.** Protease-activated receptors: contribution to physiology and disease. *Physiol Rev* 84: 579-621, 2004.

139. **Pacha J, Frindt G, Antonian L, Silver RB, and Palmer LG.** Regulation of Na channels of the rat cortical collecting tubule by aldosterone. *J Gen Physiol* 102: 25-42, 1993.

140. **Palmer LG.** Epithelial Na channels: function and diversity. *Annu Rev Physiol* 54: 51-66, 1992.

141. **Palmer LG and Frindt G.** Conductance and gating of epithelial Na channels from rat cortical collecting tubule. Effects of luminal Na and Li. *J Gen Physiol* 92: 121-138, 1988.

142. **Palmer LG and Frindt G.** Gating of Na channels in the rat cortical collecting tubule: effects of voltage and membrane stretch. *J Gen Physiol* 107: 35-45, 1996.

143. **Paulais M, Lachheb S, and Teulon J.** A Na+- and Cl- -activated K+ channel in the thick ascending limb of mouse kidney. *J Gen Physiol* 127: 205-215, 2006.

144. **Paunescu TG, Blazer-Yost BL, Vlahos CJ, and Helman SI.** LY-294002-inhibitable PI 3-kinase and regulation of baseline rates of Na(+) transport in A6 epithelia. *Am J Physiol Cell Physiol* 279: C236-247, 2000.

145. **Pearce D.** SGK1 regulation of epithelial sodium transport. *Cell Physiol Biochem* 13: 13-20, 2003.

146. **Pintigny D and Dachary-Prigent J.** Aprotinin can inhibit the proteolytic activity of thrombin. A fluorescence and an enzymatic study. *Eur J Biochem* 207: 89-95, 1992.

147. **Planes C, Leyvraz C, Uchida T, Angelova MA, Vuagniaux G, Hummler E, Matthay MA, Clerici C, and Rossier BC.** In vitro and in vivo regulation of transepithelial lung alveolar sodium transport by serine proteases. *Am J Physiol Lung Cell Mol Physiol*, 2005.

148. **Pochynyuk O, Staruschenko A, Tong Q, Medina J, and Stockand JD.** Identification of a functional phosphatidylinositol 3,4,5-trisphosphate binding site in the epithelial Na+ channel. *J Biol Chem* 280: 37565-37571, 2005.

149. **Pochynyuk O, Tong Q, Staruschenko A, Ma HP, and Stockand JD.** Regulation of the epithelial Na+ channel (ENaC) by phosphatidylinositides. *Am J Physiol Renal Physiol* 290: F949-957, 2006.

150. **Poirot O, Vukicevic M, Boesch A, and Kellenberger S.** Selective regulation of acid-sensing ion channel 1 by serine proteases. *J Biol Chem* 279: 38448-38457, 2004.

151. **Puoti A, May A, Canessa CM, Horisberger JD, Schild L, and Rossier BC.** The highly selective low-conductance epithelial Na channel of Xenopus laevis A6 kidney cells. *Am J Physiol* 269: C188-197, 1995.

152. **Renard S, Lingueglia E, Voilley N, Lazdunski M, and Barbry P.** Biochemical analysis of the membrane topology of the amiloride-sensitive Na+ channel. *J Biol Chem* 269: 12981-12986, 1994.

153. **Rick R, Dorge A, von Arnim E, and Thurau K.** Electron microprobe analysis of frog skin epithelium: evidence for a syncytial sodium transport compartment. *J Membr Biol* 39: 313-331, 1978.

154. **Rokaw MD, Benos DJ, Palevsky PM, Cunningham SA, West ME, and Johnson JP.** Regulation of a sodium channel-associated G-protein by aldosterone. *J Biol Chem* 271: 4491-4496, 1996.

155. **Rokaw MD, Wang JM, Edinger RS, Weisz OA, Hui D, Middleton P, Shlyonsky V, Berdiev BK, Ismailov I, Eaton DC, Benos DJ, and Johnson JP.** Carboxylmethylation of the beta subunit of xENaC regulates channel activity. *J Biol Chem* 273: 28746-28751, 1998.

156. **Rossier BC.** The Epithelial Sodium Channel: Activation by Membrane-bound serine proteases. *Proc Am Thorac Soc* 1: 4-9, 2004.

157. **Salako LA and Smith AJ.** Changes in sodium pool and kinetics of sodium transport in frog skin produced by amiloride. *Br J Pharmacol* 39: 99-109, 1970.

158. **Salako LA and Smith AJ.** Effects of amiloride on active sodium transport by the isolated frog skin: evidence concerning site of action. *Br J Pharmacol* 38: 702-718, 1970.

159. **Schild L, Schneeberger E, Gautschi I, and Firsov D.** Identification of amino acid residues in the alpha, beta, and gamma subunits of the epithelial sodium channel (ENaC) involved in amiloride block and ion permeation. *J Gen Physiol* 109: 15-26, 1997.

160. **Schultz SG.** Homocellular regulatory mechanisms in sodium-transporting epithelia: avoidance of extinction by "flush-through". *Am J Physiol* 241: F579-590, 1981.

161. **Scott CF, Wenzel HR, Tschesche HR, and Colman RW.** Kinetics of inhibition of human plasma kallikrein by a site-specific modified inhibitor Arg15-aprotinin: evaluation using a microplate system and comparison with other proteases. *Blood* 69: 1431-1436, 1987.

162. **Segal A, Awayda MS, Eggermont J, Van Driessche W, and Weber WM.** Influence of voltage and extracellular Na(+) on amiloride block and transport kinetics of rat epithelial Na(+) channel expressed in Xenopus oocytes. *Pflugers Arch* 443: 882-891, 2002.

163. **Sheng S, Carattino MD, Bruns JB, Hughey RP, and Kleyman TR.** Furin cleavage activates the epithelial Na+ channels by relieving Na+ self-inhibition. *Am J Physiol Renal Physiol*, 2006.

164. **Sheppard DN, Carson MR, Ostedgaard LS, Denning GM, and Welsh MJ.** Expression of cystic fibrosis transmembrane conductance regulator in a model epithelium. *Am J Physiol* 266: L405-413, 1994.

165. **Shimkets RA, Lifton R, and Canessa CM.** In vivo phosphorylation of the epithelial sodium channel. *Proc Natl Acad Sci U S A* 95: 3301-3305, 1998.

166. **Shimkets RA, Lifton RP, and Canessa CM.** The activity of the epithelial sodium channel is regulated by clathrin-mediated endocytosis. *J Biol Chem* 272: 25537-25541, 1997.

167. **Shipway A, Danahay H, Williams JA, Tully DC, Backes BJ, and Harris JL.** Biochemical characterization of prostasin, a channel activating protease. *Biochem Biophys Res Commun* 324: 953-963, 2004.

168. **Shoelson SE, White MF, and Kahn CR.** Tryptic activation of the insulin receptor. Proteolytic truncation of the alpha-subunit releases the beta-subunit from inhibitory control. *J Biol Chem* 263: 4852-4860, 1988.

169. **Simson JA, Spicer SS, Chao J, Grimm L, and Margolius HS.** Kallikrein localization in rodent salivary glands and kidney with the immunoglobulin-enzyme bridge technique. *J Histochem Cytochem* 27: 1567-1576, 1979.

170. **Snyder PM.** The epithelial Na+ channel: cell surface insertion and retrieval in Na+ homeostasis and hypertension. *Endocr Rev* 23: 258-275, 2002.

171. **Snyder PM.** Liddle's syndrome mutations disrupt cAMP-mediated translocation of the epithelial Na(+) channel to the cell surface. *J Clin Invest* 105: 45-53, 2000.

172. **Snyder PM, Bucher DB, and Olson DR.** Gating induces a conformational change in the outer vestibule of ENaC. *J Gen Physiol* 116: 781-790, 2000.

173. **Snyder PM, McDonald FJ, Stokes JB, and Welsh MJ.** Membrane topology of the amiloride-sensitive epithelial sodium channel. *J Biol Chem* 269: 24379-24383, 1994.

174. **Snyder PM, Olson DR, and Bucher DB.** A pore segment in DEG/ENaC Na(+) channels. *J Biol Chem* 274: 28484-28490, 1999.

175. **Snyder PM, Olson DR, Kabra R, Zhou R, and Steines JC.** cAMP and serum and glucocorticoid-inducible kinase (SGK) regulate the epithelial Na(+) channel through convergent phosphorylation of Nedd4-2. *J Biol Chem* 279: 45753-45758, 2004.

176. **Snyder PM, Olson DR, and Thomas BC.** Serum and glucocorticoid-regulated kinase modulates Nedd4-2-mediated inhibition of the epithelial Na+ channel. *J Biol Chem* 277: 5-8, 2002.

177. **Staruschenko A, Medina JL, Patel P, Shapiro MS, Booth RE, and Stockand JD.** Fluorescence resonance energy transfer analysis of subunit stoichiometry of the epithelial Na+ channel. *J Biol Chem* 279: 27729-27734, 2004.

178. **Staruschenko A, Pochynyuk O, and Stockand JD.** Regulation of epithelial Na+ channel activity by conserved serine/threonine switches within sorting signals. *J Biol Chem* 280: 39161-39167, 2005.

179. **Staub O, Gautschi I, Ishikawa T, Breitschopf K, Ciechanover A, Schild L, and Rotin D.** Regulation of stability and function of the epithelial Na+ channel (ENaC) by ubiquitination. *Embo J* 16: 6325-6336, 1997.

180. **Stockley RA.** New approaches to the management of COPD. *Chest* 117: 58S-62S, 2000.

181. **Takagi T and Doolittle RF.** Amino acid sequence studies on factor XIII and the peptide released during its activation by thrombin. *Biochemistry* 13: 750-756, 1974.

182. **Takeuchi T, Harris JL, Huang W, Yan KW, Coughlin SR, and Craik CS.** Cellular localization of membrane-type serine protease 1 and identification of protease-activated receptor-2 and single-chain urokinase-type plasminogen activator as substrates. *J Biol Chem* 275: 26333-26342, 2000.

183. **Tang J, Abramcheck FJ, Van Driessche W, and Helman SI.** Electrophysiology and noise analysis of K+-depolarized epithelia of frog skin. *Am J Physiol* 249: C421-429, 1985.

184. **Tavernarakis N and Driscoll M.** Molecular modeling of mechanotransduction in the nematode Caenorhabditis elegans. *Annu Rev Physiol* 59: 659-689, 1997.

185. **Taylor NA, Van De Ven WJ, and Creemers JW.** Curbing activation: proprotein convertases in homeostasis and pathology. *Faseb J* 17: 1215-1227, 2003.

186. **Tong Q, Gamper N, Medina JL, Shapiro MS, and Stockand JD.** Direct activation of the epithelial Na(+) channel by phosphatidylinositol 3,4,5-trisphosphate and phosphatidylinositol 3,4-bisphosphate produced by phosphoinositide 3-OH kinase. *J Biol Chem* 279: 22654-22663, 2004.

187. **Tong Q and Stockand JD.** Receptor tyrosine kinases mediate epithelial Na+ channel inhibition by epidermal growth factor. *Am J Physiol Renal Physiol*, 2004.

188. **Tong Z, Illek B, Bhagwandin VJ, Verghese GM, and Caughey GH.** Prostasin, a membrane-anchored serine peptidase, regulates sodium currents in JME/CF15 cells, a cystic fibrosis airway epithelial cell line. *Am J Physiol Lung Cell Mol Physiol* 287: L928-935, 2004.

189. **Travis J, Giles PJ, Porcelli L, Reilly CF, Baugh R, and Powers J.** Human leucocyte elastase and cathepsin G: structural and functional characteristics. *Ciba Found Symp*: 51-68, 1979.

190. **Ussing HH.** The frog skin potential. *J Gen Physiol* 43: 135-147, 1960.

191. **Vallet V, Chraibi A, Gaeggeler HP, Horisberger JD, and Rossier BC.** An epithelial serine protease activates the amiloride-sensitive sodium channel. *a* 389: 607-610, 1997.

192. **Vallet V, Pfister C, Loffing J, and Rossier BC.** Cell-surface expression of the channel activating protease xCAP-1 is required for activation of ENaC in the Xenopus oocyte. *J Am Soc Nephrol* 13: 588-594, 2002.

193. **Van Driessche W and Lindemann B.** Concentration dependence of currents through single sodium-selective pores in frog skin. *a* 282: 519-520, 1979.

194. **Van Driessche W and Lindemann B.** Low-noise amplification of voltage and current fluctuations arising in epithelia. *Rev Sci Instrum* 49: 53-57, 1978.

195. **Van Driessche W and Van Deynse N.** *Channels and Noise in Epithelial Tissues*. San Diego [etc.]: Academic Press, 1990.

196. **Verrey F.** Transcriptional control of sodium transport in tight epithelial by adrenal steroids. *J Membr Biol* 144: 93-110, 1995.

197. **Vinci JM, Zusman RM, Izzo JL, Jr., Bowden RE, Horwitz D, Pisano JJ, and Keiser HR.** Human urinary and plasma kinins: relationship to sodium-retaining steroids and plasma renin activity. *Circ Res* 44: 228-237, 1979.

198. **Vogel R and Werle E.** Handbook of Experimental Pharmacology. Bradykinin, Kallidin, and Kallikrein. In: *Kallikrein Inhibitors*, edited by Erdos EG. Berlin: Springer, 1970, p. 213-249.

199. **Vu TK, Wheaton VI, Hung DT, Charo I, and Coughlin SR.** Domains specifying thrombin-receptor interaction. *a* 353: 674-677, 1991.

200. **Vuagniaux G, Vallet V, Jaeger NF, Hummler E, and Rossier BC.** Synergistic activation of ENaC by three membrane-bound channel-activating serine proteases (mCAP1, mCAP2, and mCAP3) and serum- and glucocorticoid-regulated kinase (Sgk1) in Xenopus Oocytes. *J Gen Physiol* 120: 191-201, 2002.

201. **Vuagniaux G, Vallet V, Jaeger NF, Pfister C, Bens M, Farman N, Courtois-Coutry N, Vandewalle A, Rossier BC, and Hummler E.** Activation of the amiloride-sensitive epithelial sodium channel by the serine protease mCAP1 expressed in a mouse cortical collecting duct cell line. *J Am Soc Nephrol* 11: 828-834, 2000.

202. **Vukicevic M, Weder G, Boillat A, Boesch A, and Kellenberger S.** Trypsin Cleaves Acid-sensing Ion Channel 1a in a Domain That Is Critical for Channel Gating. *J Biol Chem* 281: 714-722, 2006.

203. **Wang H, Traub LM, Weixel KM, Hawryluk MJ, Shah N, Edinger RS, Perry CJ, Kester L, Butterworth MB, Kleyman TR, Frizzell RA, and Johnson JP.** Clathrin-mediated endocytosis of ENaC: Role of epsin. *J Biol Chem*, 2006.

204. **Weisz OA, Wang JM, Edinger RS, and Johnson JP.** Non-coordinate regulation of endogenous epithelial sodium channel (ENaC) subunit expression at the apical membrane of A6 cells in response to various transporting conditions. *J Biol Chem* 275: 39886-39893, 2000.

205. **Yang LM, Rinke R, and Korbmacher C.** Stimulation of the Epithelial Sodium Channel (ENaC) by cAMP Involves Putative ERK Phosphorylation Sites in the C Termini of the Channel's beta- and {gamma}-Subunit. *J Biol Chem* 281: 9859-9868, 2006.

206. **Yu JX, Chao L, and Chao J.** Prostasin is a novel human serine proteinase from seminal fluid. Purification, tissue distribution, and localization in prostate gland. *J Biol Chem* 269: 18843-18848, 1994.

207. **Zhang YH, Alvarez de la Rosa D, Canessa CM, and Hayslett JP.** Insulin-induced phosphorylation of ENaC correlates with increased sodium channel function in A6 cells. *Am J Physiol Cell Physiol* 288: C141-147, 2005.

208. **Zimmerman M and Ashe BM.** Sbustrate specificity of the elastase and the chymotrypsin-like enzyme of the human granulocyte. *Biochim Biophys Acta* 480: 241-245, 1977.